NTNU

Norwegian University of
Science and Technology

Experimental study of multiphase flow in an upward-inclined pipe

Magnus Kallager
Marit Vassmyr

Master of Energy and Environmental Engineering
Submission date: June 2017
Supervisor: Zhilin Yang, EPT
Co-supervisor: Nicolas La Forgia, EPT

Norwegian University of Science and Technology
Department of Energy and Process Engineering

NTNU

Norwegian University
of Science and Technology

Department of Energy
and Process Engineering

EPT-M-2017-40 & EPT-M-2017-92

MASTER THESIS

for

Magnus Kallager & Marit Vassmyr

Spring 2017

Experimental study of multiphase flow in an upward-inclined pipe

Eksperimentell studie av flerfasestrømning i et oppoverhellende rør

Background and objective

A correct prediction of multiphase flow dynamics in an inclined pipe is critical for the design of pipeline for the deep-water riser and production tubing of a production well in offshore oil and gas field development. The focus on multiphase flow studies has been on the flow in a pipe close to horizontal and flow in a vertical pipe, since such pipe geometry and topology are quite common. The exploration into deep water and development of horizontal well drilling make it more actual for the pipe or flow channel with inclination between 10 and 85 degree, little information on the flow in the pipe with such inclination angle range is available. The industry has identified that there is a big gap for the existing model prediction for the flow in such pipe geometry.

The objective of the current thesis is to conduct an experimental study of multiphase flow in an upward pipe flow with pipe inclination between 10 and 80°, focus will be on liquid dominated flow.

The following tasks are to be considered:

1. Conduct literature survey on the flow in inclined pipe flow, and collect the flow model on pressure gradient and liquid holdup, as well as the flow regime information.
2. The modification of the current rig in the laboratory should be conducted to meet the experimental requirement: inclination angles, pipe with i.d of around 60 mm;
3. Necessary instrumentation and calibration: pressure sensor, differential pressure sensor, temperature, flowrate meter for each phases, holdup measurement, video record for the flow structure;
4. Conduct experimental study with gas-liquid two-phase, and three-phase flow if time allowed;
5. Analysis of the experimental data, and assessment of the existing model and observation with the experimental results obtained from this thesis work.

Within 14 days of receiving the written text on the master thesis, the candidate shall submit a research plan for his project to the department.

When the thesis is evaluated, emphasis is put on processing of the results, and that they are presented in tabular and/or graphic form in a clear manner, and that they are analyzed carefully.

The thesis should be formulated as a research report with summary both in English and Norwegian, conclusion, literature references, table of contents etc. During the preparation of the text, the candidate should make an effort to produce a well-structured and easily readable report. In order to ease the evaluation of the thesis, it is important that the cross-references are correct. In the making of the report, strong emphasis should be placed on both a thorough discussion of the results and an orderly presentation.

The candidate is requested to initiate and keep close contact with his/her academic supervisor(s) throughout the working period. The candidate must follow the rules and regulations of NTNU as well as passive directions given by the Department of Energy and Process Engineering.

Risk assessment of the candidate's work shall be carried out according to the department's procedures. The risk assessment must be documented and included as part of the final report. Events related to the candidate's work adversely affecting the health, safety or security, must be documented and included as part of the final report. If the documentation on risk assessment represents a large number of pages, the full version is to be submitted electronically to the supervisor and an excerpt is included in the report.

Pursuant to "Regulations concerning the supplementary provisions to the technology study program/Master of Science" at NTNU §20, the Department reserves the permission to utilize all the results and data for teaching and research purposes as well as in future publications.

The final report is to be submitted digitally in DAIM. An executive summary of the thesis including title, student's name, supervisor's name, year, department name, and NTNU's logo and name, shall be submitted to the department as a separate pdf file. Based on an agreement with the supervisor, the final report and other material and documents may be given to the supervisor in digital format.

☒ Work to be done in lab (Water power lab, Fluids engineering lab, Thermal engineering lab)
☐ Field work

Department of Energy and Process Engineering, 15. January 2017

Zhilin Yang

Academic Supervisor

Research Advisor:

Nicolas La Forgia

Acknowledgement

We would like to thank our supervisor and professor II Zhilin Yang for his encouragement during this semester. A special thanks goes to post doctor Nicolas La Forgia for advise and support. Thanks also to Mariana Diaz who helped us with the capacitance sensors and the cameras. We would also like to thank Martin Bustadmo who did indispensable work for us in the laboratory. Thanks also goes to Stein Kristian Skånøy who assisted when there were problems with the software. We want to thank Trygve Wangensteen for his Matlab-files, which inspired and helped us to develop our own. Last, but not at least, a big thank to PhD-candidate Cleide Vieira for her help during this work.

11.06.2017

Magnus Kallager and Marit Vassmyr

Abstract

This work has been dedicated to gain knowledge about two-phase flow in an inclined pipe through experimental investigation and adaption of theoretical framework from relevant literature. Two-phase flow experiments with viscous oil and air were carried out in a 6 m long, 60 mm ID pipe with inclination angles ranging from 10° to 78°. The oil density and viscosity was 836 kg/m^3 and 0.025 $Pa\,s$, respectively. The superficial oil velocities were in the interval 0.017 m/s - 1.34 m/s, while superficial air velocities ranged from 0.028 m/s - 10.78 m/s. The observed flow patterns comprised stratified wavy from $10° - 20°$ angle, cap bubble flow from $10° - 60°$ angle, elongated bubble flow from inclinations 10°-30°, severe slug flow from $45° - 78°$ angle, churn flow at inclinations 70° and 78°, while slug and annular flow were observed for the entire range of inclinations. Flow regime maps were made for all pipe inclinations.

An important purpose of the investigation was to validate a unified model from the literature and it was observed that the flow regime predictions from the unified model was in good agreement with the measurements. Overall, the bubble-slug flow transition at inclination $45° - 78°$ was highly equivalent with measurements. The transition to stratified flow was predicted at lower oil flow rates compared to the measurements, although the maximal inclination angle for stratified flow regime agreed quite well. The objective was also validating measurements with simulations in OLGA. The results showed that flow regime simulations in OLGA were not in sufficient agreement with the measurements. OLGA predicted stratified flow for inclination angles up to 45°, and annular flow transition was achieved at significantly higher gas flow rates than the measurements. One reason could be the different classification of the flow regimes. The capacitance sensor were used to classify flow regimes and calculate liquid holdup and pressure drop. It was found that the accuracy of liquid holdup correlations can be improved by considering each flow pattern.

Pressure drop measurements showed that two-phase oil-air flow gave lower total pressure drop compared to single phase flow for inclinations. This was more significant for low liquid flow rates and higher inclination angles. The total pressure loss reached a minimum point for lower gas flow rates and an increase in gas flow rates resulted in larger pressure drop for all inclinations. In this area, the frictional losses became more dominant. Small gas and liquid flow rates gave positive frictional pressure gradients. OLGA simulations showed the same trends as the experiments. Although the experiments and OLGA were in good agreement at low flow rates, the deviation in frictional pressure gradient was significant for medium and high gas flow rates. This resulted in deviation in the total pressure gradient. One reason could be simplifications of the experimental results, where averaged values were used.

Sammendrag

Dette arbeidet er dedikert til økt kunnskap om tofasestrømning i et oppoverhellende rør gjennom eksperimentelle undersøkelser og tilpasning av teoretisk grunnlag. Tofasestrømning med luft og viskøs olje ble eksperimentelt undersøkt i et 6 m langt, 60 mm ID rør med helningsvinkel fra 10° til 78°. Densiteten og viskositeten til oljen var henholdsvis 836 kg/m^3 og 0.025 $Pa\,s$. De overfladiske hastighetene for olje og luft var henholdsvis i intervallene 0.017 m/s- 1.34 m/s og 0.028 m/s- 10.78 m/s. De observerte strømningsregimene var lagdelt bølgestrømning for vinkler mellom $10° - 20°$, boblestrøm for vinkler mellom $10° - 60°$, ustabil slugstrømning for helning $45° - 78°$, churn for vinkler 70° og 78°, mens slug-og annulær strømning var observert for alle vinkler. Det ble utviklet strømningskart for alle vinklene.

Formålet var å undersøke hvorvidt en teoretisk uniform modell forutså strømningsregimer tilstrekkelig i forhold til eksperimentelle funn. Det ble avekket at modellen fastslo dette fordelaktig, spesielt i overgangen boble-slugstrømning for vinkler mellom $45° - 78°$. Modellen forutså samme maksimale vinkelhelning for lagdelt strømning. Det aktuelle strømningsregimet ble forutsett for lavere strømningsrate av olje sammenlignet med målinger. Systemet ble også simulert i OLGA. Strømningskart i OLGA stemte ikke tilstrekkelig med eksperimentelle resultater. Resultater viste at OLGA forutså lagdelt strømning opp til 45 °. Vesentlig høyere strømningsrate av luft ble beregnet for annulær strømning sammenlignet med målinger. Årsaken til dette kan være ulik klassifisering av strømningsregimer. En kapasitans sensor ble brukt til å klassifisere strømningsregimer og videre i kalkulasjoner av væskefraksjoner og trykkfall. Resultater viste at væskefraksjon-korrelasjoner bør være tilpasset strømningsregimet. Dette bør undersøkes i videre arbeider.

Resultater fra trykkmålinger viste at tofase olje-luft strømning ga et lavere trykktap enn ved enfase strømning for rør med helning. Det ble funnet et minimumpunkt for totalt trykktap for lave gass rater der videre økning av luftstrømning resulterte i ytterligere økt trykktap. Ved høye luftstrømninger var friksjonstapene dominante. Fordelen med luftinjeksjon var størst for lave oljestrømmer og høye vinkelhelninger. Simuleringer i OLGA ga samme resultat ved samme betraktninger. En observasjon var at friksjonsgradienten ble positiv når olje-og luftstrømningsratene var lave. Selv om sammenfallende trender ble observert mellom eksperimenter og OLGA, var de faktiske friksjonstapverdiene avvikende. Dette førte også til avvik i det totale trykktapet. Avvikene var størst ved høye luftstrømningsrater. Årsaker kan være ulik bestemmelse av strømningsregimer, eller forenklinger ved analyse av eksperimentelle resultater der gjennomsnittsverdier ble anvendt. Dette bør undersøkes i videre arbeid.

Contents

List of Tables

List of Figures

Nomenclature

Roman Symbols

A	Cross section area, $[m^2]$
C_L	Lift coefficient, $[-]$
D	Pipe diameter, $[m]$
d	Bubble diameter, $[m]$
f	Friction, $[-]$
Fr	Froude number, $[-]$
g	Gravity, $[\frac{m}{s^2}]$
h	Liquid level, $[m]$
L	Length, $[m]$
P	Pressure, $[Pa]$
Pe	Wettet perimeter, $[m]$
Q	Volume flow rate, $[\frac{m^3}{s}]$
r	Pipe radius, $[m]$
Re	Reynolds number, $[-]$
R_{sm}	Minimal liquid holdup, $[-]$
S	Interface, $[m]$
U	Velocity, $[\frac{m}{s}]$
x	Horizontal length, $[m]$
X	Lockhart Martinelli parameter, $[-]$
y	Vertical length, $[m]$
Y	Lockhart Martinelli parameter, $[-]$

Greek Symbols

α Volume fraction, $[-]$

γ Distortion coefficient, $[-]$

δ Film thickness, $[m]$

ϵ Roughness, $[m]$

θ Angle, $[^\circ]$

μ Dynamic viscosity, $[\frac{kg}{sm}]$

ν Kinematic viscosity, $[\frac{kg}{sm}]$

ρ Density, $[\frac{kg}{m^3}]$

σ Surface tension, $[\frac{N}{m}]$

τ Shear stress, $[Pa]$

Subscripts

$()_{CAP}$ Capacitance

$()_c$ Critical

$()_e$ Entry

$()_G$ Gas phase

$()_{GL}$ Interface gas and liquid phase

$()_{GW}$ Interface gas and pipe wall

$()_h$ Hydraulic

$()_i$ Phase

$()_L$ Liquid phase

$()_{LW}$ Interface liquid and pipe wall

$()_M$ Mixture

$()_{new}$ New

$()_o$ Bubble rise

$()_S$ Superficial

$()_{SL}$ Interface length

$()_{slip}$ Slip

$()_{noslip}$ No-slip condition

Chapter 1

Introduction

The demand of comprehension of multiphase transport of oil and gas is increasing, and technical solutions for handling and controlling its behavior are required. While most of the available experimental data on viscous fluids in long multiphase pipelines concerns horizontal and vertical pipes, the amount of information on inclined pipelines is scarce. Multiphase flow in inclined pipes occurs during production and transportation of petroleum related fluids. The aim of the thesis is to investigates two-phase flow with viscous fluids in a pipeline with inclination angles from 10° to 78°.

Several models for flow pattern predictions are available in the literature and most of them state that flow patterns in horizontal and vertical pipes can be predicted sufficiently by solving the momentum equations for two-phase flow, (Zhang et al. (2003)). Taitel et al. (1980) modelled flow regime patterns for upward gas-liquid flow in vertical tubes, while Taitel and Dukler (1976) presented a theoretical model for predicting flow regimes in horizontal and near horizontal gas-liquid flow. Nevertheless, a unified model for all inclination angles which could predict two-phase flow behaviour was required. A unified model should include correlations and equations for different flow patterns, inclination angles, liquid hold up, flow rates and other parameters, (Gokcal et al. (2008)). Thus, a unified model regarding flow pattern predictions for the entire range of pipe inclinations was proposed by Barnea (1987) and more recently Zhang et al. (2003) presented a unified model which predicted flow pattern, pressure gradient, liquid holdup and slug characteristic.

This thesis will investigate the existing model Barnea (1987) experimentally. The multiphase laboratory at NTNU was used and the findings are compared with the model. This will include assessment of flow regimes and liquid holdup. In addition, the experimental results on flow regime determination, liquid holdup and pressure drop will be compared to results obtained in OLGA. The thesis will cover the fundamental theory and literature behind single-and two-phase flow in pipelines which is applied in the unified model and OLGA.

1.1 Objectives

The thesis investigates flow regimes and the transition between them, pressure and liquid holdup in two-phase flow for different inclination angles. The research approach is mainly experimental, however, numerical calculations and simulations were applied to accommodate the experimental results. Moreover, the tasks accomplished are:

- Careful preparation of the experimental facility, which includes test section design, improvements and calibration of the existing instrumentation, in addition to fluids selection.
- Performance of experiments with viscous two-phase flow in a test section pipe with inclination ranging from 10° to 78°.
- Collection of experimental data from the literature in addition to models with information on flow pattern, liquid holdup and pressure drop for horizontal, inclined and vertical pipes. Extraction of useful information and implementing into numerical calculations in order to compare with experimental results.
- Numerical simulations in a dynamic multiphase flow simulator, OLGA. Comparison of simulations flow regime predictions, pressure drop and liquid holdup measurements in OLGA with experimental data achieved.

1.2 Scope and limitations

The scope only includes gas-liquid two phase flow with air and oil as working fluids and the highest inclination angle possible is equal 78°. Due to security issues, the test section was allowed to be increased with 5° angle intervals for angles $10° - 30°$, 15° intervals for angles $30° - 60°$, 10° interval from 60° to 70° and lastly 8° interval from 70° to 78°.

1.3 Structure of the thesis

The thesis contains six chapters in total where the first chapter is an introduction. A literature review will be presented in chapter two and this chapter will provide the necessary information and explanation of concepts and parameters that will be used and investigated in the study. The literature review will also contain a presentation of the unified model for two-phase flow and present the OLGA model. Further, chapter three contains a presentation of the experimental facility with instruments used for the investigation. The experimental results are presented in chapter four. Chapter five includes comparison with

the model encountered in chapter two in addition to OLGA simulations. The conclusion is summarized in chapter six along with recommendations for further work.

Chapter 2

Literature review

2.1 Fluid properties

The experimental and modelling methods of two-phase flow requires knowledge about the properties of the fluids which depends on pressure and temperature. In particular, the liquid viscosity is an important property that should be known. Maurice Marie Alfred Couette used the Couette flow geometry to measure viscosity, (Piau et al. (1994)). It is common to present the shear stress based on this description of Couette‘s two-dimensional shear. The geometry involves two large, parallel flat surfaces where one is stationary while the other moves with a constant velocity. The shear stress that occurs in a fluid placed between the plates can then be measured. Hence, the viscosity is the ratio of the tangential wall stress to the shear rate. Fluids that have a constant viscosity over a wide range of shear rates are considered as Newtonian fluids. Thus, there is a linear relationship between the shear stress and shear rate. The experimental fluid selection in chapter 3.1.1 is based on Equation 2.1.

$$\tau = \mu \frac{\partial U}{\partial y}, \tag{2.1}$$

where μ is the fluid viscosity, τ is the shear stress and $\frac{\partial U}{\partial y}$ is the share rate.

2.2 Two phase gas-liquid flow

Multiphase flow is characterized by the flow of multiple phases across surfaces and elsewhere in nature. The phenomena can be imposed naturally as well as in industrial processing. As an example of its application areas, better understanding of the interaction between air and water in weather situations could result in more accurate forecasts. Having that said, the complex nature of multiphase flow makes it demanding and mastering it

requires knowledge in several fields including fluid mechanics, thermodynamics, mechanical engineering, chemical engineering, discrete mathematics, automation and computer science. Numerical methods are necessary for solving the hyperbolic equations related to the conservation equations, (Zhang et al. (2003)). Similarly, it is important to understand how chemical properties of the fluids change with different scenarios in order to achieve reliable models.

Overall, the prediction of the flow pattern in gas-liquid flow is highly important, (Barnea (1986)). For that reason, the knowledge at which flow rate combination the different flow pattern transitions occur, is crucial. The flow pattern can consequently be applied as a necessary input when calculating the flow variables such as pressure drop and liquid holdup which will be further discussed.

2.2.1 Flow regimes and flow pattern maps

A flow regime is a representation of how the phases and fluids interact with each other. The flow pattern prediction is inevitable in several industries that operates with multiphase flow. As an example, different combinations of oil, water and gas will occur in wells in the petroleum industry, (Beggs et al. (1973)). The combination depends on conditions such as temperature, pressure, pipe geometry and mass fractions. Furthermore, can inhibitors, geology and terrain influences affect the flow.

The flow regime will categorize the flow into either separated flow, bubble flow or slug flow and the different flow regimes will occur due to different compositions of gas and liquid as well as the change in their velocities, (Bratland (2010)). A flow regime map is usually used to illustrate the flow regimes whereas several researchers have tried to generalize these flow regime maps with non-dimensional variables, but a perfect unified method does not exist yet. However, it is quite common to present the map with the superficial velocities at the axis. The superficial velocity, expressed in Equation 2.2, can be described as the velocity a phase would have, if it was the only phase to flow in the pipe.

$$U_{Si} = \alpha_i U_i = \frac{Q_i}{A}, \tag{2.2}$$

where i represent G or L for gas or liquid phase, respectively, α is the volume fraction, Q is the volume flow rate and A is the cross section area of the pipe.

As mentioned in the introduction, the thesis will investigate the flow regimes for different pipe angles and flow conditions. In order to do so, it is important to understand the more relevant cases. Both horizontal and vertical pipelines will be reviewed first followed by inclined flow regimes which are similar and based on those. An usual approach in determining flow regime pattern is by observing the flow visually in a transparent pipe and

note the different flow regime for a set of flow rates. This approach makes the definition of the different flow regimes possible to plot in a flow regime map. The approach is however subjective and can vary in reliability, (Barnea et al. (1980a)). Therefore, it is not always scientifically reliable and adaptable although a great amount of investigation have been done in the last decades.

It is useful to theoretically investigate the flow regime transition and for which there are different dedicated computational programs. This will be studied later in the thesis.

Horizontal flow regimes

The general flow regimes for two-phase gas-liquid flow in horizontal pipelines have been characterized by many researches. A recent description can be found in Bratland (2010) and Shoham (2005), and Figure 2.1 illustrates common horizontal flow regimes. Further, the related flow regime map is illustrated in Figure 2.2. In cases where the flow is within the boundaries of two or three flow regimes, the uncertainties are significant.

The following section is based on theory in Bratland (2010). Stratified flow is recognized when the gas and liquid flows separately in a pipe with a defined surface interface. If the flow rates of the phases are sufficiently low, the liquid phase will flow at the bottom due to its higher density, as illustrated in Figure 2.1. However, as the gas velocity increases, the interface becomes more wavy and unstable. This flow regime is called stratified wavy. A further increase in the gas velocity will form larger waves that eventually reach the top of the pipe and thereby block the flow. This blockage will capture the air in a pocket until the pressure is build up such that it manage to escape. Consequently, the air will blow out as a bullet-shaped bubble, named Taylor bubble. This bullet-shaped Taylor bubble with alternately liquid flow, is recognized, as slug flow. The alternately liquid flows at high velocity at the upper part of the pipe cross section area, while a continuous liquid phase flows at the bottom. Slug flow is transient and inconvenient due to the pressure becoming discontinuous. Discontinuous pressure could lead to gas/liquid entering a processing facility unevenly, which can cause reservoirs to flood. Another type of transient flow, where the bubbles are shorter compared to the bubbles in slug flow, is called elongated bubble flow.

As the gas increase even further, the high velocity of gas will force the liquid phase to creep up on the periphery of the pipe, due to capillary effect, while the gas phase flows in the core in-between the liquid film. When the liquid phase covers the whole circumference of the pipe, separating the pipe wall from the gas core, the flow is characterized as annular flow. Even though the phases are separated, liquid droplets can entrain from the liquid film due to drag forces from the fast moving gas phase. Droplets of the right sizes can accelerate up to the gas velocity and make a dispersed droplet phase in the gas phase. However, the droplets can deposit back into the liquid film, when the droplets becomes

too large. This is classified as annular flow. Lastly, dispersed bubble flow regime can occur in cases where there is small amounts of gas compared to liquid. The liquid flow rate is dominate, such that it creates sufficient turbulence and the gas is adequately mixed into the liquid.

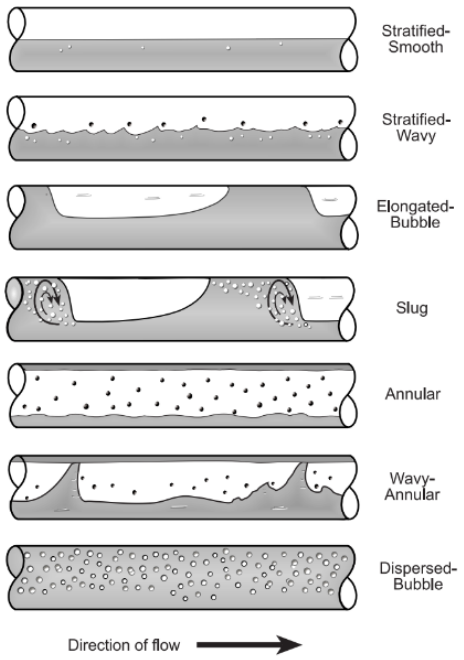

Figure 2.1: Horizontal flow regimes, (Shoham (2005)).

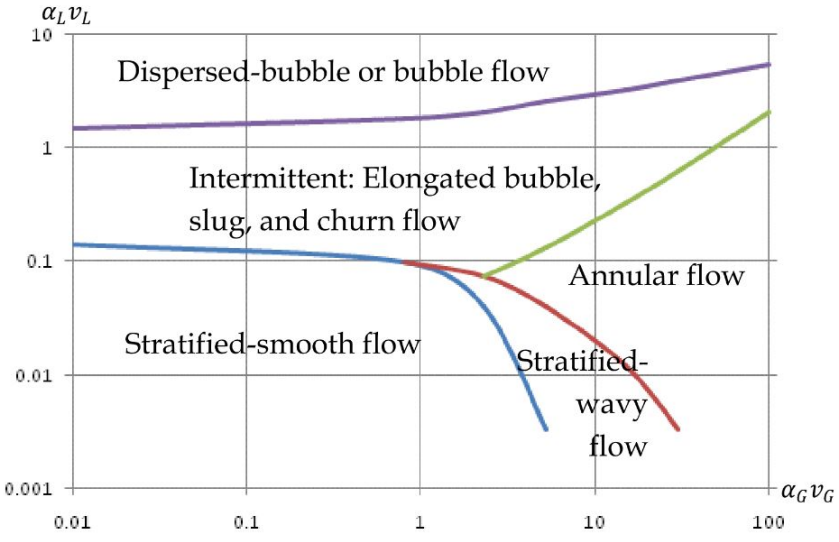

Figure 2.2: Typical flow regime map for horizontal flow, (Bratland (2010)).

Horizontal flow regime determination can be done by using existing correlations. Beggs and Brill (1973) provided a model based on air-water experiments for the whole range of inclination angles between ±90 °. Their model applies the horizontal liquid holdup

with correlations to predict the flow regime. They found that the flow regime could be determined based on two criteria, namely the Froude number of the mixture and the no-slip liquid fractions, which is presented in Equation 2.3 and 2.4.

$$Fr_M = \frac{\alpha_G U_G + \alpha_L U_L}{\sqrt{g}D}, \tag{2.3}$$

$$\alpha_{Lnoslip} = \frac{\alpha_L U_L}{\alpha_G U_G + \alpha_L U_L}, \tag{2.4}$$

where Fr_M is the mixed Froude number and $\alpha_{Lnoslip}$ is the no-slip liquid fraction. Further, α_G is the gas volume fraction, α_L is the liquid volume fraction, U_G and U_L are the velocities of the gas and liquid, respectively, g denotes gravity and D is the diameter of the pipe. For horizontal flow, they state that it is possible to determine the flow patterns from 4 critical Froude numbers. By using these definitions together with Equation 2.3 and 2.4, they concluded that the flow patterns could be determined as segregated, transition, intermittent or distributed. For that reason, their model is simple, but unfortunately uncertain, particularly for uphill flows. No flow pattern maps were reported, although data were taken from the whole range of pipe inclination.

Later, Taitel and Dukler (1976) developed a model for horizontal pipelines, as well as nearly horizontal pipes; the model is valid for ± 10 °. This is based on a more physical understanding of the transition where the transition from stratified flow is determined by a stability analysis, taking the Bernoulli effect of the flow into account. If the gas velocity is below this proposed instability criteria, as expressed in Equation 2.5, the flow is considered stratified. Otherwise, the flow would either be intermittent, dispersed or annular. Furthermore, an intermittent-slug transition could be determined by the liquid height of the flow. Annular flow would be the case if the liquid height fall below a certain value.

$$U_G \geq (1 - \frac{h_L}{D})\sqrt{\frac{(\rho_L - \rho_G) g \cos\theta A_G}{\rho_G S_{SL}}}, \tag{2.5}$$

where U_G is the gas velocity, h_L is the liquid level, D is the inner pipe diameter, ρ_G and ρ_L is the gas and liquid densities, respectively, g is gravity acceleration, θ is the pipe inclination from the horizontal, A_G is the area occupied by gas and S_{SL} is the interface length.

Vertical flow regimes

This section is mainly based on theory from Bratland (2010) as well. Two-phase vertical flow are considered more chaotic than horizontal flow. The main difference between

horizontal and vertical pipe flow is the absence of stratified flow regime in a vertical pipe. Stratified flow is impossible in vertical pipes due to the impossibility of liquid nor gas phase to flow in the lower part of the pipe. However, low flow rates in vertical pipes will provide a bubbly flow of which buoyancy is the driving force. The flow regime map proposed for vertical flow is illustrated in Figure 2.4.

In addition to slug flow, dispersed bubble flow and annular flow, churn flow is a usual flow regime in vertical pipe flow. Churn flow is more chaotic compared to slug flow, and the difference can be seen in Figure 2.3. In churn flow, the interface between gas and liquid is not well defined and the Taylor bubbles are short and narrow, Bratland (2010). Shoham (2006) suggests that the flow is always churn at the pipe inlet for vertical flow. Barnea et al. (1980b) explains this by the liquid slug alternating between rising and falling, incapable of creating a stable bridge separating the Taylor bubbles. This entry region is described in Shoham (2005) as Equation 2.6.

$$\frac{L_e}{D} = 40.6(\frac{U_M}{\sqrt{gD}} + 0.22), \tag{2.6}$$

where L_e is the entry length, D is the pipe diameter and U_M is the mixture velocity. The Taylor bubbles almost cover the whole pipe diameter in vertical pipes. Only a small back flowing liquid film circumference the bubble and separates it from the pipe wall. The liquid slug creates a stable support to the air slugs keeping the Taylor bubbles flowing consequently at the same speed. Larger bubbles, but not large enough to occupy the whole cross-section, are also characterized as bubble flow, (Bratland (2010)). Bubble flow occurs when the agglomeration or coalescence of the discrete gas bubbles are kept below a certain level. The bubble flow regime also has an upper limit when the liquid flow rate is increased and the flow behaves more turbulent, it starts to break up larger bubbles and prevent coalescence. The bubbles will flow as small discrete bubbles in the continuous liquid flow, and create the dispersed bubble flow regime. The turbulent forces due to high liquid flow rate causes larger bubble to break down while the small spherical resist further break down. Annular flow is the flow regime that occurs in vertical pipes at which the gas phase is dominant. Hence, the gas phase tends to flow in the core of the pipe and the liquid flows in a film separating the gas core and the pipe. Due to the relatively fast flowing gas phase, the liquid film experience a drag making the gas-liquid interface wavy. The drag also cause droplet entrainment from the liquid film to the gas core and can form annular flow with droplets as in Figure 2.3 illustrates.

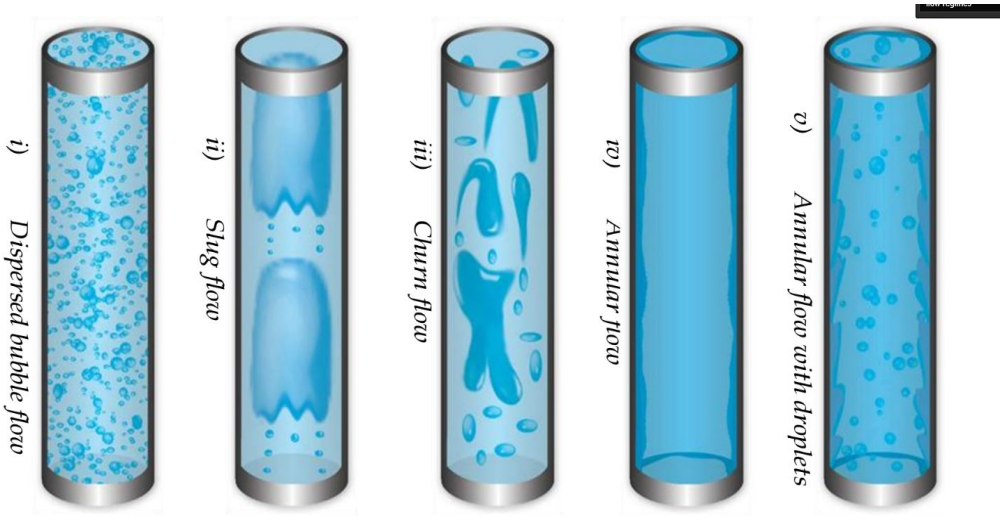

Figure 2.3: Vertical flow regimes, (Bratland (2010)).

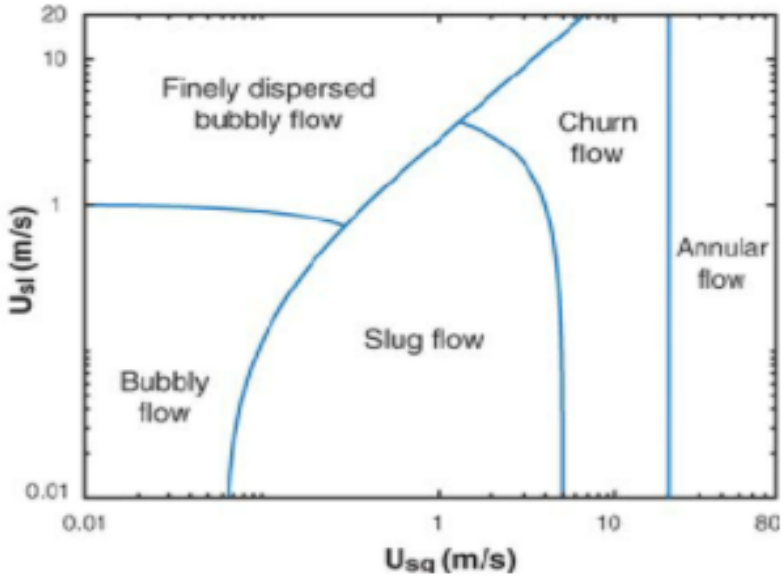

Figure 2.4: Typical flow regime map for vertical flow, (Taitel et al. (1980)).

Flow regimes in inclined pipelines

As the oil and gas industry is moving towards production from non-conventional reservoir and challenging locations, the effect of large inclination changes on the pipeline is important to understand. However, there is a lack of knowledge regarding stronger pipe inclinations and the verification of slugs generated in this region, (Zhang et al. (2003)). The natural elevations in the terrain in addition to the shape of the riser contributes to an inclination in the pipeline. Gravity can work with or against the flow for downhill or uphill geometries, respectively. A slug flow, called severe slugging, can occur in this

situations. This can form a local elevation minimum, due to the liquids tendency to accumulate in the bottom section and thereby block the air flow. Slugs are then created when the air pressure manage to escape around the elbow. The severe slug flow condition could be several kilometers long, and the elevation does not have to be significantly steep to create the slugs. Nevertheless, it could cause several operational difficulties, (Bratland (2010)).

Authors have done investigations on the flow regimes in inclined pipelines throughout time. Kosterin (1949) was one of the first to do a general observation regarding the flow regime with change in pipe diameter and inclination. He found that the effect of inclination was greatest at low liquid rates. Many years later, Beggs et al. (1973) presented the effect of full range $\pm 90°$ pipe inclination with focus on liquid holdup and pressure loss. They conducted an experimental study and correspondingly developed correlations for liquid holdup and friction factor for predicting pressure gradients. It was discovered that holdup had a significant dependency on angle due to the effects of gravity and viscosity. As the angle of the pipe increased from horizontal, gravity forces acting on the liquid caused a decrease in velocity and thus increasing liquid holdup. At last, the liquid holdup was normalized by dividing the holdup at any angle by the holdup at $0°$ and a liquid holdup could be predicted for all flow rates at angles $\pm 90°$. Values for the friction factor were normalized by dividing it by a no-slip friction factor obtained from Moody diagram for smooth pipe.

Experiments by Mukherjee (1979) showed that angle of inclination had no appreciable effect on the slug to annular-mist transition. Barnea et al. (1980b), did a comparison of experimental data with theory for flow pattern transition for horizontal and inclined pipes. In this case it was found that the greatest effect on the flow pattern is in the transition between stratified and intermittent or annular flow regimes. Upward inclination resulted in intermittent flow regimes over a larger range of flow conditions. In addition, stratified smooth flow was not observed for upward inclinations larger than $0.25°$. Spedding et al. (1982) conducted experiments which covered pressure drop for the same range of inclination. They found that an annular flow regime was observed for total velocity between $10 - 30m/s$, while for the range less than $10m/s$, there was a maximum in the total pressure loss at an angle between $60°$ and $70°$. Over all, it was seen that for upward vertical flow the higher total pressure loss was recorded for the lowest total flow rate, while a minimum pressure loss was achieved at total flow velocity of about $15m/s$.

Barnea (1987) presented a unified model based on previous works by Taitel and Dukler (1976), Taitel et al. (1980) and Barnea et al. (1985) which was applicable for all inclination angles, and incorporated the effect of fluid properties and pipe size. The model has been a standard for experimental comparison and development of other, more recent models. Kokal and Stanislav (1989) made a comprehensive study on light oil-air flow in a slightly inclined pipe. They found that the transition between stratified flow and intermittent flow

regime was highly sensible to the inclination angle, which is the same as Kosterin (1949) discovered. The intermittent to annular and intermittent to dispersed flow transition was nearly independent of the inclination. Kokal and Stanislav (1989) conducted experiments in inclination angles of $\pm 9^\circ$ for two phase oil and air flow in a pipe. They found that the pressure gradient was much higher at greater inclination angles due to the additional static pressure drop in inclined pipes. The increase in pressure gradient was also explained by the intermittent flow regime, which is associated with higher pressure drop. However, for high gas and liquid flow rates, the pressure drop became nearly independent of the inclination angle.

Another unified model was presented by Zhang et al. (2003), which was indeed based on the Barnea (1987) model. Zhang et al. (2003) covers all inclination angles which are based on slug dynamics. As Barnea et al. (1980b) had no appearance of stratified smooth flow above 0.25°, a more unstable wavy stratified flow was observed for angles up to 20° according to Shoham (2005). He made a comprehensive study earlier, which is explained in his book, of two-phase air-water flow for the whole range of inclinations from -90°and +90°. Over all, he conducted experiments for both 2.54 and 5.1 cm ID pipes, where the bubble flow was only observed in the 5.1 cm pipe. He observed that the bubble flow regime area decreased when the inclination angle from horizontal increased and finally disappeared between $50^\circ - 70^\circ$ inclination. The same was observed for the churn flow, which is associated with vertical flow. Churn flow was not observed for inclination angles of 70°or below. Also, he observed that the transition to dispersed bubble flow and annular flow was quite sensitive to change in inclination angle. The annular-intermittent transition moved slightly to the right, appearing at higher superficial gas velocity for steeper inclination.

Lately, Jeyanchandra (2011) confirmed the observations that Kokal and Stanislav (1989) achieved, and he explained that the frictional components became the dominating forces for high flow rates. He also showed that the total pressure gradient varied with gas and liquid flow rates, inclination angle and viscosity.

2.2.2 Liquid holdup

Liquid holdup is an important parameter that must be predicted in order to calculate the pressure gradient. It is a crucial parameter when calculating the elevation, frictional and acceleration components of the total pressure drop. More important, it is dependent on the flow pattern, which illustrates how important the prediction of the flow pattern is as well. While flow patterns and transition boundaries are obtained through visual observations, the liquid holdup is generally predicted through empirical or semi-empirical correlations derived from experimental data, (Chen and Spedding (1983)).

The liquid hold up is expressed in Equation 2.7 and represents the more dense phase,

which is moving slowly compared to the lighter phase. The liquid and gas area is denoted A_L and A_G, respectively, while the total cross section area is A.

$$\alpha_L = \frac{A_L}{A}. \tag{2.7}$$

In contrast, the fraction of the gas phase in a two-phase flow is called gas holdup, or more commonly referred to as the void fraction. This is the area of the pipe that is not occupied by liquid, and is consequently given as in Equation 2.8. The liquid holdup can be calculated directly as $\alpha_L = 1 - \alpha_G$.

$$\alpha_G = \frac{A_G}{A}. \tag{2.8}$$

No-slip holdup is the volumetric flow rate of the liquid in a two-phase flow if there is no slip between the two phases.

In the literature several correlations for liquid holdup can be found for horizontal and vertical flow, however few correlations are found for inclined pipelines. Chen and Spedding (1983) did an investigation to cover a wider range of application than holdup equations for the cases of ideal stratified and ideal annular horizontal flow. The purpose of the work was to review and extend the application of the correlation technique for horizontal flow and expand its application to the case of inclined flow. They found correlations for bubble-slug flow and annular flow. Barnea et al. (1980a) proposed a conductivity probe technique for horizontal, near horizontal and upward flows. The experiments were conducted using air and water and a aim was to clearly detect all flow patterns using a set of probe system to see the significantly different electrical conductivity of air and water.

An expression for liquid holdup can be found for a horizontal stratified flow using the wetted perimeter, Pe, the pipe radius, r, the liquid level, h, and the angle, θ, which is defined as in Figure 2.5, and given in Equation 2.12, based on Equations 2.9-2.11.

$$\theta = \frac{Pe}{r}. \tag{2.9}$$

$$h = rcos\Big(\frac{\theta}{2}\Big). \tag{2.10}$$

$$A_G = \Big(\pi - \frac{\theta}{2}\Big)r^2 + hrsin\Big(\frac{\theta}{2}\Big). \tag{2.11}$$

$$\alpha_L = 1 - \frac{A_G}{A}. \tag{2.12}$$

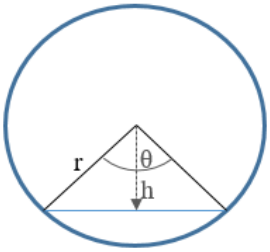

Figure 2.5: Geometrical properties of stratified, horizontal two-phase flow.

2.2.3 Pressure drop

Determination of two-phase flow pressure drop is based on the same concepts as in single phase flow. For that reason, the equations for pressure drop in single phase flow will firstly be presented as a prerequisite. In any case, the pressure drop is dependent on fluid properties, such as density and viscosity and flow parameters including the velocity and friction factor.

Pressure drop in single phase flow

Single phase pressure drop in circular pipes is mainly affected by three factors, namely acceleration, gravity and friction. The steady state momentum conservation equation in x-direction yields;

$$\frac{dP}{dx} = \rho g \sin\theta + f\frac{\rho U^2}{2D}, \tag{2.13}$$

where the terms represented are gravitational pressure drop $\rho g \sin\theta$, and the frictional pressure drop $f\frac{\rho U^2}{2D}$. For the frictional pressure drop, f represents the Darcy friction factor.

The frictional losses in single phase flow have been investigated thoroughly over the years with the aim of finding an universal relationship between the pressure drop and the flow conditions. Flow conditions might include fluid properties, the inertia of the flow, pipe roughness and more. For laminar flow, the velocity profile and friction factor is analytically obtainable and found to be inversely dependent on the Reynolds number. Laminar flow occur at Reynolds number lower than 2300 and is independent of the surface roughness. It means that the friction factor for laminar flow will be equal for smooth and rough surfaces. The Darcy friction factor for laminar flow yields;

$$f = \frac{64}{Re}, \tag{2.14}$$

where the Reynold number is defined as

$$Re = \frac{UD}{\nu}, \tag{2.15}$$

with U as velocity, D as pipe diameter and ν as kinematic viscosity.

More complications arises regarding the mechanisms behind turbulent flow. A flow in a circular pipe is assumed to be turbulent if the Reynolds number exceed 4000. Von Karman describes the velocity profile of turbulent flow as highly fluctuating, where collisions between the fluid particles in addition to viscous shear stresses makes the profile complex, (Bratland (2009)). However, averaging the fluctuations is sufficiently accurate for engineering purposes. Two of the most common equations are the Blasius friction factor, expressed in Equation 2.16, and the Colebrook, Equation 2.17.

$$f = \frac{0.3156}{Re^{0.25}} \tag{2.16}$$

$$\frac{1}{\sqrt{f}} = -2log(\frac{\epsilon/D}{3.7} + \frac{2.57}{Re\sqrt{f}}), \tag{2.17}$$

where ϵ is the roughness.

An approximation of Colebrook equation is Haaland equation, which is given by

$$\frac{1}{\sqrt{f}} = -1.8log\Big[\Big(\frac{\epsilon/D}{3.7}\Big)^{1.11} + \frac{6.9}{Re}\Big]. \tag{2.18}$$

Pressure drop in two-phase flow

Correlations for predicting the pressure drop in two-phase flow have been successfully conducted in horizontal and vertical pipes, but these correlations have not been correct when applied to inclined pipes, (Beggs et al. (1973)). Compared to single phase flow, the pressure drop in two-phase flow is more complex and difficult to predict. Mukherjee (1979) explains that forces like gravity and buoyancy in the individual phases make most of the flow regime heterogeneity. In bubble and slug flow, the slippage and the velocity difference between the phases may cause problems when evaluating the mixture velocity. As a consequence, the calculation of the frictional losses are complicated.

In a simplified stratified flow model, explained in Bratland (2010), the pressure gradient for the two phases can be expressed as Equation 2.19 for gas and Equation 2.20 for liquid. The equations, which are derived from momentum balance over a control volume, are assumed to be steady state, one dimensional in x-direction, incompressible and thermal changes are neglected.

$$\alpha_G \frac{\partial P}{\partial x} = -\tau_{GL} S_{GL} + \tau_{GW} S_G - \alpha_G \rho_G g \sin\theta, \tag{2.19}$$

$$\alpha_L \frac{\partial P}{\partial x} = \tau_{GL} S_{GL} + \tau_{LW} S_L - \alpha_L \rho_L g \sin\theta, \tag{2.20}$$

where τ is the shear stress, α_G and α_L are the volume fractions, ρ_G and ρ_L are the densities and g represents the gravity. The subscript $_{GL}$ is the liquid gas interface while $_{GW}$ and $_{LW}$ is the interface between each phase and the pipe wall. The momentum from gravity due to pipe inclination is given by $\alpha_G \rho_G g \sin\theta$ and $\alpha_L \rho_L g \sin\theta$ for each phase. S is the perimeter over which the stress act. Shear stresses and friction factors include the hydraulic diameter, which is defined in Bratland (2010) as

$$D_h = \frac{4A}{Pe}, \tag{2.21}$$

where the wetted perimeter of the cross-section is Pe and the cross-sectional area is A and will equal A_G for the gas section and similarly A_L for the liquid.

In annular flow, Bratland (2010) also explains that the force balance for steady flow provides the momentum conservation equation for the two phases as follows

$$\alpha_G \frac{\partial P}{\partial x} = -\tau_{GL} S_{GL} - \rho_G \alpha_G g \sin\theta, \tag{2.22}$$

for the gas core, and for the liquid film

$$\alpha_L \frac{\partial P}{\partial x} = -\tau_L S_L + \tau_{GL} S_{SL} - \rho_L \alpha_L g \sin\theta. \tag{2.23}$$

It is important to mention that the complexity of the equations will increase for compressible gas and flows with thermal changes or transient situations. For other flow regimes, for example slug or bubble flow, different equations must be derived.

The procedure for solving the flow models starts with assuming or guessing a flow regime. For a given flow regime, the corresponding conservation equations must be solved. Afterwards, the flow characteristics that occur must be checked against the criteria for the represented flow regime. These flow characteristics can be liquid fractions and gas velocities. If they do not meet the criteria, a new guess must be executed.

2.3 Modeling

One of the main objective in research of multiphase flow is to be able to assess models which can recreate the physics of the flow. In this thesis one of the most acknowledged model in the literature is used, accordingly the unified model of Barnea (1987). The following section will provide the theory behind the model. The model is also implemented

in Matlab with its criteria and equations for flow regime determination. This will provide flow regime transition boundaries which later will be compared to flow regime maps obtained by experimental investigation of two-phase flow in the multiphase lab at NTNU. The comparison can be used to validate the unified model flow regime determination at all inclination angles and liquid holdup criteria. This chapter will also explain the OLGA model, which additionally is used for comparison with experimental results.

2.3.1 Unified Model Barnea (1987)

The unified model, Barnea (1987), for flow regime prediction is a mechanistic model applicable for the whole range of inclination angles. It involves steady-state, two-phase gas-liquid flow and is based on work done by Taitel and Dukler (1976) who presented a model for predicting flow regime transitions in horizontal and slightly horizontal gas-liquid flow.

A unified model should be applicable to the entire range of inclination and the aim is smooth changes in flow pattern boundaries with continuous increase in pipe inclination. The unified model by Barnea (1987) satisfies this criteria although only upward inclination will be handled in the thesis. Flow rates, geometry, inclination angle and fluid properties are specified and transition criteria for each transition are applied. The procedure of flow-pattern determination is explained with information from Barnea (1987). The model begins with the transition from dispersed bubbles. It continues in a decision tree, to the stratifies-non stratified transition, where the transition boundaries are illustrated in Figure 2.8. Annular and intermittent flow-patterns are determined before criterion for slug-churn transition is applied.

The transition from dispersed bubbles

At high liquid flow rates, dispersed bubble flow occur over a whole range of pipe inclinations. Low liquid flow rates can form bubbly flow, nonetheless only in vertical and off-vertical pipes with large diameter. Thus, bubble flow can exist only when the following two criteria are met:

1. The Taylor bubble velocity exceeds the bubble velocity, which is satisfied for large diameter, D, (Taitel et al. (1980)):

$$D > 19\Big[\frac{(\rho_L - \rho_G)\sigma}{\rho_L^2 g}\Big]^{1/2}, \tag{2.24}$$

   where ρ_L and ρ_G are the liquid and gas densities, g is gravity and σ is the surface tension.

2. The angle of inclination, θ is large enough to avoid bubbles to move to the top of the pipe wall

$$\frac{\cos\theta}{\sin\theta} = \frac{3}{4}\cos 45 \frac{U_o^2}{g}\frac{C_L\gamma^2}{d}, \tag{2.25}$$

where d denote the bubble diameter, U_o denote the bubble rise velocity of relatively large bubbles and γ denote the distortion coefficient, which, based on observations, ranges from 1.1 to 1.5. The lift coefficient of the bubbles is C_L and the value suggested is 0.8 (Barnea (1987)). From sources in Barnea (1987), U_o is given by the relation:

$$U_o = 1.53\Big[\frac{g(\rho_L - \rho_G)\sigma}{\rho_L^2}\Big]^{1/4} \tag{2.26}$$

Taitel et al. (1980) initially found that the transition from bubbly to slug flow, for low liquid flow rates, occur when the gas void fraction exceeds a critical value of $\alpha_c = 0.25$. This value is later applied in the studies carried out by Barnea (1987) and Shoham (2005). When $\alpha_c = 0.25$, the transition is given by Equation 2.27.

$$U_{SL} = 3.0U_{SG} - 11.5\Big[\frac{g(\rho_L - \rho_G)\sigma}{\rho_L^2}\Big]^{1/2}\sin\theta, \tag{2.27}$$

where U_{SL} and U_{SG} are the superficial velocities.

The transition from dispersed bubble flow for upward vertical flow was first presented by Taitel et al. (1980) and revisited in Barnea (1986). The bubble diameter on the transition boundary is given as

$$d_c \geq \Big[0.725 + 4.15\Big(\frac{U_{SG}}{U_M}\Big)^{1/2}\Big]\Big(\frac{\sigma}{\rho_L}\Big)^{2/5}\Big(\frac{2f_M}{D}U_M^3\Big)^{-2/5}, \tag{2.28}$$

where U_M is the mixture velocity, $U_M = U_{SG} + U_{SL}$, and f_M is the friction factor based on the mixture velocity. According to Taitel et al. (1980), Barnea (1986) and Barnea (1987), the transition boundary is valid for gas void fractions $\alpha < 0.52$. At $\alpha = 0.52$ the coalescence to intermittent flow occurs because the bubbles reach the maximum volumetric packing density. The transition curve that describe this condition is given by Equation 2.29

$$U_{SL} = U_{SG}\frac{1-\alpha}{\alpha}, \tag{2.29}$$

The critical bubble size above d_c is the bubble size small enough to cause bubbles to remain spherical. The value of d_c is taken as the smallest between d_{CB} and d_{CD}, where d_{CD} is the critical bubble size above which the bubble is deformed,

$$d_{CD} = 2\Big[\frac{0.4\sigma}{(\rho_L - \rho_G)g}\Big]^{1/2}, \tag{2.30}$$

and d_{CB} is the critical bubble size below the point where migration of bubbles to the upper part of the pipe is prevented,

$$d_{CB} = \frac{3}{8}\Big[\frac{\rho_L}{\rho_L - \rho_G}\Big]\frac{f_M U_M^2}{g\cos\theta}, \tag{2.31}$$

where all parameters are as described above.

The Transition from Stratified to Non-stratified Flow

Taitel and Dukler (1976) illustrates the equilibrium stratified flow as shown in Figure 2.6. The equilibrium stratified flow momentum equations correspond to Equation 2.19 and 2.20 in section 2.2.3. The combined momentum equation, by substituting the pressure gradients from the two phases, results:

$$\tau_{GW}\frac{S_G}{\alpha_G} - \tau_{LW}\frac{S_L}{\alpha_L} + \tau_i S_i\Big(\frac{1}{\alpha_L} + \frac{1}{\alpha_G}\Big) + (\rho_L - \rho_G)g\sin\theta = 0. \tag{2.32}$$

The wall shear stresses are evaluated by

$$\tau_{LW} = f_L\frac{\rho_L U_L^2}{2}, \qquad \tau_{GW} = f_G\frac{\rho_G U_G^2}{2}, \qquad \tau_{GL} = f_{GL}\frac{\rho_G(U_G - U_{GL})^2}{2} \tag{2.33}$$

with the gas and liquid gas friction factors

$$f_L = C_L\Big(\frac{Dh_L U_L}{\nu_L}\Big)^{-n}, \qquad f_G = C_G\Big(\frac{Dh_G U_G}{\nu_G}\Big)^{-m}, \tag{2.34}$$

where Dh_L and Dh_G are the hydraulic diameters for liquid and gas, as explained in section 2.2.3, U_G and U_L are the gas and liquid velocities, A_G and A_L are the gas and liquid cross-sectional areas, C_L and C_G are liquid and gas coefficients, and ν is viscosity.

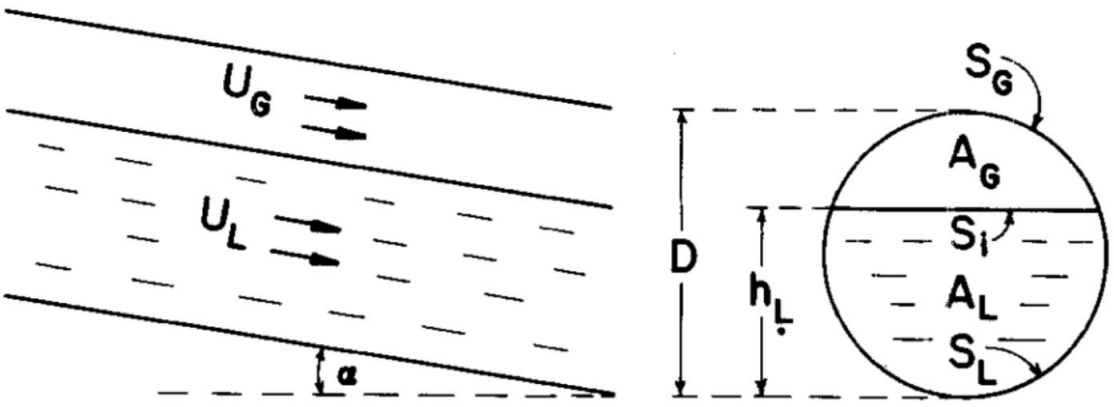

Figure 2.6: Equilibrium stratified flow, (Taitel and Dukler (1976)).

As the gas accelerates over a finite wave on the surface of the stratified flow, the pressure decreases due to Bernoulli effect. Pressure drop will make the waves grow. In contrast, gravity forces acting will cause the waves to decay. In order to suggest a criterion at which the wave will grow and the transition from stratified to non-stratified flow it is useful to transform the equations to dimensionless form. The dimensionless numbers are defined by

$$\tilde{h_L} = \frac{h_L}{D}, \qquad \tilde{A_L} = \frac{A_L}{D^2}, \qquad \tilde{A_G} = \frac{A_G}{D^2}, \qquad \tilde{U_L} = \frac{U_L}{U_{SL}} = \frac{A}{A_L}, \qquad \tilde{U_G} = \frac{U_G}{U_{SG}} = \frac{A}{A_G},$$

where h_L is the liquid level as illustrated to the right in Figure 2.6. All the dimensionless variables depend only on the equilibrium level, $\tilde{h_L}$.

From Taitel and Dukler (1976) it is stated that the criterion becomes

$$Fr^2 \left[\frac{1}{\left(1 - \tilde{h_L}^2\right)} \frac{\tilde{U_G}^2 \frac{d\tilde{A_L}}{d\tilde{h_L}}}{\tilde{A_G}} \right] \geq 1, \tag{2.35}$$

in dimensionless form, where the Froude number, Fr is evaluated as

$$Fr = \sqrt{\frac{\rho_G}{\rho_L - \rho_G}} \frac{U_{SG}}{\sqrt{Dg\cos\theta}} \tag{2.36}$$

In addition, the dimensionless momentum equation takes the form

$$X^2 \left[(\tilde{U_L} D\tilde{h}_L)^{-n} \tilde{U_L}^2 \frac{\tilde{S_L}}{\tilde{A_L}} \right] - \left[(U_G \tilde{D}\tilde{h}_G)^{-m} \tilde{U_G}^2 \left(\frac{\tilde{S_G}}{\tilde{A_G}} + \frac{\tilde{S_{GL}}}{\tilde{A_L}} + \frac{\tilde{S_{GL}}}{\tilde{A_G}} \right) \right] - 4Y = 0, \tag{2.37}$$

where

$$X^2 = \frac{\frac{4}{D} f_{SL} \frac{\rho_L U_{LS}^2}{2}}{\frac{4}{D} f_{SG} \frac{\rho_G U_{GS}^2}{2}} = \frac{\left(\frac{dp}{dx}\right)_{SL}}{\left(\frac{dp}{dx}\right)_{SG}} \tag{2.38}$$

and

$$Y = \frac{(\rho_L - \rho_G) g \sin\theta}{(\frac{dp}{dx})_{GS}}, \tag{2.39}$$

$(\frac{dp}{dx})_S$ denotes the pressure drop of one phase as if it was flowing alone in the pipe. This is the Lockhart-Martinelli correlation, (Lockhart and Martinelli (1949)). The equilibrium level is represented as a function of X for parameter values of Y. It is an important observation that small changes in inclination angle have a major effect on the transition between stratified to non-stratified boundary due to dependence of $sin\theta$ in Y. For turbulent liquid, and turbulent or laminar gas, it is illustrated as in Taitel and Dukler (1976),

in Figure 2.7. The predicted transition criteria can also be presented in a flow regime map with superficial velocities along the axis.

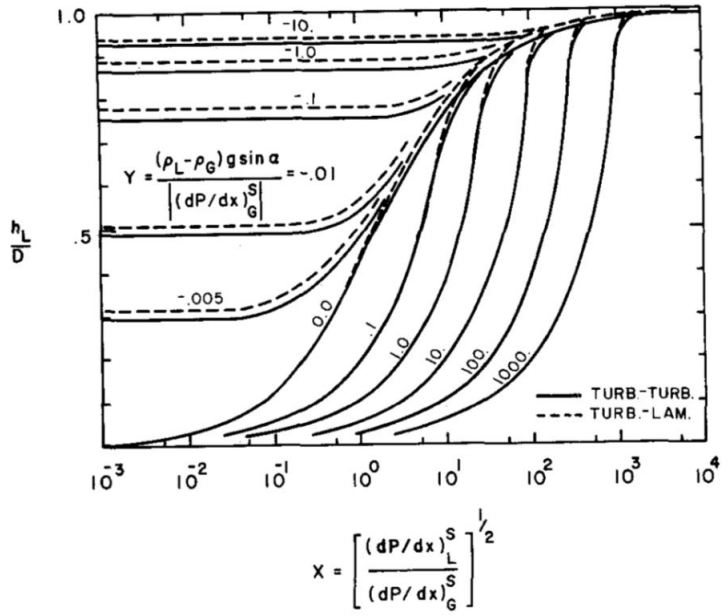

Figure 2.7: Equilibrium liquid level for stratified flow, (Taitel and Dukler (1976)).

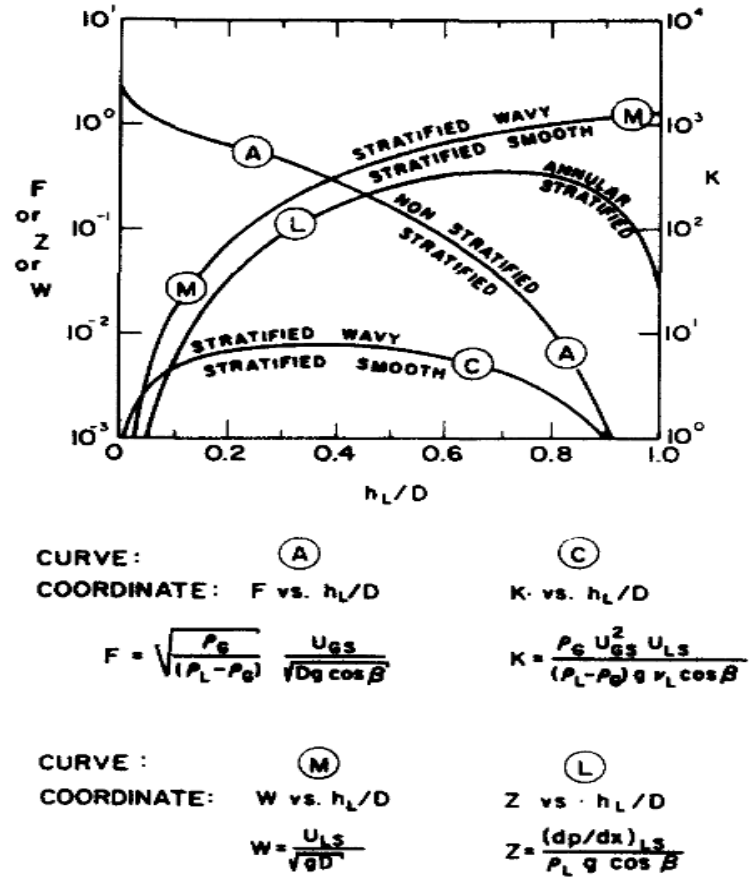

Figure 2.8: Generalized transition boundaries, (Barnea (1987)).

The Transition from Annular to Intermittent Flow

Barnea (1986) explains that annular flow has high gas flow rates, and as long as the gas flow rate is sufficient, it carries the entrained liquid droplets. The concept of annular flow regime is explained in section 2.2.1 with the corresponding momentum conservation equations presented in section 2.2.3. By substituting the pressure gradient in Equation 2.22 into Equation 2.23 gives the following combined momentum equation:

$$\tau_{GL} S_{GL} \Big(\frac{1}{\alpha_L} + \frac{1}{\alpha_G} \Big) - g(\rho_L - \rho_G) \sin\theta - \tau_{LW} \frac{S_{LW}}{\alpha_L} = 0, \tag{2.40}$$

where the liquid shear stress τ_{LW}, τ_{GL} is the gas-liquid shear stress, and the liquid-wall friction factor f_{LW} is equally defined as in Equation 2.33 and 2.34.

The transition from annular to intermittent flow occur if the gas core is blocked by the liquid. According to Barnea (1986) this situation may be the result from two different mechanisms:

1. instability of annular flow that prevents a stable annular configuration;
2. the liquid film to cause a spontaneous blockage as a result of axial transfer of liquid in the film. Accumulation of liquid in the mixing section due to backflow in the film is an example of this criteria.

The film geometry is given in regards of the film thickness, δ, and the diameter of the pipe, D. The geometry for the annular flow is summarized in Equation 2.41 where parameters are explained as before.

$$S_{LW} = \pi D \qquad S_{GL} = \pi(D - 2\delta) \qquad A_L = \pi(D\delta - \delta^2) \qquad A_G = \pi \Big(\frac{D}{2} - \delta \Big)^2. \tag{2.41}$$

Inserting equation 2.41 into 2.40, the result yields

$$\tau_{GL} = g(\rho_L - \rho_G) D \sin\theta (\tilde{\delta} - \tilde{\delta}^2)(1 - 2\tilde{\delta}) + \frac{1}{32} C_L \rho_L \Big(\frac{D}{\nu_L} \Big)^{-n} (U_{SL})^{2-n} \Big[\frac{(1 - 2\tilde{\delta})}{(\tilde{\delta} - \tilde{\delta}^2)} \Big], \tag{2.42}$$

which in dimensionless form becomes

$$Y = \frac{1 + 75\alpha_L}{(1 - \alpha_L)^{5/2} \alpha_L} - \frac{1}{\alpha^3} X^2, \tag{2.43}$$

where $\tilde{\delta} = \delta / D$ is the dimensionless film thickness while X and Y are defined as before. Barnea (1987) states the following:

$$Y \geq \frac{2 - \frac{3}{2}\alpha_L}{\alpha_L^3 (1 - \frac{3}{2}\alpha_L)} X^2. \tag{2.44}$$

For vertical upward flow the shear stress between the two phases is, according to Barnea (1986), given as:

$$\tau_{GL} = \frac{1}{2} f_{GL} \rho_G \frac{U_{SG}^2}{(1 - 2\tilde{\delta}^4)}, \tag{2.45}$$

The friction factor yields

$$f_{GL} = C_G \Big(\frac{U_{SG} D}{\nu_g} \Big)^{-m} \Big(1 + 300\tilde{\delta} \Big). \tag{2.46}$$

The aim is to find the $\tilde{\delta}$ that yields the value of U_{SG} at the transition. In order to obtain that result, equation 2.42 is differentiated with respect to $\tilde{\delta}$ and equated to zero. Equation 2.42 and 2.45 must be solved simultaneously with the value that satisfies $\tilde{\delta}$ from the differentiated equation.

Blockage of the gas core may occur when the supply of the liquid film is large enough to provide a liquid bridge. Barnea (1986) suggest that intermittent flow will develop when

$$\frac{A_L}{AR_{sm}} = \frac{\alpha_L}{R_{sm}} \geq 0.5, \tag{2.47}$$

where R_{sm} is the minimal liquid holdup within the formed liquid bridge that will allow blockage of the gas core. Barnea (1986) use previous research and state that R_{sm} equals approximately 0.48.

The leaps in change of inclination is large and consequently does not give a properly picture of how the transition develops. For horizontal flow, the solution is always stable which means that the transition from annular to slug only occur due to 2). However, in vertical upward flow the transition is a consequence of both 1) and 2).

Slug-Churn Transition

According to Taitel et al. (1980), slug flow is characterized by the liquid velocity between two Taylor bubbles which moves at a constant velocity and the tail have constant speed. Opposed to churn flow, where the liquid slug between two Taylor bubbles is too short to obtain a stable bridge between the bubbles. There are difficulties identifying the transition between slug and churn flow because to identify churn flow itself is challenging. However, one observes an oscillatory motion of the liquid in churn flow. Churn flow is mostly observed in the entry region and the L_E designate the entry length of the pipe required to establish stable slug flow. The entry length is expressed in Equation 2.6. This would consequently be the region where churn flow is observed. In calculating the entry length or length for churn flow, it is assumed that near the gas liquid inlet coalescence

is instantaneous. Short Taylor bubbles and liquid slugs are formed. When a Taylor bubble merges into the leading bubble and a larger bubble and liquid slugs take place, At approximately the same time, a third and a fourth Taylor bubble will merge as well. This process will go on until a stable liquid slug is obtained.

The velocity of a Taylor bubble depends on center line velocity plus its rise velocity (Equation 2.48). For a case with two subsequent Taylor bubbles, the liquid slug must reestablish the turbulent distribution otherwise the second bubble will overtake the first. As a result, two Taylor bubbles will coalesce and churn flow is created.

$$U_G = 1.2U_L + 0.35\sqrt{gD} \tag{2.48}$$

Experimental observation suggest that the length of a stable slug relative to its diameter is constant and independent of gas and liquid flow rates. The stable slug relative to its diameter is 16D according to Taitel et al. (1980) . The criteria $\alpha_c = 0.52$ may be adapted as the criteria for churn flow in the whole range of pipe inclinations.

2.3.2 OLGA Modeling

In order to compare the experimental results with a commercial model, the multiphase simulator OLGA has been used. The aim is to validate the performance of flow regime determination, and pressure and liquid holdup measurements in OLGA for upward inclination angles. This section will cover the OLGA modeling process.

The following summary is mainly based on the OLGA 7.3 user manual, Schlumberger (2014), in addition to the investigation by Bendiksen et al. (1991). Olga is a commercial dynamic multiphase flow simulation program, which was first developed by the institute for Energy Research (IFE) in 1980. Oil companies have since then supported the continuously development of OLGA. It is used for networks of wells, flow lines, pipelines and process equipment.

Set up

The flow regimes were plotted by fixing necessary parameters and provide superficial velocities from experiments in addition to inclination angle. The range of superficial velocities gave flow regime predictions, that provided the liquid holdup and the pressure drop. The multiphase flow toolkit was used for the thesis t. It applies the OLGA S-point model to predict flow regime, liquid holdup and pressure losses.

Fluids

OLGA requires input of the fluid properties, with their pressure and temperature dependencies. This can be provided in PVT tables made in the editor or from pre-made tables. OLGA offers pre-made tables for oil, water and gas for a wide range of temperature and pressures. The simulations in the thesis have applied fluid properties as presented in Table 3.1. Due to assumption of constant temperature in the lab, a constant input temperature is applied in the simulations. Additionally, surface tension between air and oil is set to 0.028 N/m.

Simulations

According to Bendiksen et al. (1991), the flow regimes in OLGA are treated with separate flow regime maps as functions of void fractions and mass flow only. The approach of determining flow regimes are treated as an integrated part of the two fluid system, where the correct flow regime, as a function of the average flow parameters, is required for flow regime prediction. Two basic flow regime classes are applied, namely distributed and separated where the first contributes to bubble and slug flow and the latter includes

stratified and annular flow. In total, OLGA distinguish between four flow regimes; stratified, bubble, slug and annular. The transition between distributed and separated flow regimes is based on the assumption of continuous average void fraction which means the flow regime yielding when the minimum gas velocity is chosen.

Bendiksen et al. (1991) also explains that stratified flow in OLGA is represented as either smooth or wavy. To distinguish between them, an expression for the average wave height must be obtained. If this value is zero, the flow regime is stratified smooth. The transition between annular and stratified flow is based on wetted perimeter of the liquid film, and annular flow is obtained when the wetted perimeter becomes equal to the film inner circumference. In other words, it occurs when the wave height reaches the top of the tube and $Pe = \pi D$. Apparently, this definition is different from what is defined as annular flow in the experiments and OLGA can be considered more conservative for annular flow transition. The experiments allowed for liquid droplets in the core in annular flow. Data from SINTEF Two-Phase Flow laboratory in 1983 showed that bubble-slug flow regime was described adequately, while stratifies-annular was not. The problems that arose were pressure drop too high in vertical flow and liquid holdup too high, at some cases by a factor of two. The discrepancies in this regime were explained by the neglect of droplet field, moving at approximately the gas velocity. Later, the flow regime has been incorporated and improved as liquid flow at which forms a wall layer and a possible droplet flow in the core and this is called stratified-annular mist in OLGA. Nevertheless, it seems like it is not defined with the same conditions as in the measurements, as will be seen in the analysis.

Regarding holdup, OLGA is a unified model, and does not require separate user-specified correlations for liquid holdup. The pressure drop at slug-bubble to stratified-annular flow experience a discontinuity at upward inclinations, which is partly justified in the experiments conducted by Bendiksen et al. (1991).

Chapter 3

Experimental study of two phase flow in inclined pipeline

The experiments were carried out at the Multiphase Flow Laboratory at the Norwegian University of Science and Technology in Trondheim. The Multiphase Flow Laboratory is flexible and includes several test loops for different purposes. Overall, the facility includes risers, horizontal and inclined pipe sections, flexible pipes and mini loops. However, the experiments in this thesis were conducted in the inclined pipe section and it is presented in Figure 3.1.

(a) Side view of rig during experiments.

(b) Front view of rig.

Figure 3.1: Inclined test section.

3.1 Experimental Facility and Set up

The multiphase flow facility at NTNU consists of several flow loops and test sections where two of them can be connected to the supply system at once. The liquids are stored in a large separator in the basement where the density difference of water and oil keeps the fluids separated in the tank. Several oil and water pumps in the basement secure a wide range of usage and application. The air system supplies the lab with air at 7 bar, but it is reduced to 4 bar by a pressure reduction valve before entering the flow control system upstairs. A steel pipe network for each of the fluids connects the supply area downstairs with the flow loops upstairs. The flow lines can be further investigated in Appendix A.

An inclined test section pipe with $60mm$ ID, which covers the inclination range from 10° to 78°, was used. The inlet to the test section can be seen in Figure 3.2 with the trolley which supported the setup for change in inclination angle. New improvements to the loop allowed 5° interval changes for angle $10° - 30°$ and an illustration of the instrumentation used for inclination change is provided in Figure 3.3. The experimental investigation included inclinations from 10° to 78°, however it was important to have a horizontal test section as a reference. Additional effort was required to achieve a horizontal test section, and Figure 3.4 shows the construction where the test section was lifted 1.5 m above the ground.

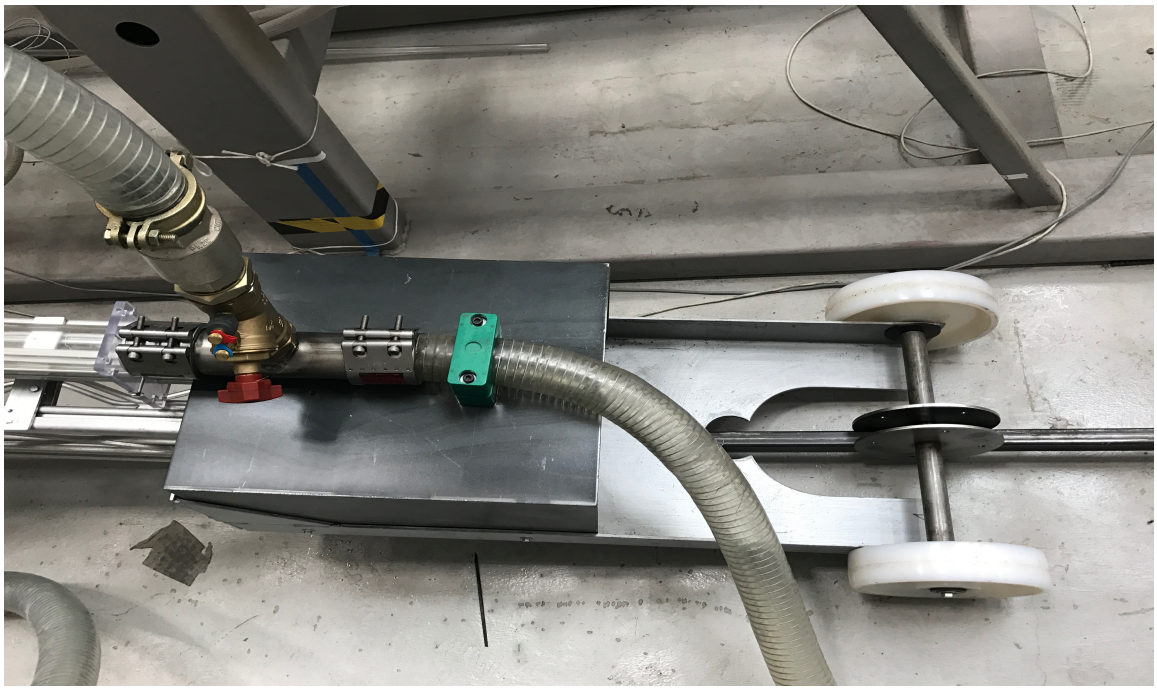

Figure 3.2: Inlet to test section and trolley.

(a) Control device for changing pipe inclinations.

(b) Support beam for test section.

Figure 3.3: Control device and construction to support change in inclination angle.

Figure 3.4: Horizontal set up.

The inclined loop has two possible mixing sections. Thus, two different T-sections allows the air to be injected at two locations. The desired mixing point is chosen using the red valves. The first mixing section is located before the flexible pipe, which is illustrated in Figure 3.5a. This option provided higher air flow rates to the test section. The other mixing option is placed at the test section entrance, right after the flexible pipe. This setup is illustrated by Figure 3.5b, where the air is supplied through the small flexible pipe on top of the test section inlet. The purpose of this option was to prevent instabilities prior to the test section, which will be the case if the mixing occurs several meters before the test section.

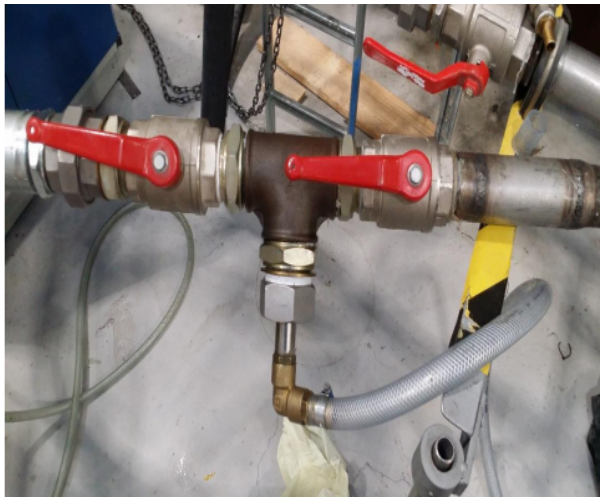

(a) T-section before the flexible pipe.

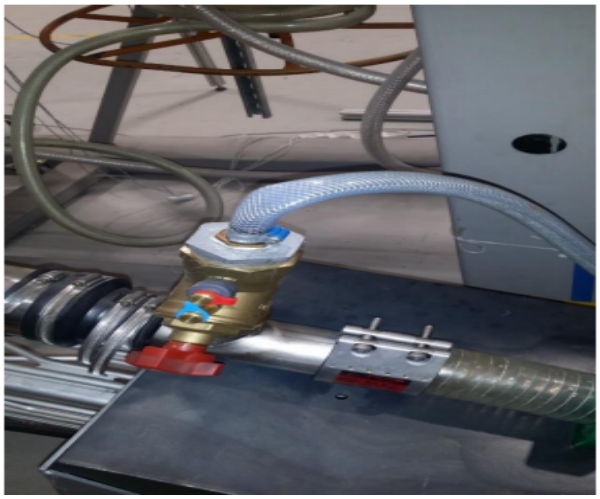

(b) T-section at the test section inlet.

Figure 3.5: Mixing sections.

However, during experiments it was observed that the flow rate of air did not reach a sufficiently high value with the mixing option in Figure 3.5b, which was critical in order to obtain annular flow. To achieve higher air flow rates, the mixing point had to be changed to the option in Figure 3.5a. Unfortunately, this resulted in considerably changes in the oil flow rates. Hence, the instabilities and lower flow rates affected the flow regime before it entered the test section pipe. The flexible pipe with air supply was consequently changed from a 0.5 inch pipe to a 2 inch pipe during the experimental period. Figure 3.6 and Figure 3.7 show the new configuration with air supply. The results presented in this thesis are done after the new configuration. The increase of dimension allowed for higher air flow rates, and consequently annular flow, which required air flow rate of approximately 25 l/s. The improvement increased the maximum flow rate of air from approximately 4.8 m/s to approximately 10.0 m/s. Further increase was not required for this work, and therefore not tested.

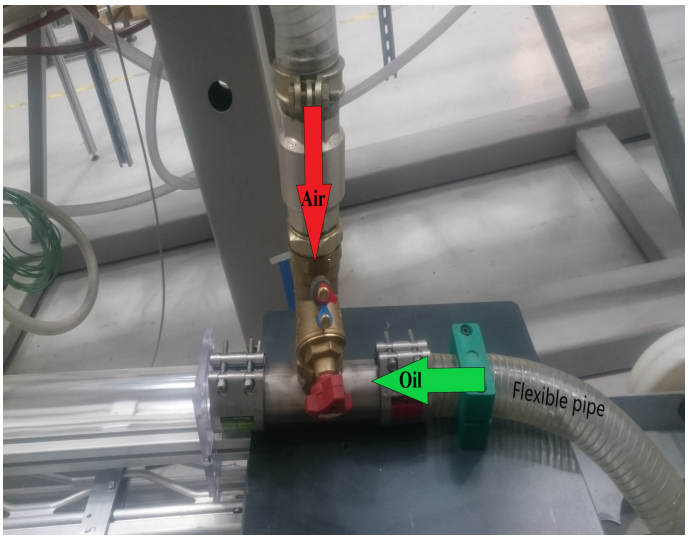

Figure 3.6: Improvement to air supply at the test section inlet.

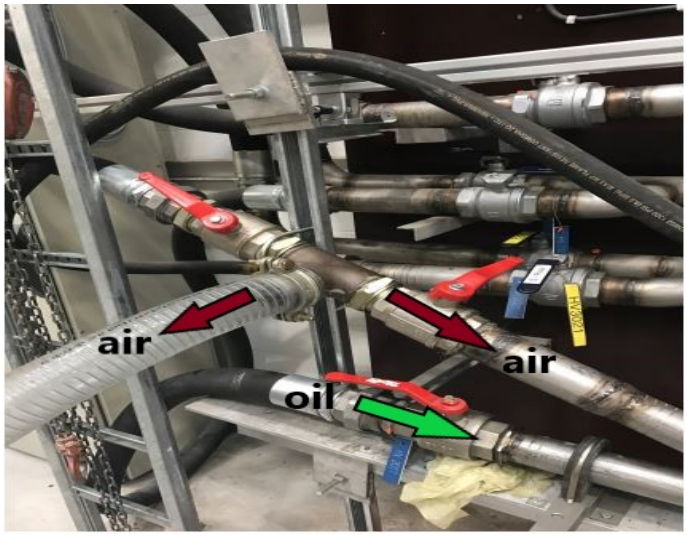

Figure 3.7: Improvement to air supply at the mixing section before the flexible pipe.

A program written in LabView was used for the experiments. The main control program include monitors for capacitance sensors, pressure transducer, pressure transmitter and flow meters. Additionally, valves, pumps and flow meters were used to secure the desired flow condition and acceptable pump frequencies. Pressure transducer and capacitance sensors were installed and used to study pressure drop and liquid holdup, respectively, and LabView provided output signals and logging. A further explanation of the instrumentation is given in section 3.1.2-3.1.6.

3.1.1 Fluids selection

The facility has three available fluids, which is oil, water and air. The oil used in the loop was a mixture of Marcol 52 and Nexbase 3080 and the properties of the fluids are listed in Table 3.1. Only air and oil were utilized in the experimental results. The oils had individually different densities and density measurement using a picnometer was done, illustrated in Figure 3.8. The fluid in the illustration is water, but the same procedure was practiced for the oil. The coriolis oil flow meter in the loop measured the density of the oil as well, but the value from the picnometer is applied due to higher accuracy. Temperature for oil measurements was 20°C, while water and air measurements were conducted at atmospheric conditions.

Fluid	**Density** $[kg/m^3]$	**Viscosity** $[Pa\,s]$
Water	1000	0.001
Oil	836	0.025
Air	1.22	$1.81x10^{-5}$

Table 3.1: Fluid properties.

Figure 3.8: Density measurement using a picnometer.

Viscosity measurement was done to confirm the viscosity of the oil mixture. For this purpose, a rotational rheology meter Ares-G2 from TA Instruments was used. A rheology meter measures the shear stress between the plate and the fluid while varying the shear rate. Figure 3.9a show the linear relation between shear stress and shear rate, which is characteristic for a Newtonian fluid and expressed in Equation 2.1. The rheology meter also has a heating plate, which allows to measure the change in viscosity for different temperatures. Figure 3.9b illustrates how the oil from the loop vary with temperature for a constant shear rate.

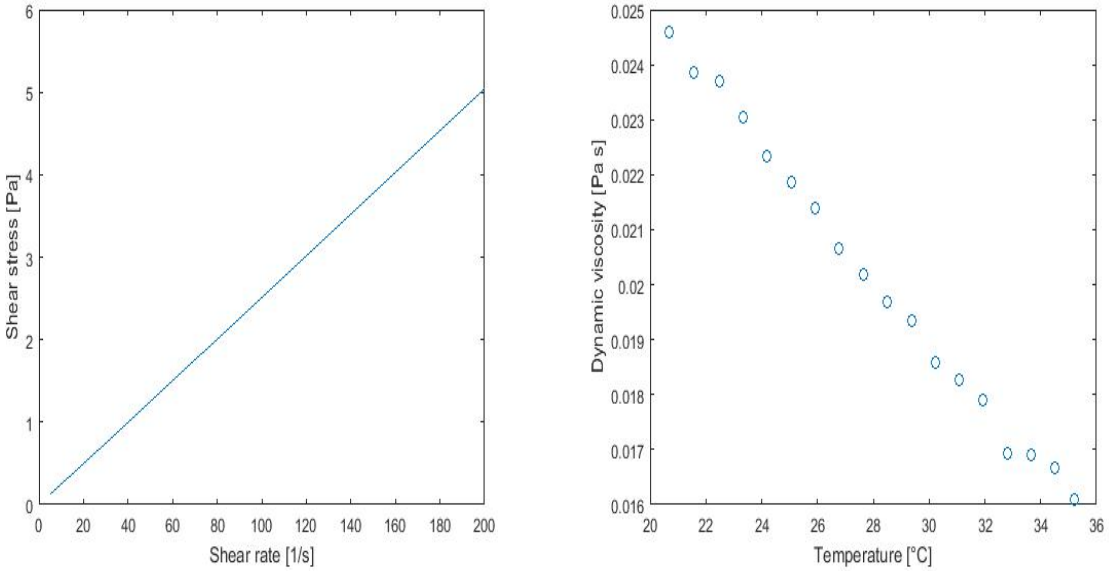

(a) Measured viscosity of oil at 20 $°C$.

(b) Measured viscosity of oil.

Figure 3.9: Viscosity measurements of oil in the loop.

3.1.2 Flow rate

The different flow lines are connected to flow meters of various types. Table 3.2 summarizes the flow meters connected to the facility. The flow meters can be chosen accordingly to the experiments.

Flow Meter	Model	Type	Range	Name	Accuracy
Air	Micro motion CMF	Coriolis	0.12-80 kg/h	FIT 1.01	0.25 %
	Endress & Hauser Flowirl 77A	Vortex	9-110 l/s	FIT 1.02	0.25 %
Water	Endress & Hauser Promag 33	Electromagnetic	0.053 -0.987 l/s	FIT 2.01	0.5%
	Fisher Porter COPA XM Series 3000	Electromagnetic	0.83-10 l/s	FIT 2.02	0.5 %
Oil	Micromotion F025	Coriolis	100-1000 kg/h	FIT 3.01	0.2 %
	Micromotion T150	Coriolis	1000-5000 kg/h	FIT 3.02	0.15 %

Table 3.2: Flow meter characteristics.

3.1.3 Pumps

The facility provides several types of pumps. However, the experiments conducted in this thesis required high flow rates and consequently the large centrifugal oil pumps were used exclusively. Table 3.3 shows the maximum obtained oil flow rate for a 60 mm ID horizontal pipe. The air provided at 80% valve opening was 37 m/s.

Fluid	Type of pump	Density $[kg/m^3]$	Maximum flow rate $[m/s]$
Oil	Grundfoss CR64-1	836	2.78

Table 3.3: Pump characteristics.

3.1.4 Pressure

The differential pressure was measured at two locations in the test section pipe, with two pressure transmitter of the same type. The differential pressure transmitters used

were FUJI FCX-A, illustrated in Figure 3.10, and properties are summarized in Table 3.4. Range and span are specified by the manufacturer, however the range was changed by the technician at NTNU prior to the calibrations.

Name in the lab	**Range** $[mbar]$	**Span** $[kPa]$
PDT 4.02	-20 - $+44$	0 1/6
PDT 4.03	-5 - $+55$	0 1/6

Table 3.4: Pressure transmitters.

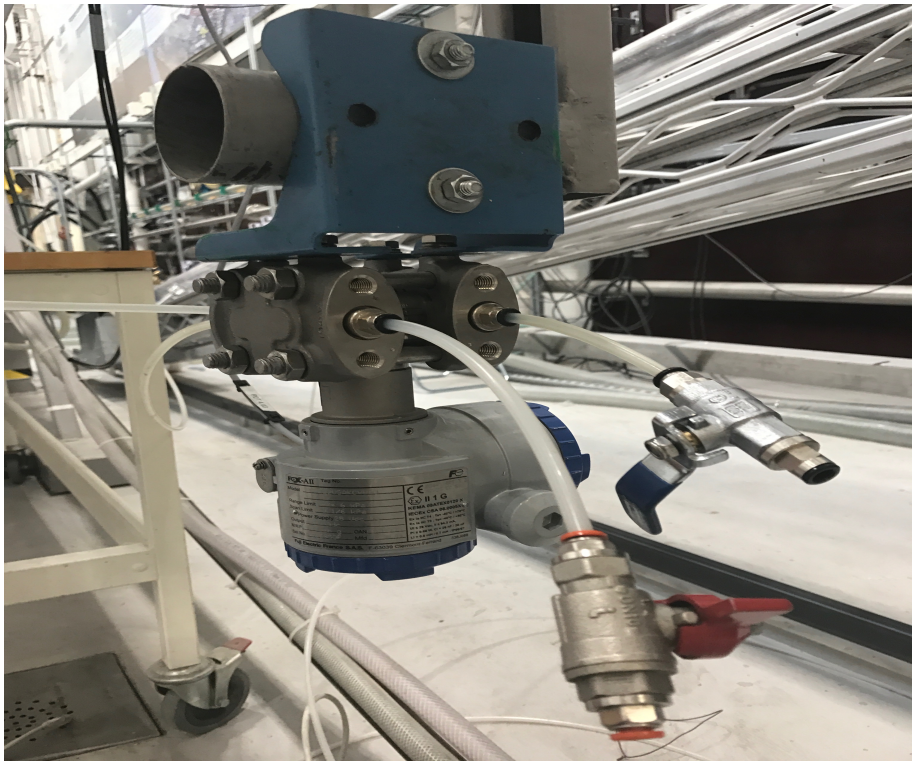

Figure 3.10: Differential pressure transmitter.

To ensure a correct signal output, the transmitters were calibrated with a HART bilingual communication module before taken into use. The digitize input range was -20 mA to +20 mA with 10 samples/second. During calibration, a given pressure were set manually using a pump and thereby an output current, $[mA]$, was recorded in LabView. This set up is illustrated in Figure 3.11. The logged values were checked with the accuracy range provided by the manufacturer, summarized in Table 3.5. Figure 3.12 show plots of the calibration results with the HART communication module against the targeting current. An approximately linear relation and values within the range of accuracy restrictions indicated a successful calibration.

Figure 3.11: HART bilingual communication module.

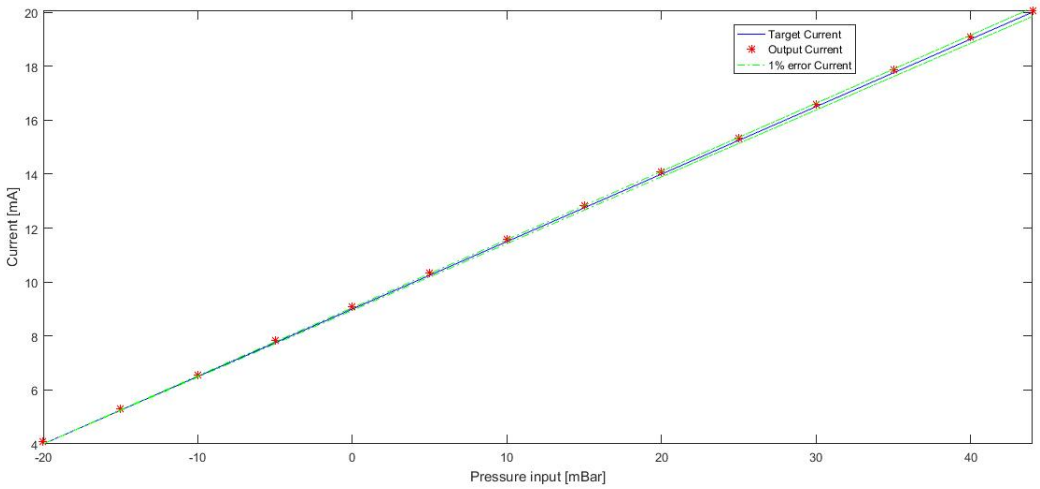

Figure 3.12: Calibration differential pressure transmitter PDT 4.02.

Measurement category	**Actual**	**Accuracy** 0.1%	**Accuracy** 0.2%
Percent display (%)	0, 25, 50, 75, 100	±0.1	±0.2
Current measurement (mA)	4, 8, 12, 16, 20	±0.016	±0.032
Voltage measurement (V)	1, 2, 3,4, 5	±0.004	±0.008

Table 3.5: Differential pressure transmitter.

Further, a single phase flow calibration of the differential pressure transmitters had to be performed for every inclination angle and consequently be used as reference in the

two-phase flow measurements. To validate the measured pressure drop values, they were compared with the theoretical pressure drop presented in section 2.2.3. The results are presented in Figure 3.13 in terms of the non dimensional parameters Darcy friction factor and Reynolds number. From Figure 3.13, it can be seen that the measured friction factor fits the laminar curve for Reynolds number up to 2000, before it changes abruptly. In the region of $Re > 2000$, the flow is in an intermittent region before it becomes fully turbulent at Reynolds number above 10000. However, it does not exist good correlation for the friction factor in the transition area between laminar and turbulent flow. Therefore, the results were considered valid as they were close to the calculated values for laminar flow and for intermittent Reynolds number it moves towards the Blasius correlation. The capacity of the pump was reached at Reynolds number around 2600, therefore a fully turbulent flow was not achieved.

A similar calibration was conducted for air and the same results could be seen, although not displayed here. The results were not equally accurate compared with the oil calibration, but it was assumed to be sufficient due to considerably lower pressure drop for air than for oil.

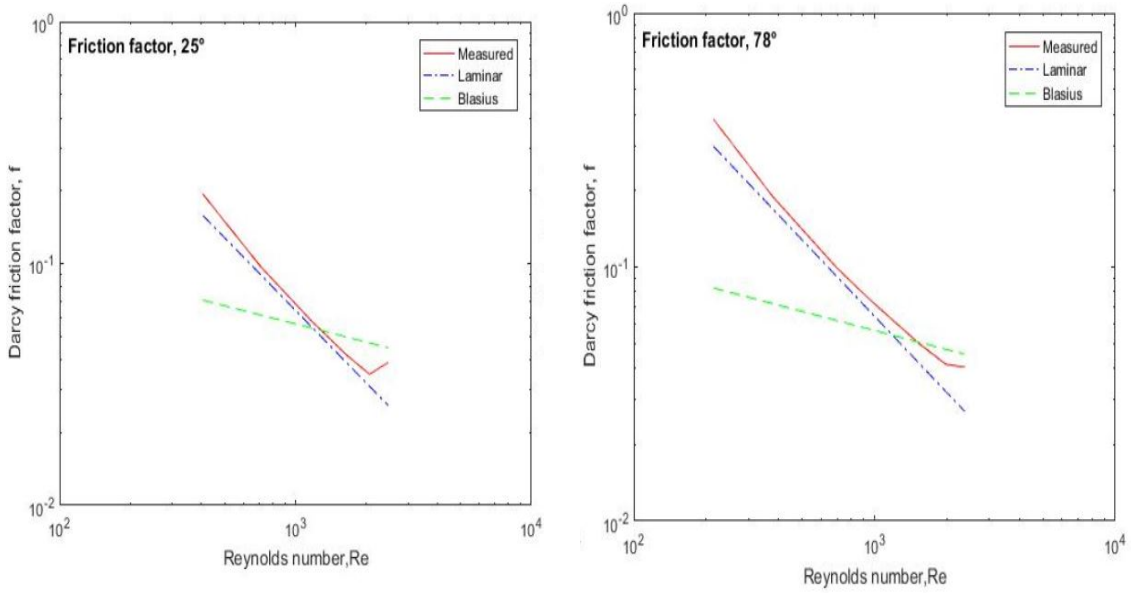

Figure 3.13: Measured and calculated friction factor for oil.

During the calibration it was questioned whether the pressure sensors measured the static pressure head correctly, which lead to uncertainties regarding the reference pressure head at zero flow. For that reason, it was tested if the pressure sensors measured difference in height correctly. This was done as illustrated in Figure 3.14 where a container, filled with water, was connected to the pressure sensor and thereby changed in height. The corresponding pressure was logged in LabView. Figure 3.15 was used to conclude that the relationship between the static pressure and an increase in height was appropriate as

it show approximately linear relation. A comparison with the calculated values concludes that the correlation is sufficient. The test also confirmed that the range of the pressure transmitters were limited and not sufficient to cover pressure measurements for the whole range of inclination angles. However, for most of the two-phase cases, the measurements were within the range. The concerns regarding the reference pressure head are discussed later.

Figure 3.14: Set up for verification of static pressure with water.

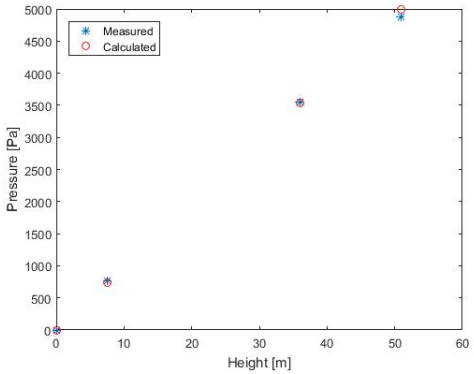

Figure 3.15: Measured and calculated pressure drop.

More over, small discrepancies in the pressure measurements were observed, which could originate from instrumentation errors. However, the friction factor was considered acceptable compared to known correlations. The trends also agrees with other researchers, and that validated the experimental measurements for pressure drop.

3.1.5 Capacitance

Reliable measurements of the void fraction and flow pattern identification are important for accurate modeling of two-phase flow. Several techniques can be used to measure the void fraction, including radiation attenuation or impedance technique using capacitance sensors, (Ahmed (2006)). The instantaneous output signal from the sensors can be used to identify the flow pattern. This thesis will use capacitance sensor due to simple design and economic aspects. Capacitance probes are provided by the multiphase laboratory at NTNU Trondheim and have previously measured slug flow successfully (Johansen (2006) and Diaz (2016)). They were designed to detect the liquid fraction in oil-air two-phase flow, which was their purpose in this thesis as well. The instrumentation was made from models from Johansen (2006), and the design is presented in Figure 3.16. The purpose of the instrumentation is to detect the change of values of conductivity and permittivity for gas and oil mixtures. The sensor is mounted externally around the pipeline and consists of copper foil strips. Thus, the inner strips on the foil act as electrodes while the outer strips work as an active guard. In order to avoid external interference, the sensor is covered with a thin copper foil which forms an outer shield. Figure 3.17 illustrates the installed instrumentation.

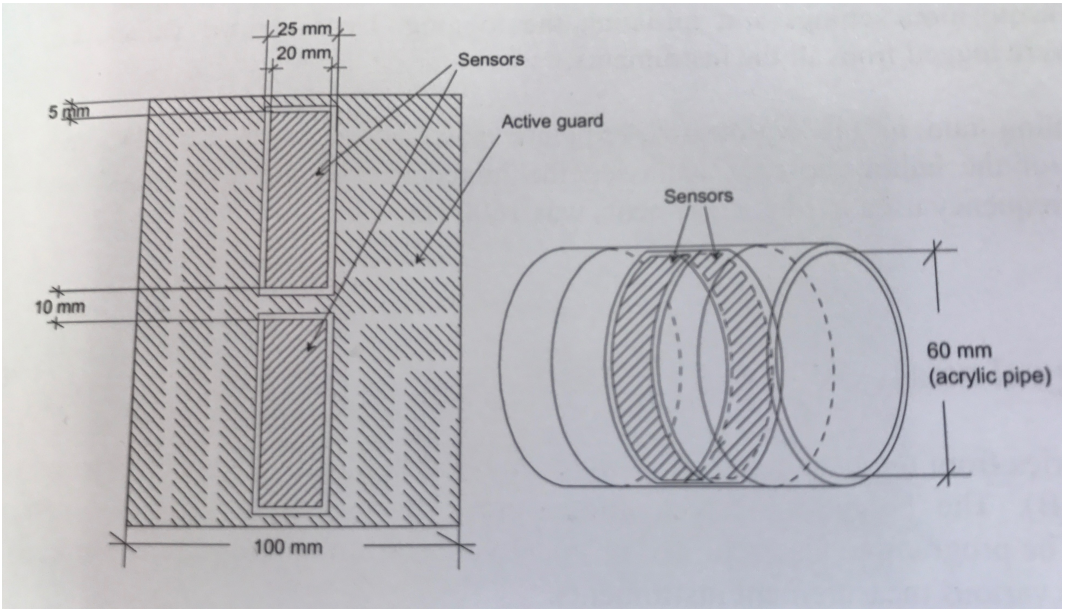

Figure 3.16: Capacitance sensors design, (Johansen (2006)).

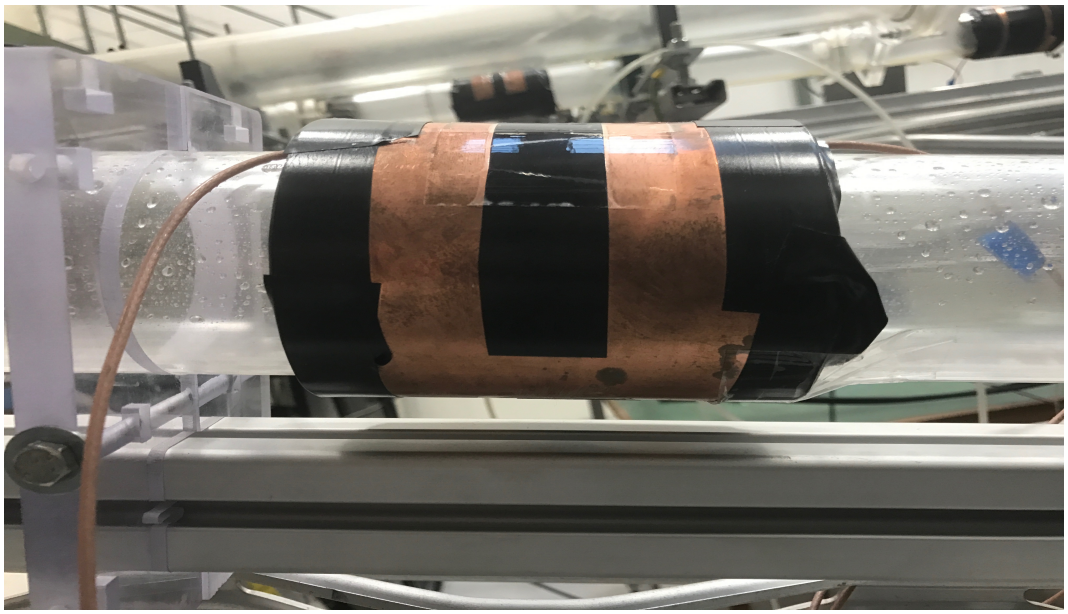

Figure 3.17: Capacitance sensor.

The capacitance sensors had to be calibrated every day before conducting experiments. They were highly sensitive and could be influenced by small changes in the environment such as loud noise in the room or vibration in the test section. The electrical circuit contains a power supply that provides a voltage from 2 V to 10 V, and the purpose of the circuit was to measure conductance as a function of time. A minimum and maximum value were accordingly calibrated within those limits such that signals and signal noises could be detected. Thus, the limits were set to 3.2 V and 9.2 V. To achieve the minimum capacitance, the pipe was completely emptied for liquid, and a tap inside the electrical box was manually adjusted to reach a value of 3.2 V. The same procedure was applied with the pipe filled with oil, and the tap corresponding to maximum was adjusted. The taps inside the electric box is shown in Figure 3.18a. Due to inclination of the pipe, and consequently inability to obtain stratified flow, it was more difficult to calibrate the capacitance in a non-horizontal pipe. For that reason, the pipe was set in a horizontal position and stratified flow was achieved. By controlling the liquid level, the wetted perimeter for the different capacitance situations could be detected. A measuring tape, Figure 3.18b, was used to determine the wetted perimeter. As explained in chapter 2.2.2, the wetted perimeter can be converted into liquid holdup. Thereby, a function for liquid holdup is obtainable by using the voltage from the capacitance sensor. Figure 3.19 show the relationship between liquid holdup and the voltage obtained from the calibration. The line is a curve-fitting of the data points. For $V*$, defined in Equation 3.1, between 0.2 and 0.9 (V/V), there is almost a linear relationship between the liquid holdup and the voltage. This can be explained by small changes in the curvature in this region. On the other hand, the liquid level changes a lot for small changes of liquid volume outside of this region. In the region with significant changes, the best curve fitting is a third order

polynomial, at which was also found by Diaz (2016). An alternative way to the calibrate the sensor for inclined pipes is to use the static liquid level. By increasing the liquid level in the pipe, the wetted perimeter can be achieved for all situations between empty and filled pipe. However, this would be difficult for high inclination angles were the liquid level is almost normal to the pipe.

The normalized voltage is defined as:

$$V* = \frac{V - V_{min}}{V_{max} - V_{min}} \tag{3.1}$$

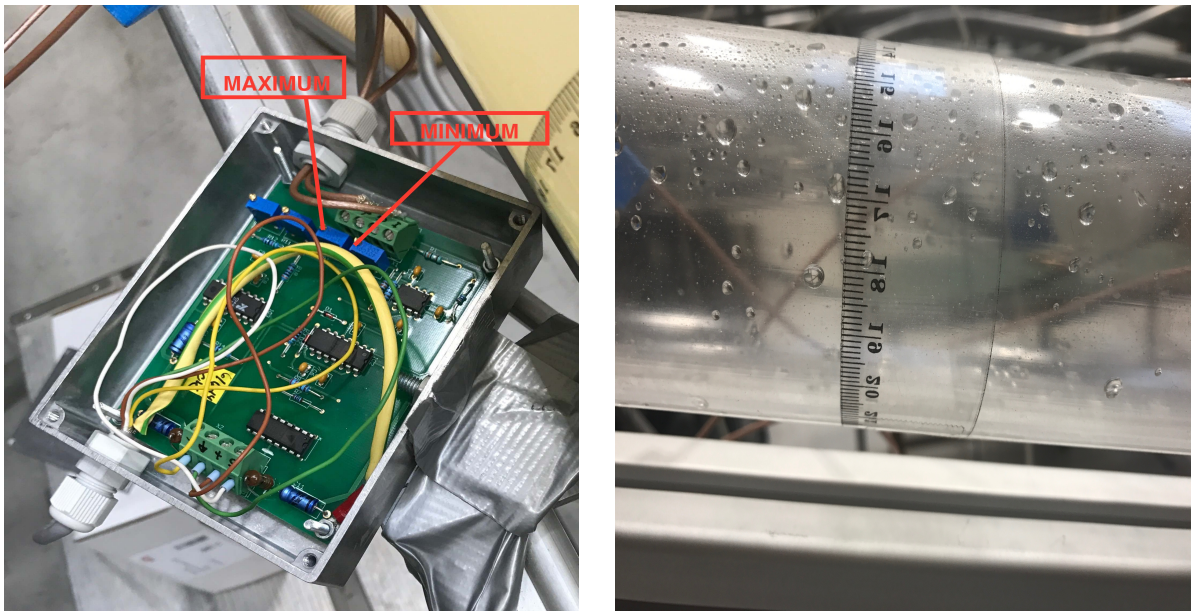

(a) Electronics capacitance sensor. (b) Measuring tape.

Figure 3.18: Calibration capacitance sensor.

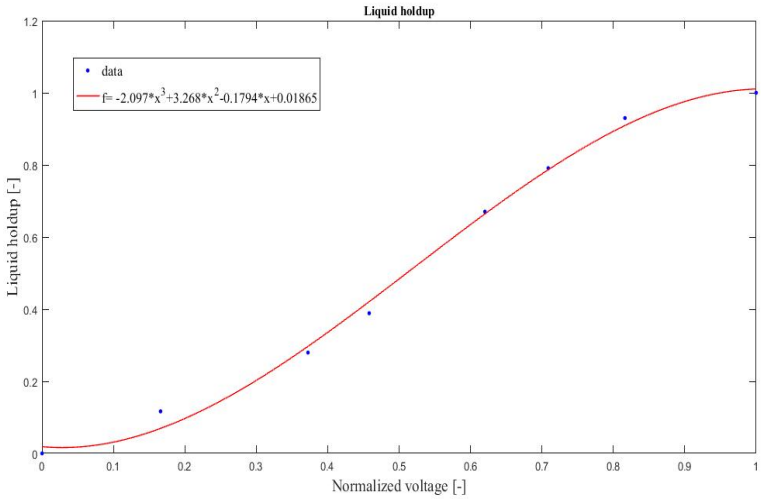

Figure 3.19: Liquid holdup and voltage at horizontal pipe.

As mentioned, the sensors are highly sensitive and originally three sensors were installed on the test section pipe. As the capacitance is a function of geometry and the permittivity of the dielectric material between the plates it was important that the body of capacitance sensor was entirely rounded around the pipe to obtain a uniform electrical field. The capacitance sensors had to be investigated carefully and although there were several sensors installed, it was found that only one of the sensors measured accurate values. Nevertheless, it was decided that it was sufficient with measurements from one of the sensors only.

3.1.6 Visualization

Flow regimes were determined by capacitance measurements and visualization. In order to examine the flow regimes carefully, video recordings were conducted and saved. All videos were recorded with synchronised GigE cameras at 120 fps. The full visualization system included 3 synchronized GigE cameras model Basler acA640-120fps, a computer Intel ® core ™ i7 and a GigE Vision frame grabber of National Instrument model PCLe-8233.

The camera settings were changed in the software or directly on the camera. Exposure time settings were particularly taken into consideration to keep a uniform color distribution and obtain a adequate frame rate as a maximum exposure time was at the expense of the frame rate. A long exposure time provided acquisition of fewer frames per second. Also, the height of the frame influenced the allowed frame rate and could be adjusted according to the area of interest. The preferred frequency of frame caption was minimum 40-50 Hz.

A separate acquisition structure was used for the camera system, which was not synchronized with the main control program. The acquisition was done with a program written in LabView, which allowed recording and stopping the video simultaneously for all the cameras. The program allowed to chose between saving the recording in frames, as a video, or both.

The image processing was conducted as following:

1. Set up: The location of the cameras varied for different inclination angles depending on the accessibility around the test section. Consequently, the distance from the test section pipe, the mixing point and between the cameras changed. For inclination angles 10°, 15° and 20°, the location of the cameras was equal. All three cameras were set up along the side of the pipeline, with approximately the same distance between them, as can be seen in 3.20b. For angles above 20°, only two cameras were used due to inconvenient and impossible access in heights as the position of the scaffold and other equipment in the facility blocked the passage. One camera

was placed along the side of the pipeline and the other camera was placed at the top. These set ups can be seen in Figure 3.21. The camera for the horizontal test section was allocated 2.73 m from the test section inlet and can be seen in Figure 3.20a

(a) Camera set up for horizontal pipe.

(b) Camera set up inclination angles $10° - 20°$.

Figure 3.20: Camera set up for horizontal and lower inclination angles.

(a) Camera set up for inclination angles $25° - 60°$.

(b) Camera set up for inclination angles 70° and 78°.

Figure 3.21: Camera set up for higher inclination angles.

.

2. Recording: Recording was done in a program written in LabView. The recording started when the flow was stable. In addition, the recording time was adapted to the relevant flow regimes. The recording time was extended when the flow regimes was in transition regions.

3. Processing: Due to a subjective and memorable based impact of live visualization, pictures and videos were used to support the decision making regarding the flow regimes. The pictures were also used as reference for upcoming flow regime maps. In many situations, especially in the transitions region, the different flow regimes were hard to define. However, the illustrations of the observed flow regimes are presented in Figure 3.22 - 3.30.

   Figures 3.22 -3.25 show the flow regimes in a horizontal pipe. They correspond to the horizontal flow regimes explained in section 2.2.1 and were uncomplicated to categorize visually. On the other hand, the flow regimes in an inclined pipe were more chaotic and therefore more challenging to distinguish from each other. Figures 3.26 - 3.30 illustrate the flow regimes for the inclined cases. Figure 3.28 and 3.29 originate from 15° angle while Figure 3.26, 3.27 and 3.30 are illustrations from 20° angle. For inclination angles larger than 45°, the repeated cycle of severe slugging occurred. This is not displayed in the figures, but the video recordings can be used to determine slug frequency and size. Elongated bubble flow is defined in Barnea et al. (1980b) as the distinction between elongated bubble and slug is based on the "bubble-shape" and the film thickness below the bubble. In elongated bubble flow, the gas bubble has a smooth bullet-formed shape, the liquid part does not contain dispersed bubbles and the phases move slowly compared to the corresponding phases in slug flow. A variation of elongated bubble flow were classified as cap bubble flow which is categorized as smaller, more frequent bubbles. This flow regime can be seen in Figure 3.29.

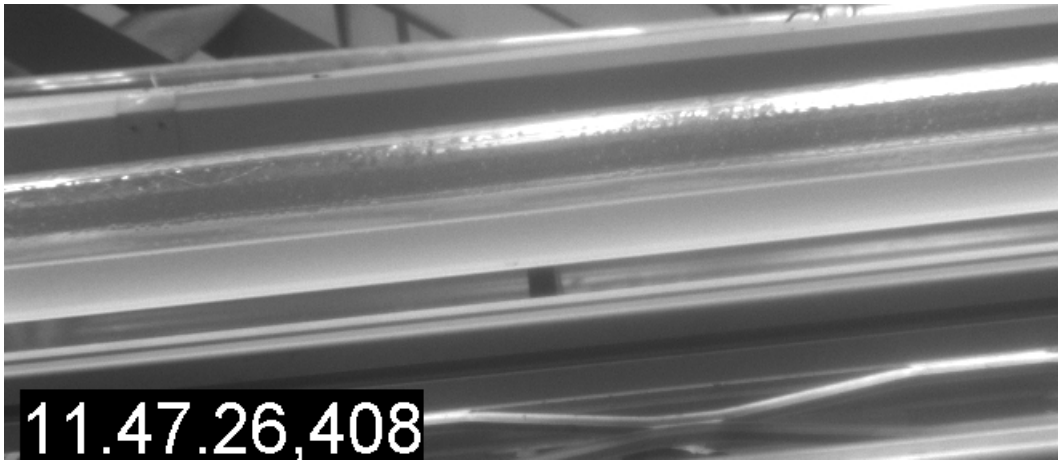

Figure 3.22: Stratified flow in horizontal pipe.

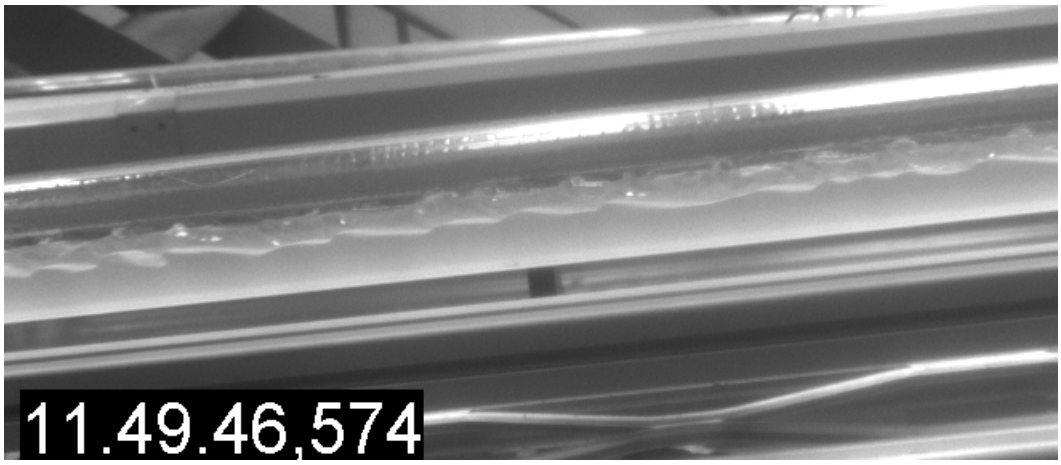

Figure 3.23: Stratified wavy flow in horizontal pipe.

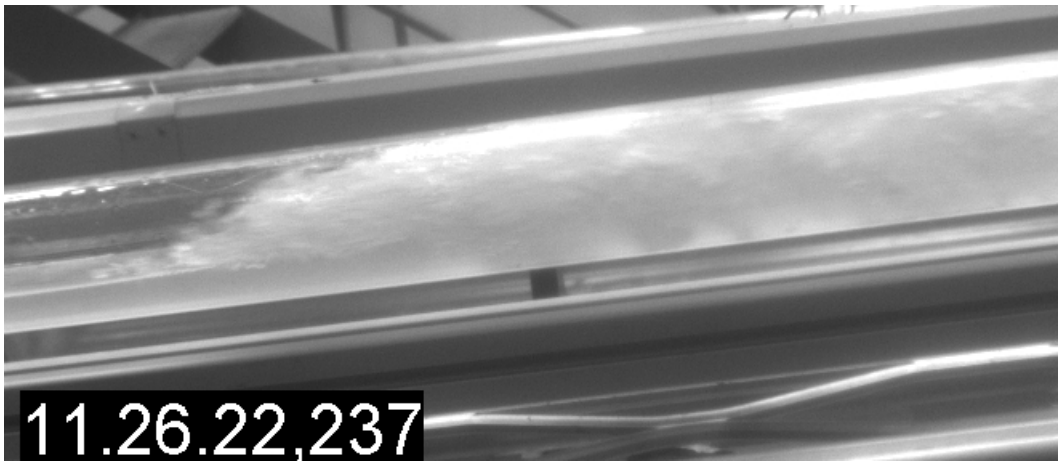

Figure 3.24: Slug flow in horizontal pipe.

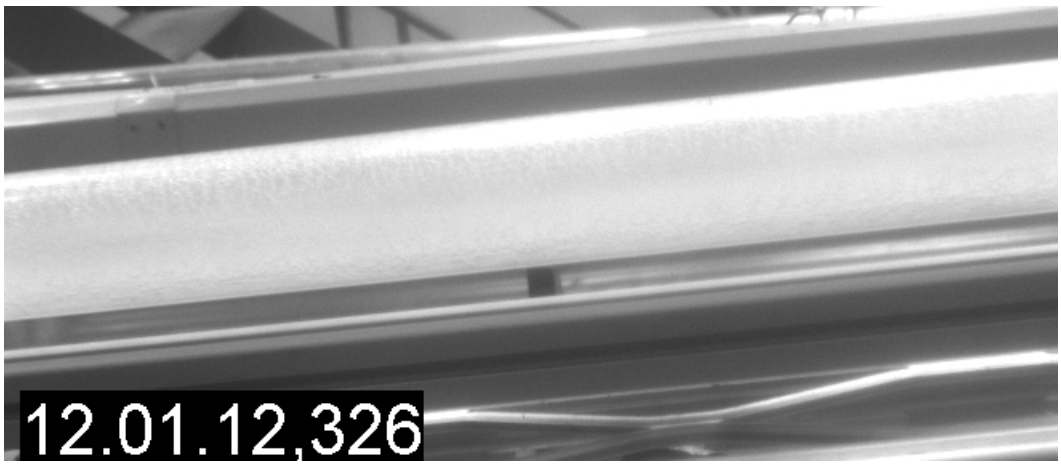

Figure 3.25: Annular flow in horizontal pipe.

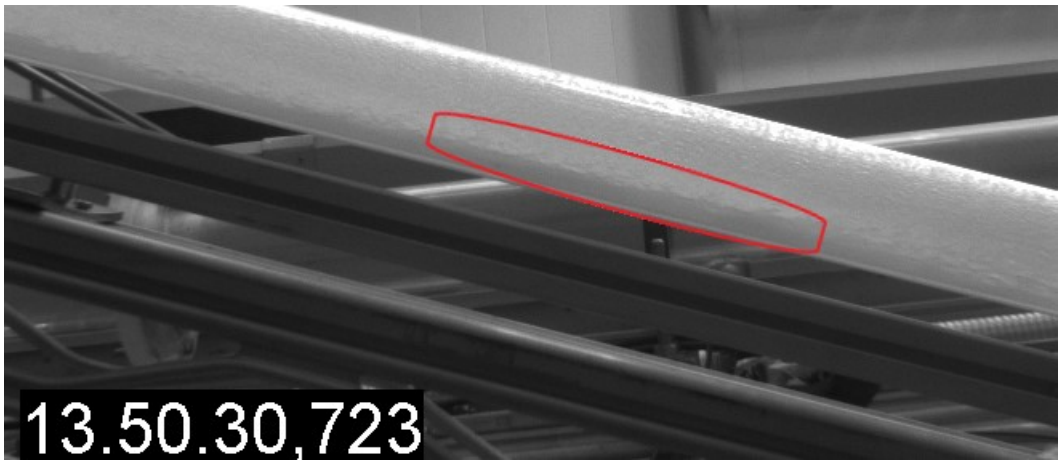

Figure 3.26: Stratified wavy flow in inclined pipe.

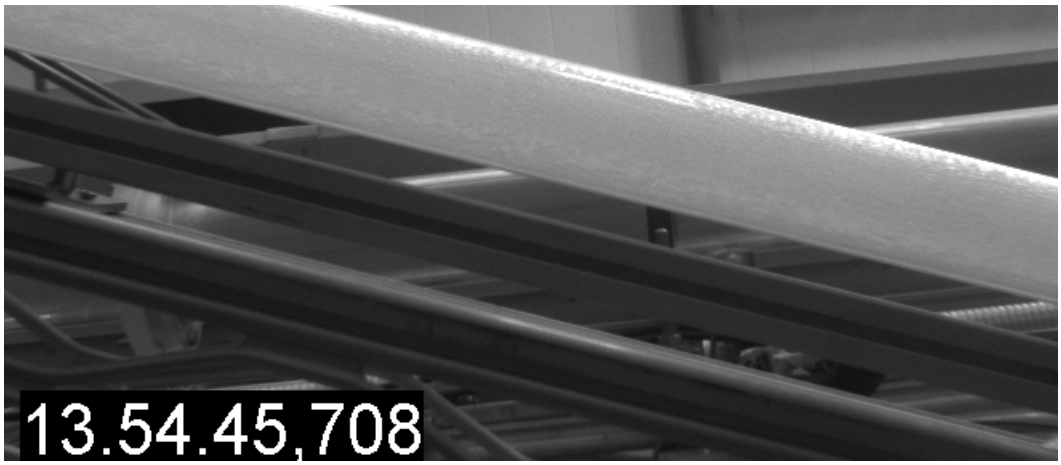

Figure 3.27: Annular flow in inclined pipe.

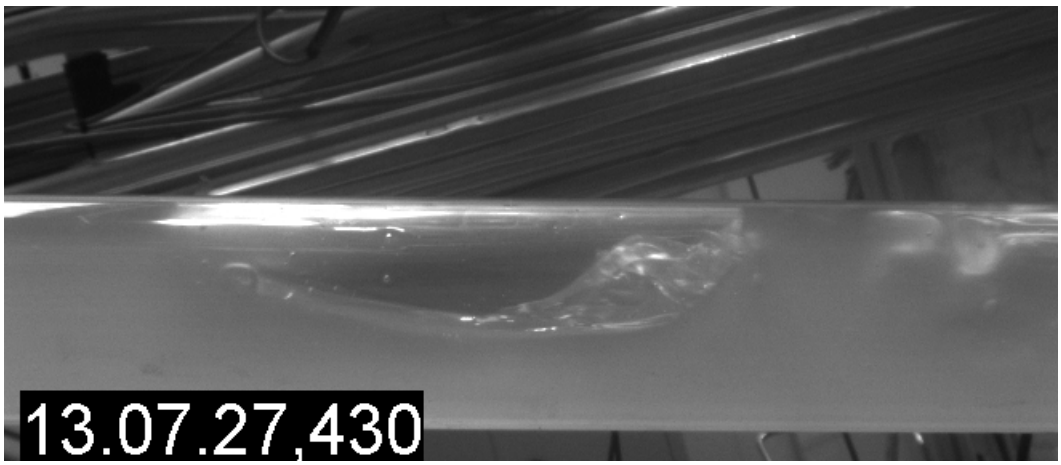

Figure 3.28: Elongated bubble flow in inclined pipe.

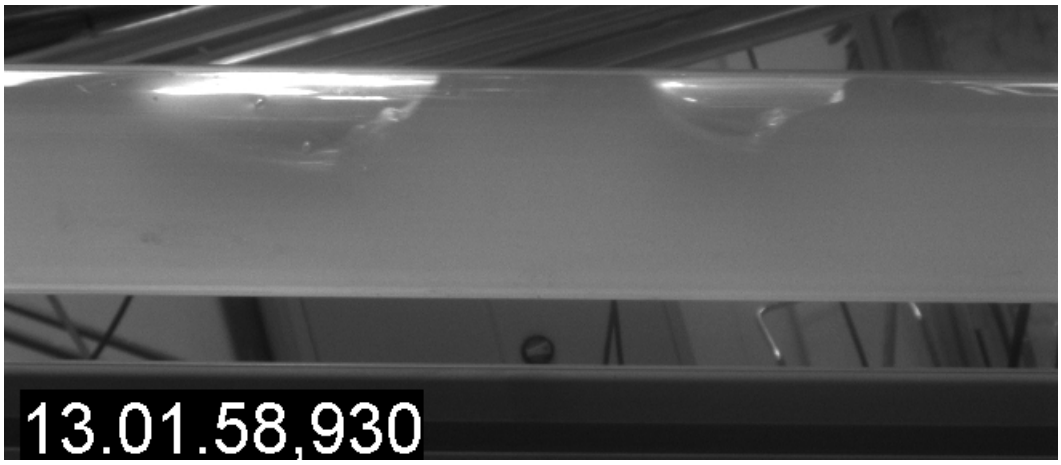

Figure 3.29: Cap bubble flow in inclined pipe.

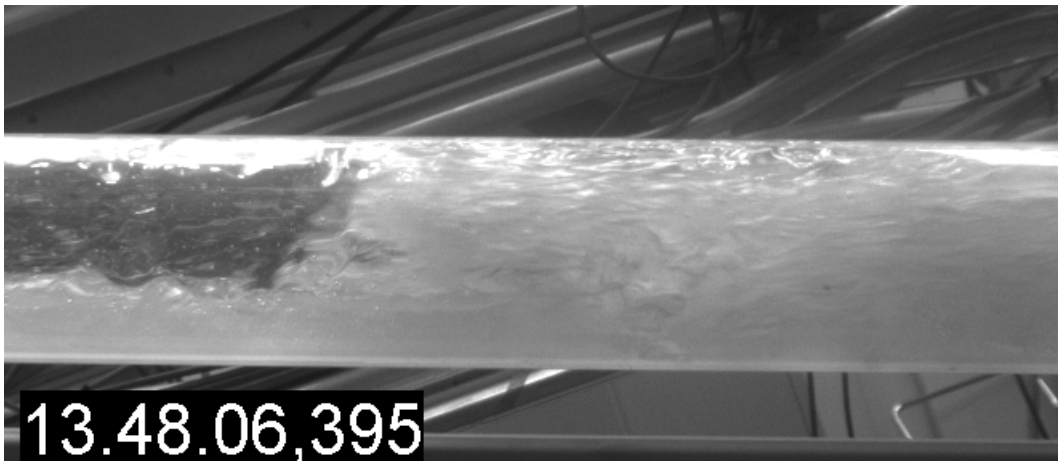

Figure 3.30: Slug flow in inclined pipe.

3.1.7 Capacitance for Flow Regime Determination

The capacitance measurements were used to determine flow regimes, together with visual observation. As explained by Barnea et al. (1980a), the major difficulty of visual observation, even when using high speed cameras, is that the classification itself is highly questionable and the pictures can be blurry and confuse rather than help. Similar to the Barnea et al. (1980a), capacitance measurements were used for horizontal pipe as well as upward inclination pipe in the the thesis. The horizontal measurements are presented in Figure 3.31 and the associated visualization of the flow regimes is presented in Figures 3.22-3.25. The measurements are compared with the investigation by Barnea et al. (1980a), where the basic horizontal flow regimes are classified as stratified, intermittent, annular and dispersed bubble. Thereby the flow regime decision for the measurements can be made with comparison of similar shapes and trends. Stratified smooth and stratified wavy is similar in shape, but stratified wavy contains fluctuations with higher amplitude.

For slug flow the difference between minimum and maximum voltage is clearly larger than for stratified wavy. This is reasonable as slug flow associated with higher liquid holdup. In annular flow, the pipe is almost completely filled with air, and consequently the normalized voltage low. However, the liquid film surrounding the tube wall can provide capacitance fluctuations if the liquid surface towards the gas core is wavy.

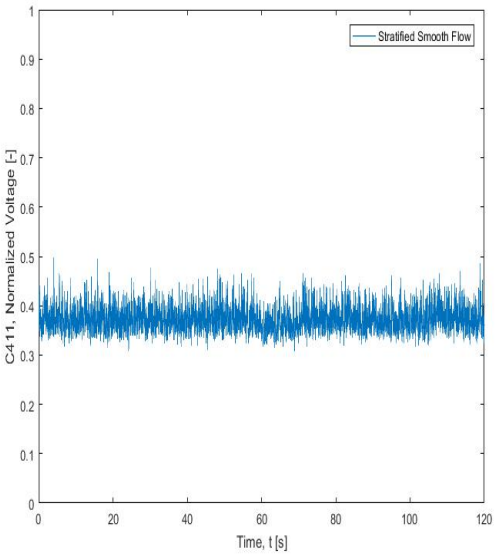

(a) Stratified smooth, $U_{SG} = 5.3l/s$.

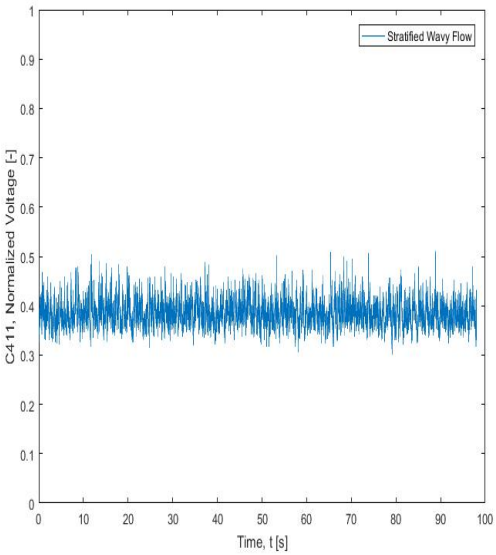

(b) Stratified wavy $U_{SG} = 9.4l/s$.

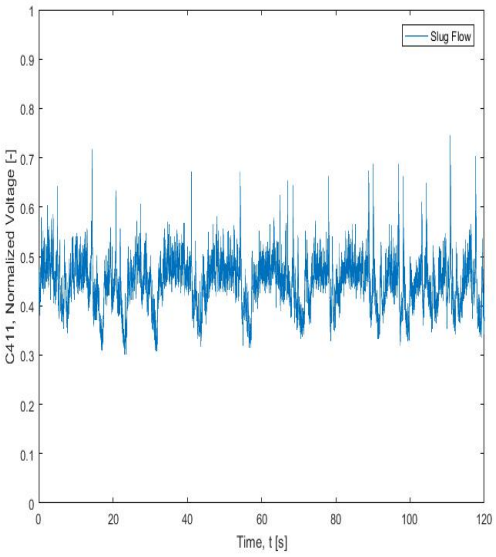

(c) Slug flow, $U_{SG} = 15.2l/s$.

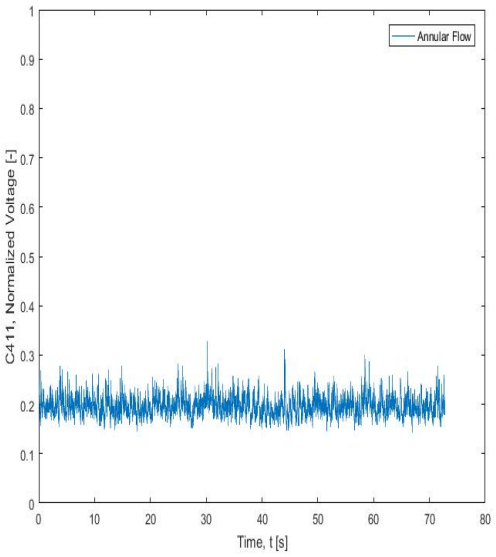

(d) Annular flow, $U_{SG} = 29.7l/s$.

Figure 3.31: Capacitance sensor in horizontal pipe with oil flow rate equal $2500kg/h$.

Figure 3.32 shows how the electrical voltage obtained from the capacitance sensors at 78° for different gas flow rates at a constant time-averaged oil flow rate of 3000 kg/h, approximately. This is included to illustrate the transition from slug flow to churn and

lastly annular flow. The amplitude of churn flow at 13.9 l/s is between high amplitude slug flow, at 9.3 l/s air, and low voltage for annular flow at 19.4 l/s. A flow containing only oil, shown in the top left plot, gives a voltage around 9.2 V. A single flow of air will give a voltage around 3.2 V, and will approximately have the same output as the bottom right plot, which is annular flow. In between these boundaries, the other flow regimes will provide different values and plots. For the severe slug flow regime, which is associated with high liquid fractions, the signal drops when the air bubbles appear before the voltage stabilize again at 9.2 V. This behaviour is observed at air flow rates up to 7.6 kg/h, however the frequency of these air bubble trains increases with increased gas flow rates.

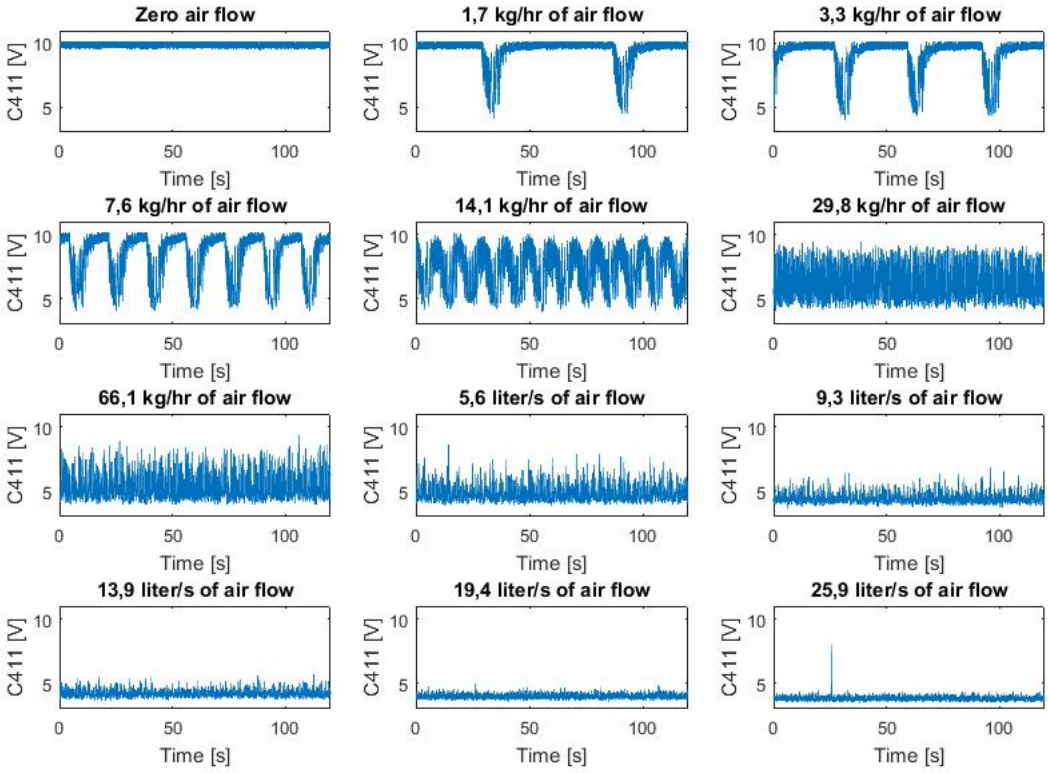

Figure 3.32: Capacitance sensor at 78° with oil flow rate approximately equal 3000kg/h.

In Figure 3.32 the following air flow rates give these corresponding flow regimes. **1.7-14.1 kg/hr**: Bubble flow. **29.8-66.6 kg/hr and 5.6-9.3 [l/s]**: Slug Flow. **13.9 [l/s]**: Churn Flow. **19.4-25.9 [l/s]**: Annular Flow

3.1.8 Test Matrix

Table 3.6 provides the test matrix. The experimental procedure can be further investigated in Appendix B and C.

Inclination $^\circ$	Number of experimental points [-]	Superficial oil velocity $[m/s]$	Superficial air velocity $[m/s]$
10	65	$0.017 - 1.34$	$0.038 - 11.79$
15	71	$0.048 - 1.33$	$0.035 - 10.25$
20	79	$0.047 - 1.31$	$0.036 - 9.20$
25	72	$0.13 - 1.28$	$0.037 - 9.29$
30	82	$0.10 - 1.32$	$0.036 - 9.24$
45	71	$0.11 - 1.29$	$0.039 - 9.18$
60	72	$0.088 - 1.27$	$0.036 - 9.19$
70	66	$0.077 - 1.25$	$0.028 - 10.78$
78	61	$0.082 - 1.25$	$0.037 - 8.93$

Table 3.6: Test matrix oil/air.

17 experiments, which were used as reference, were carried out in a horizontal pipe in addition.

Chapter 4

Results

In this chapter the experimentally obtained flow regime maps for two-phase flow in an inclined test section are presented. Results from liquid holdup and pressure measurements are provided in this chapter as well.

4.1 Experimental Results Flow Regime Maps

Figures 4.1-4.9 show the flow regime maps obtained from experiments. The most important results are outlined in Table 4.1.

Findings	Angle
No dispersed bubble flow	$10° - 78°$
Annular and slug flow	$10° - 78°$
Stratified flow	$10° - 20°$
Elongated bubble	$10° - 30°$
Cap bubble flow	$10° - 60°$
Severe slug flow	$45° - 78°$
Churn flow	$70°$ and $78°$

Table 4.1: Experimental flow regime results.

Overall, the experimental investigation showed neither stratified smooth flow or dispersed bubble flow. This is not surprising considering previous research, among Barnea et al. (1985) and Barnea et al. (1980b), which states that stratified smooth flow pattern does not exist after $0.25°$ inclination. Stratified wavy flow was observed for inclination angles up to $20°$, which is also valid compared to results presented by Shoham (1982). On the other hand, Barnea et al. (1980b) had no occurrence of stratified flow higher than $10°$ inclination. One possible explanation for the different results could be annular wavy

flow at which is named stratified wavy in the thesis, which was discussed in section 3.1.6. Also, it is important to mention that the experiments conducted by Barnea et al. (1980b) and Barnea et al. (1985) included air and water. Further there were no existence of dispersed bubble flow due to limited oil flow rate in the experiments. According to Barnea et al. (1980b) this flow regime requires $U_{SL} = 5m/s$ for horizontal flow, while Barnea et al. (1985) obtained dispersed bubbles at approximately $U_{SL} = 2m/s$ at 10° angle. Nevertheless, the highest measured superficial velocity of oil was $U_{SL} = 1.34m/s$.

Similar to the study by Barnea et al. (1985), the experiments found that for low inclination angles, up to 20°, there exist a range of liquid rates for which, as the gas rate is increased, the pattern changes from intermittent to stratified and then to annular. An observation by Barnea et al. (1980b), was that the intermittent flow regime takes place over a wider range of flow conditions with increasing inclination angle, which is in good agreement with the measurements.

Inclination angles $25° - 45°$ have an annular-intermittent transition at which is a vertical line, which Barnea et al. (1985) also model for these angles, but also for higher inclination angles. Elongated bubble flow does not exist for inclinations above 30° in the experiments. Although Barnea et al. (1980b) observed elongated bubble flow over a wide range of flow conditions up to 10° there were found no available literature that could validate the measurements for higher inclination angles. Cap bubble flow was observed for inclination angles $10° - 60°$, despite Barnea et al. (1985) mentioned in their report that this region disappears for low liquid flow rate and totally disappears somewhere between 50-70°of inclination. Cap bubble can exist for 70° and 78° but in the experiments the flow regime is included in the severe slug flow classification. At inclination angles higher than 45°, low liquid flow rate and medium gas flow is associated with severe slug. Annular flow is generally observed at lower superficial gas velocities compared to literature, Spedding et al. (1982) states that annular flow regime usually occur at $U_{SG} = 10 - 30m/s$, while the measurements gave annular flow at $U_{SG} = 5 - 10m/s$. As mentioned,Barnea et al. (1980b) has a flow regime called annular wavy which is present in 10° angle with onset at $U_{SG} = 6m/s - 7m/s$. For the experimental case, this region seems to equal the stratified wavy flow regime.

All the discussed flow regimes in section 3.1.6 are present at angle **10-25**°, except churn flow and severe slug, which occurs at higher inclination angles. Stratified wavy flow is present at $U_{SG} = 5 - 9m/s$. As the superficial velocity of gas increases up to 10.2 m/s, the flow becomes annular. The transition line from cap bubble flow to elongated bubble flow is almost the same for 15° and 20°. Between the same angles and at high superficial liquid velocities, slug flow at 15° changes to elongated bubble flow at 20°.

An inclination of **25**° requires more pressure to push the liquid upstream, compared to the smaller angles. Hence, it results in a cap bubble flow for low gas and oil flow rates, where elongated bubble flow occurs in the same flow condition region for smaller angles.

Annular flow starts to occur at higher superficial gas velocity compared to $10° - 20°$ which is reasonable if the same trend is present as in Barnea (1986), where it is seen that an increase in inclination angle causes increase in superficial gas velocity.

For inclination angle **30**°, the flow regime map obtained by experimental investigation is given in Figure 4.5 and it reveals that the transition lines between the flow regimes are approximately vertical. At low superficial gas velocities up to 0.03 m/s, cap bubble flow occurs. A transition to elongated bubble flow is observed in the region between 0.08 m/s and 0.15 m/s. Slug flow occur at 0.3 - 0.5 m/s and is present until superficial gas velocity is equal $6m/s$ where the transition to annular flow occurs.

Figure 4.6 shows the flow regime map for **45**° and severe slug flow occurs in the region with low superficial oil and gas velocity, in the same area were elongated bubble flow existed for the angles $10° - 30°$. Low superficial gas velocity, 0.03 m/s-0.17 m/s, combined with a greater value of oil grants cap bubble flow. In the region of U_{SG}=$0.3 - 4.9m/s$, slug flow is present. As Figure 4.7 illustrates, the region where slug flow occurs is shifted to $U_{SG} = 0.7 - 7m/s$ for inclination angle **60**°, however there is one point with slug flow at low oil rate and $U_{SG} = 0.3m/s$. At 60°, the region with severe slug flow grasps a larger range of superficial gas velocity compared to inclination angle 45° and also 70°. Annular flow is present for U_{SG} above 7 m/s.

Bubble flow does not appear in the flow regime maps for **70**° and **78**°. Bubbles can however occur in the severe slug flow regime, but from what is revealed from the previous flow regime maps, the area of bubble flow shrinks with increasing inclination angle. At 70° inclination, severe slug flow occurs for low flow rates of air, at a wider range of oil rates compared to 60°. Slug flow transition occurs at superficial gas velocities approximately equal 0.25 m/s and 0.6 m/s for higher oil flow rates. The slug flow continues until U_{SG} reaches 3.4 m/s and churn flow appear at $U_{SG} = 2.3m/s - 4.9m/s$. This is the fist angle at which churn flow appear, which is similar to results in Barnea et al. (1985). The onset to churn flow is at higher superficial gas velocities at 78° compared to 70°. Even though previous studies found that churn flow exist for $70° - 80°$ it is not possible to have any knowledge of the flow regimes after 78, and experiments up to 90 degrees should be conducted to confirm the appearance of churn flow. In addition, a smaller inclination angle interval is necessary to predict when this will take place for the first time between the inclination 60° and 70°.

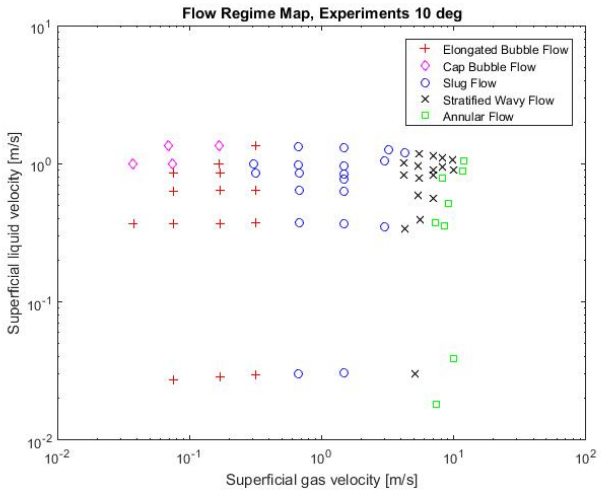

Figure 4.1: Flow regime map 10° inclination.

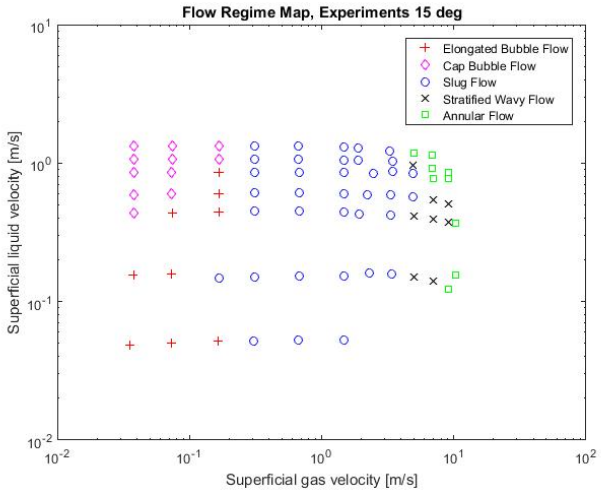

Figure 4.2: Flow regime map 15° inclination.

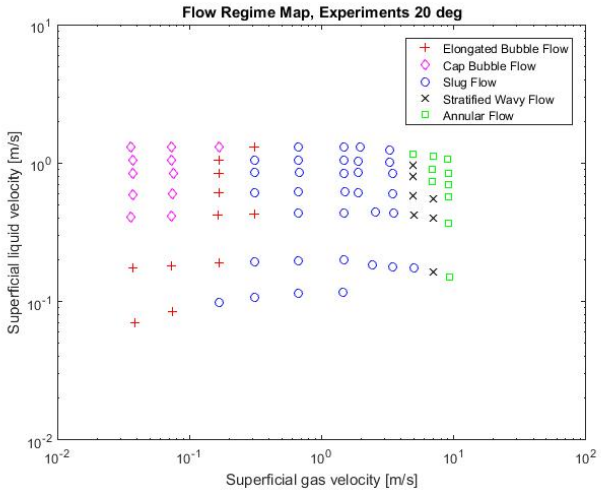

Figure 4.3: Flow regime map 20° inclination.

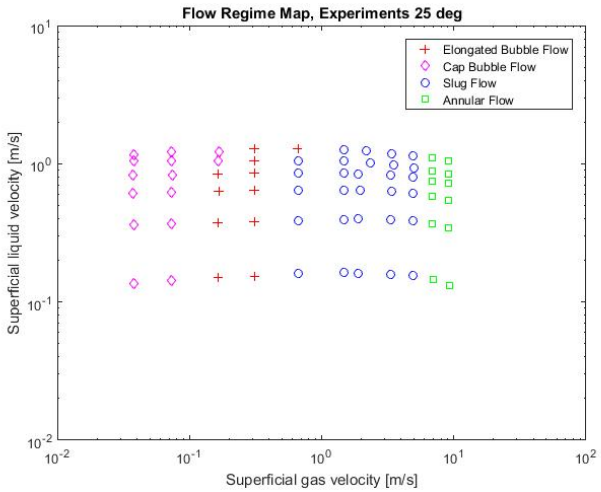

Figure 4.4: Flow regime map 25° inclination.

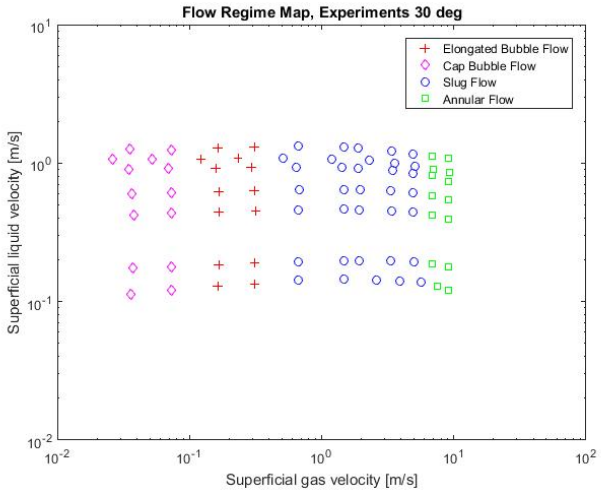

Figure 4.5: Flow regime map 30° inclination.

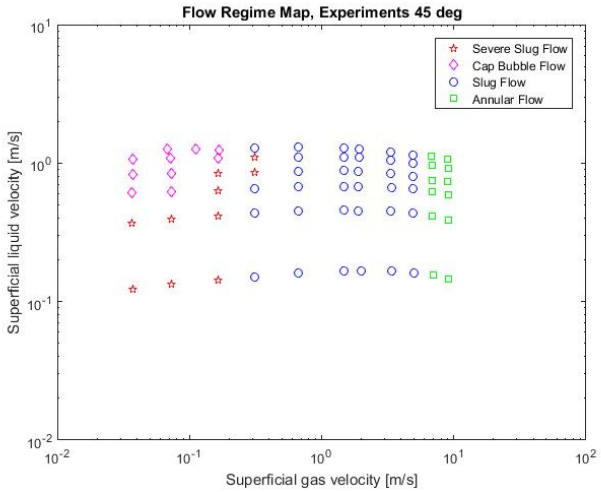

Figure 4.6: Flow regime map 45° inclination.

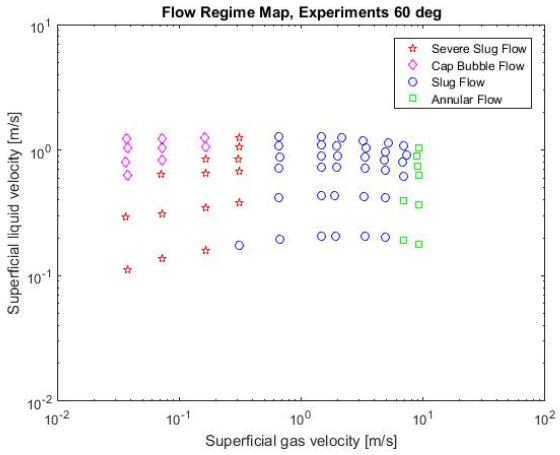

Figure 4.7: Flow regime map 60° inclination.

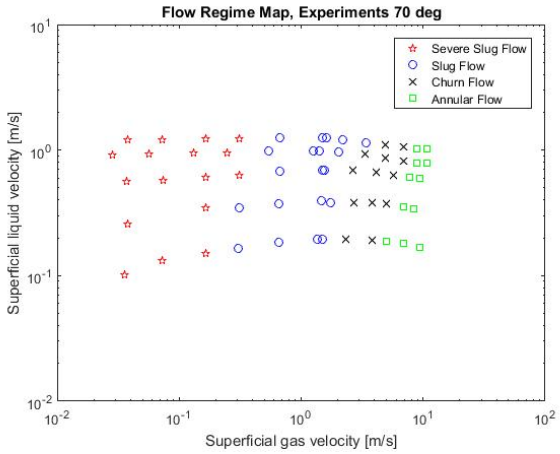

Figure 4.8: Flow regime map 70° inclination.

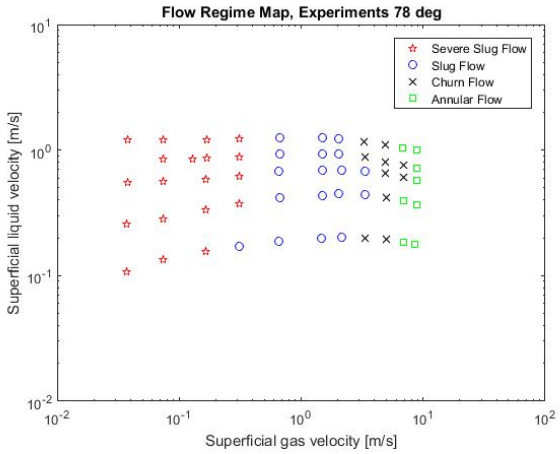

Figure 4.9: Flow regime map 78° inclination.

4.2 Experimental Results Pressure Drop, Capacitance and Flow Rates

Table 4.2 provides the outlined results from the experiments as a continuation of the test matrix in Table 3.6. The entire data set is provided additionally to the thesis and an overview of the files is seen Table F.1.

A sample of the processed raw data of the differential pressure transmitter and capacitance sensor for inclination angle 15° and 45°, and processed flow rates of 45° and 60° can be seen in Appendix E. This is included to illustrate how differential pressure, capacitance and flow rates vary with time. Overall, it is seen that the capacitance and pressure drop vary with interdependence, hence, decrease in value for increased air flow rate. Also, the pressure difference is highly dependent on the fluctuations of flow rate, particularly for severe slug flow. Liquid holdup and pressure drop values presented in the thesis are based on calculations of the average of these fluctuations.

Figures E.1-E.10 are results from 15° angle at an oil flow rate equal 3500 kg/h. For each combination of flow rates there are two figures of both pressure and capacitance, where the first is pressure and capacitance measurements over longer periods of time compared to the last two. Figures E.1-E.4 at 15° show pressure and capacitance for elongated bubble flow where capacitance values ranges from 4.5 V to 10 V and small pressure drop. Air flow rate increases and slug flow occur with slightly higher pressure drop and less frequent capacitance fluctuations. The capacitance ranges from 3.5 V to 4.5 V in annular flow which is reasonable compared to the values for elongated bubble flow.

Figures E.17-E.20 show 45° angle for oil flow rate equal 11000kg/h. Cap bubble flow occurred for air flow rate 7.5 kg/h. The voltage fluctuates from maximum conductivity, that corresponds to full liquid bridging, to low conductivity which corresponds to a gas dominating phase passing the probes. In cap bubble flow, while having the bubbles, there is still a liquid flow at the bottom of the pipe, which prevents the capacitance sensor reaching the minimum voltage. The pressure signal provides similar shaped curve. The transition to slug flow is also observed very clearly as the voltage fluctuation becomes more frequent, and the pressure drop amplitude decreases. Annular flow is discovered for gas flow rate equal 19 l/s. The high gas flow rate provide low voltage signals, however it can be seen short pulses at which a oil lump is swept around the periphery. The minimum and maximum pressure drop is equal at $m_{SG} = 7.5kg/h$ and $19l/s$, which is cap and annular flow respectively. The fluctuations are however more chaotic in annular flow.

Oil flow rate equal 3000 kg/h is presented in Figures E.13-E.16. Air flow rate equal 7.5 kg/h has similar shape as cap bubble flow at oil flow rate 11000 kg/h, however it represents severe slug for oil flow rate 3000 kg/h. In this case it provides larger pressure drop values. Similar changes can be seen in the transition to slug flow as for oil flow rate

11000 kg/h. Pressure drop results for oil flow rate at 3000 kg/h and air flow rates at 13.8 kg/h and 19.4 kg/h is mostly out of range for 45° angle. Also, at maximum pressure drop curves are flat on the top, which indicates that it is out of range This is the case for several flow rates at higher inclination angles. For that reason, the values obtained by the pressure transmitters at higher angles are not displayed. Only a few conditions were within the range at high inclinations. These are included in chapter 5.3.3. Figure E.21 show large fluctuations in the oil flow rate for severe slug compared with slug flow. The effect on the pressured drop due to fluctuating oil flow rate can be seen in Figure E.22.

At 60° angle severe slug occur and Figure E.23 show large fluctuations in the oil flow rate compared with the other flow regimes. Differential pressure transmitters are out of range in this angle.

Case no.	Angle [°]	Average Q_L $[kg/h]$	Q_G	Min/Max dP $[mBar]$	Min/Max flow rate	Comments
1	15	3500	$9.4l/s$	$-10/+20$		
2	45	3000	$7.6kg/h$	$-5/+46$		Severe slug flow causes large pressure drop.
3	45	3000	$13.8l/s$			Pressure drop out of range.
4	45	3000	$19.4l/s$			Pressure drop out of range.
5	45	11000	$7.5kg/h$	$-18/+20$		Cap flow.
6	45	11000	$19.0l/s$	$-18/+20$		Annular flow
7	60	3200	$3.3kg/h$		2300/3600	Severe slug flow. Pressure out of range for all Q_G.

Table 4.2: Experimental pressure and flow regime results.

4.3 Experimental Results Liquid Holdup

The liquid holdup at flow regime transitions are calculated with average values and the s-curve relation from Figure 3.19 and displayed in Tables 4.3-4.5.

Angle [°]	Liquid holdup [−]
10	0.098
15	0.093
20	0.132

Table 4.3: Stratified-annular flow transition.

Angle [°]	Liquid holdup [−]
10	0.80
15	0.99
20	0.87
25	0.75
30	0.80
45	0.86
60	0.97

Table 4.4: Bubble-slug flow transition.

Angle [°]	Liquid holdup [−]
10	0.49
15	0.47
20	0.40
25	0.31
30	0.33
45	0.36
60	0.31
70	0.37
78	0.38

Table 4.5: Slug-annular flow transition.

The no slip liquid holdup and actual liquid holdup were compared as Figure 4.10 illustrate. The no slip liquid holdup was found from measured superficial velocities. Further, the corresponding voltage from the capacitance measurements was found. This voltage was used as input in the s-curve which gave actual liquid holdup. Figure 4.10a show liquid holdup in slug flow and Figure 4.10b show annular flow, at all inclination angles for selected no slip liquid holdup. The greatest deviaton between no slip and measured liquid holdup from capacitance sensor is at 0° for slug flow and 60° in annular flow. The smallest deviation is at 70° and 78° for slug flow. There is generally small deviations in annular flow and the inclination angles does not have a considerable effect in that case. Figure 4.10a show the same shape as Beggs et al. (1973), except at horizontal flow.

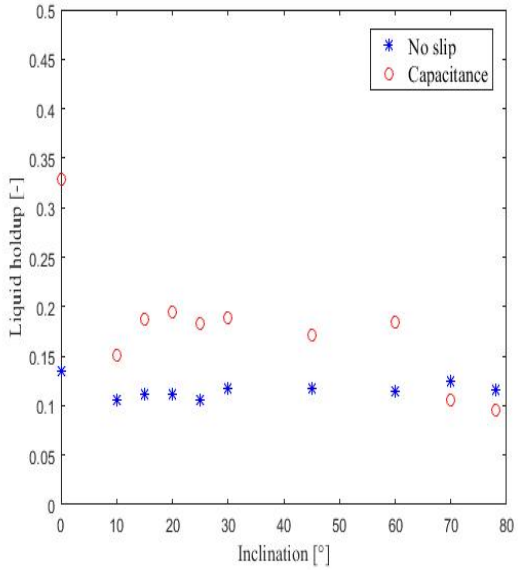

(a) Liquid holdup slug flow.

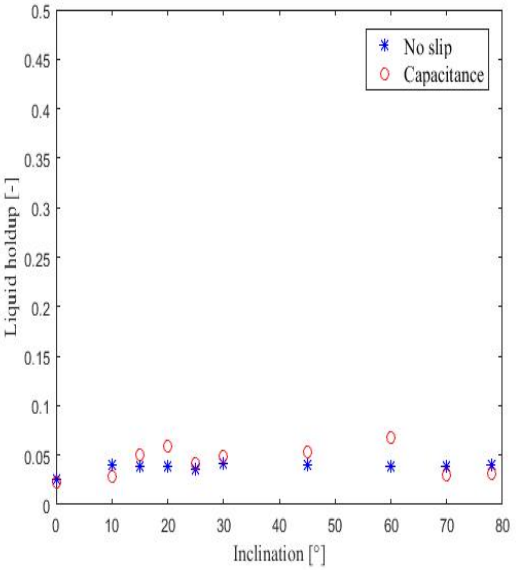

(b) Liquid holdup annular flow.

Figure 4.10: Liquid holdup for all pipe inclinations.

Chapter 5

Analysis

This chapter will start with some important operational considerations which arose during the experimental investigation. The next chapter will use the unified model of Barnea to analyze the flow regime and liquid holdup measurements. This will be an identification on the validity of the model. The last part will cover the comparison between the predicted results from OLGA and those from the experiments. This includes comparison and analysis of flow regime maps, liquid holdups and pressure drops.

5.1 Operational Considerations

A good reference point makes the validity more solid. In this case, it would be experiments in a horizontal pipe. However, with the existing design of the inclined test section, the only way to obtain a horizontal position is to lift the inlet section using a forklift. This resulted in a inlet test section 1.5 m above the ground, to ensure good drainage at the end of the test section. A complete flow regime map was not done for this inclination. However, all possible flow regimes with the current facility was found, and their corresponding data was documented.

Further, there were some considerations regarding the oil pump. One issue was the pump capacity which was not large enough to achieve the dispersed bubble flow regime. Another was for some transient flow regimes, especially for severe slug flow, where the flow rate varied a lot. In Appendix E, there are plots showing this. The flow rate also increased considerably when relatively small air flows was injected in the oil flow. For very large air flows, on the other hand, the oil flow rate decreased. Nevertheless, for most flow regimes, the oil flow rate was stable and did not increase or decrease with changing air flow.

A visual observation of flow regime patterns and transitions is not universal or general and this was no exception in the present work. In some cases it was difficult to distinguish between the flow regimes visually. An example is illustrated for 20° inclination in Figure

5.1, Figure 5.2 and Figure 5.3. This is an extreme case where the three flow regimes slug flow, stratified wavy flow and annular flow appear within a short time interval, the real time is presented in the figures. The input flow rates are $1500kg/h$ for oil and $19.2l/s$ for air. However, the stratified wavy part was more dominant and thus the flow regimes were specified with reference from pictures in section 3.1.6. Other researcher could classify this flow regime as wavy annular, (Barnea et al. (1980b) and Barnea et al. (1980a)). Barnea et al. (1980a) explains this as a type of flow with a film at the bottom of the pipe, while aerated unstable waves are swept around the pipe. This can make the flow appear both stratified wavy and slugging. It is close to stratified wavy since most of the liquid stays at the bottom of the pipe, but at the same time small amounts is swept around to wet the pipe with a thin film. The thesis do not include wavy annular in the flow regime determination, and the classification was between stratified wavy and annular.

Also, for some flow rates, the flow regime varied from the inlet of the test section pipe to the outlet. The recording was nevertheless done in the middle of the pipe for most inclinations. Uneven lightning from the environment outside caused different light exposing. This could in some cases make annular flow appear stratified due to shadow at the bottom of the pipe.

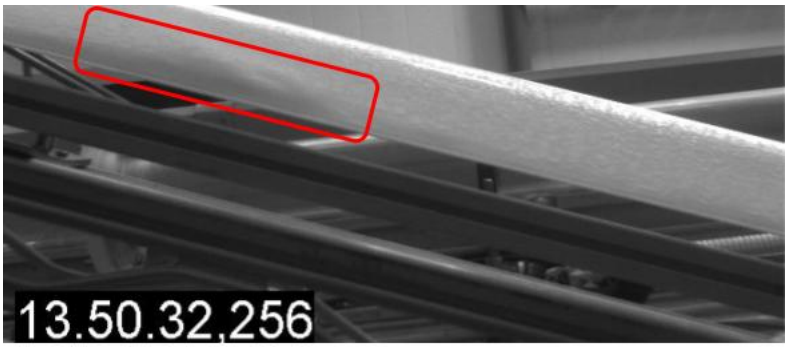

Figure 5.1: Slug flow.

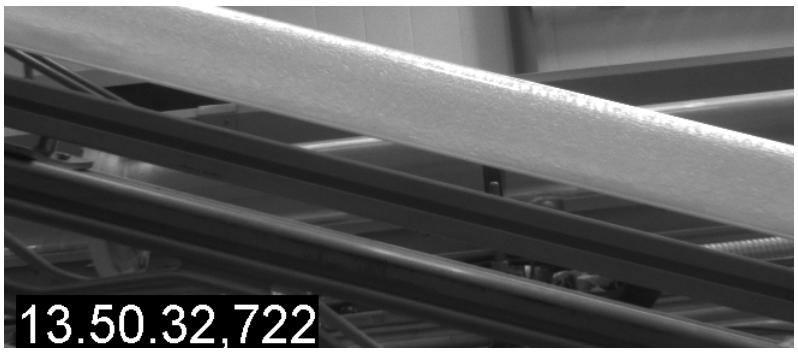

Figure 5.2: Annular flow.

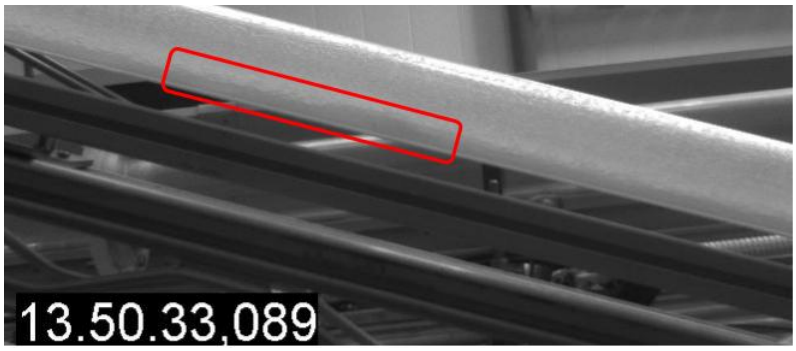

Figure 5.3: Stratified wavy flow.

Moreover, there were several concerns regarding the pressure difference measurements. Sources that could lead to inaccurate measurements are explained and summarized below:

1. The sensors are sensitive, and even vibration from the ventilation or loud noise could possibly influence the measurements. Deviation between the sensor and the logging device could cause small discrepancies as well.

2. The experience was that if the impulse pipes from the taps on the test section pipe to the transmitters were too long, the sensors did not provide accurate values. One reason could be larger frictional losses in longer pipes. The chance of having bubbles in the impulse pipes increases with length, even though the pipes were carefully investigated for bubbles. In addition, the valves and the pressure sensor itself could also contain air and had to be watched thoroughly.

3. The position of the pressure transmitters could be a source for discrepancies as well. The transmitters were mounted under the horizontal test section in the multiphase lab. It resulted in transmitters that were not located directly under the inclined test section pipe, which would minimize the distance between the taps and pressure sensors. However, it was considered to be sufficient as long as they were located below the test section pipe in elevation. They were also not moved due to concerns related to high vibration in the inclined test section pipe at high air flow rates.

4. Discrepancies in pressure measurements could be caused by inaccurate flow meter measurements.

5. There could be uncertainties due to the assumption of neglecting the surface roughness. The assumption is considered to be valid due to the acrylic material of the pipe, which has a very low surface roughness, and the fact that oil flow in most of the investigated cases can be considered as laminar.

6. There are additional uncertainties regarding the pressure loss than the surface roughness, an example is interfacial friction factor.

5.2 Barnea (1987) Comparison with Experimental Results

This section will discuss the experimental results compared to the unified model which is explained in section 2.3.1. The aim is to check the validity of the model and try to find the range of inclination angles for which the model can be considered valid. Barnea et al. (1980b), already concluded that the model is remarkable for air/water up to 10° inclination. However, they state that angles $10° - 30°$ are more uncertain.

5.2.1 Barnea (1987) Flow Pattern Map Comparison

The marks represents the experimental data while the lines are the transition boundaries modelled in Matlab using the criteria and equations from the unified model. The results for all inclination angles are plotted in Figures 5.4-5.12. The unified model does not consider elongated bubble flow. However, it can be seen as a transition flow regime from bubble to slug flow, where the bubbles gets longer and longer for increasing gas flow rate until the liquid film beneath the bubble gets small enough for slug flow to occur. It is also known that dispersed bubble flow was not achieved in either experiments, which is confirmed with the transition line from the unified model which is located above the maximum U_{SL} for all inclination angles. The next step is to determine stratified-non stratified transition, which is equivalent with transition A in Figure 2.8. Since there were no observations of smooth stratified flow during the experiments, there is no modelling regarding the stratified smooth-stratified wavy transition. Moreover, the annular-intermittent transition is represented in all flow regime maps. The transition occurs, when the the film is stable and do not block the gas core and when backflow in the liquid film is prevented. The bubble flow exists where criteria 2.24 and 2.25 are fulfilled, and the transition line is determined by Equation 2.27, transition B in Figure 2.8. Criteria 2.25 was not met for inclination angles 10° and 15°. Consequently, bubble flow transition line is absent in Figures 5.4 and Figure 5.5.

Figure 5.4 at inclination angle **10**° provides a sufficiently good correlation between the unified model and experimental results for the annular-intermittent transition although small deviations can be observed for high liquid flow rates. On the other hand, the stratified flow transition curve does not fit the experimental points accurately as the flow regime is observed at higher liquid flow rates compared to what the model of Barnea (1987) states.

At inclination angle **15**°, the stratified transition curve shows a better fit, mostly due to experimental data which is more accessible for comparison because of lower values of oil flow rate. The trend for stratified flow regime is satisfying compared to the transition curve,

however, it could be beneficial with superficial oil velocity values between $0.2 - 0.4m/s$ to be more certain of the stratified-annular flow transition. Measurements conducted at low flow rates shows adequate agreement with the stratified-annular transition curve, and as discussed in section 5.1, the transition between stratified and annular flow was in some cases unclear which means the flow regimes in this area could be classified differently by other researchers.

Bubble flow transition occurs for the first time at inclination angle **20**°. The transition curve from bubble flow to slug flow is an acceptable fit, however there are a few deviations according to Equation 2.27 if assumption $\alpha_c = 0.25$ yields. According to the unified model, a superficial gas velocity at 0.17 m/s should equal $U_{SL} = 0.46m/s$ at transition as well as a superficial gas velocity at $U_{SG} = 0.3m/s$ should equal $U_{SL} = 0.85m/s$. As can be seen in Figure 5.6, this responds with the experimental points $U_{SG} = 0.17m/s$ and $U_{SL} = 0.42m/s$, and $U_{SG} = 0.3m/s$ and $U_{SL} = 1.2m/s$, respectively. Nevertheless, it means flow regimes below the mentioned points should be slug flow, and it can be seen that there are two experimental points which deviates as they are observed as elongated bubble flow. As mentioned, elongated bubble flow could under both categorizes. Further, does stratified flow transition from the experiments agree quite well the modelled transition line.

The bubble flow transition curve moves slightly to the right, as can be seen in Figure 5.7, when the inclination angle increase to **25°.** The modelled curve satisfy the experimental data quite well, even though the curve fits the cap bubble flow regime better for low oil flow rates. However, most of the line goes through the area of elongated slug flow. The compliance for the transition curve from slug flow to annular flow is acceptable for superficial oil velocity up to 0.55 m/s. For greater values, the unified model indicates slug flow while experiments showed annular flow. The unified model confirms that there is no occurrence of stratified flow for inclination 25° or above, which is correct compared to the experimental results.

For inclination angle **30**° in Figure 5.8, $U_{SG} = 0.3m/s$ combined with $U_{SL} = 0.7m/s$ provides the transition for bubble-slug in the unified model, which is close to the transition from elongated bubble to slug flow at $U_{SG} = 0.3m/s$ and $U_{SL} = 0.65m/s$ in the experimental results. However, all U_{SL} combined with U_{SG} lower than 0.3 should, according to the unified model, correspond to a slug type of flow. In the experiments many of these points is defined are elongated bubble flow. Experimental values above the bubble line is a good fit compared with the unified model. When it comes to annular flow, the lowest value of U_{SG} that provides this flow regime is $U_{SG} = 8m/s$, according to the unified model. At $U_{SL} = 0.25m/s$ the curve for stable annular configuration turns right, which makes the transition to annular flow occur at even higher superficial gas velocities. From the experimental results it can be seen that a superficial gas velocity equal 8 m/s provides annular flow for U_{SL} up to $1.2m/s$ which is considerably higher than the model. Yet, the

trend follows the unified model at low oil flow rates from approximately 0.1 m/s to 0.6 m/s even though it would be more certain if points between $U_{SL} = 0.2 - 0.4m/s$ was measured.

The flow regime map for **45**° inclination, which is illustrated in Figure 5.9, show the annular transition curve from the unified model to the right compared with the previous inclination angle, occuring at $U_{SG} > 10m/s$. The experimental data does not capture the switch. Nor oil or gas flow rates measured are high enough to fall within this boundary. Indeed, this result yields for all inclinations greater than 45°. Slug flow occur at $U_{SL} = 1.5m/s$ at $U_{SG} = 0.3$ experimentally, while in the unified model the highest value of U_{SL} for the same value of U_{SG} equals 7.8 m/s.

The modelled bubble flow curve at 60° fits the experimental results well, with an exception of the experimental point $U_{SG} = 0.3m/s$, $U_{SL} = 0.4m/s$ at which severe slug flow was observed. The unified model indicates that all values below $U_{SG} = 0.3m/s$ and $U_{SL} = 0.6m/s$ should be slug flow. The modelled transition curve for bubble-slug flow at **70**° fits the points of transition from experiments even better than 60°, which Figure 5.11 indicates. This yields for **78**° as well, where there are experimental points at that deviates slightly from the modelled curve, except a larger deviation in the point at $U_{SG} = 0.3m/s$, $U_{SL} = 0.35m/s$ which should have been slug flow according to Barnea (1987).

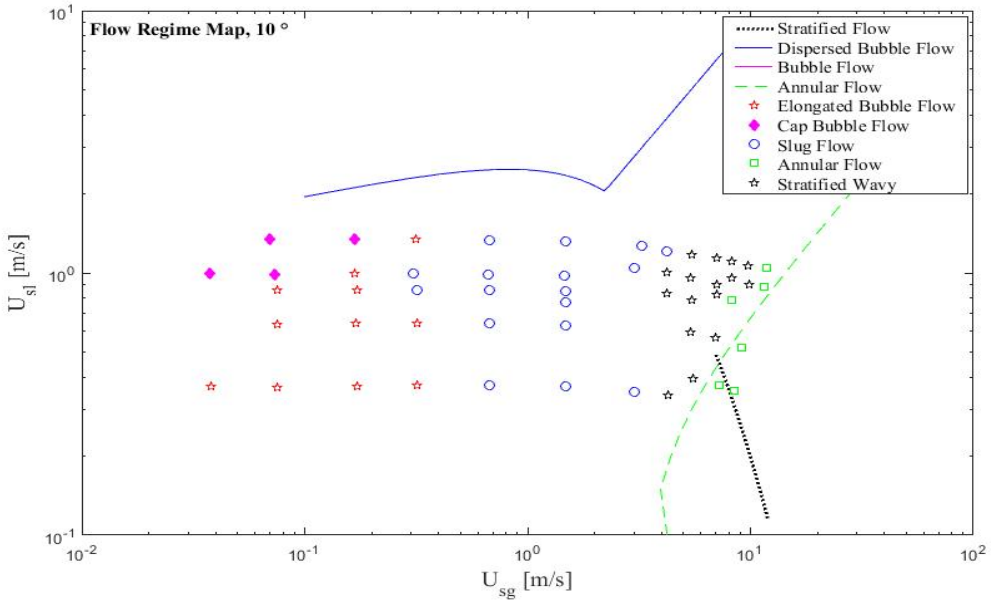

Figure 5.4: Barnea (1987) flow pattern map comparison at 10°.

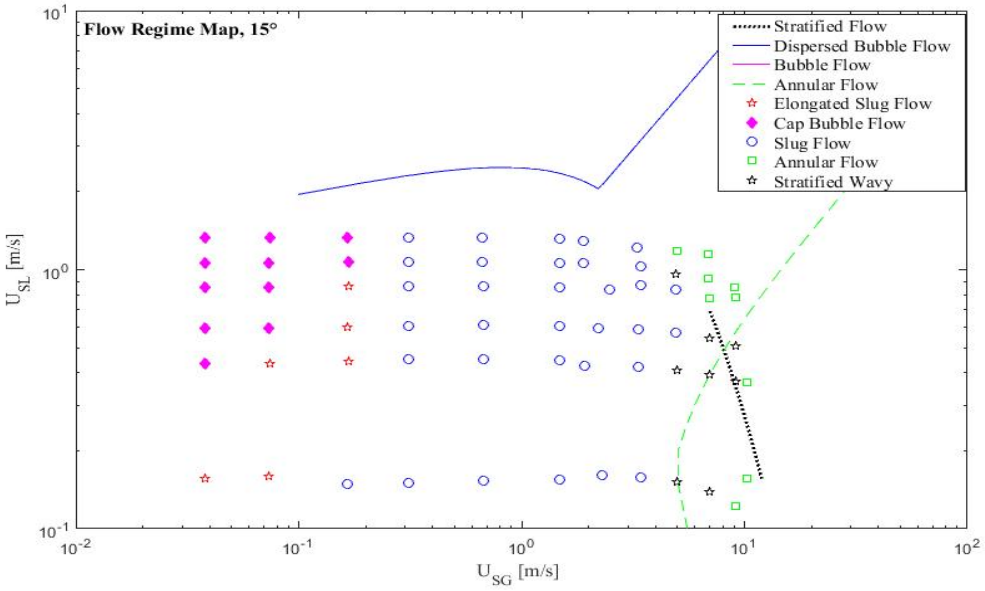

Figure 5.5: Barnea (1987) flow pattern map comparison at 15°.

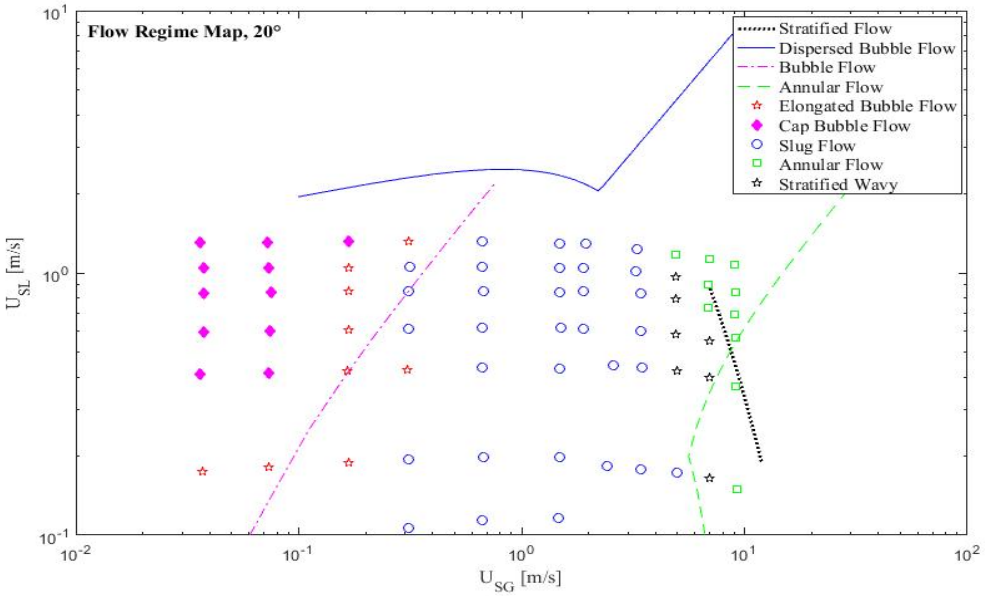

Figure 5.6: Barnea (1987) flow pattern map comparison at 20°.

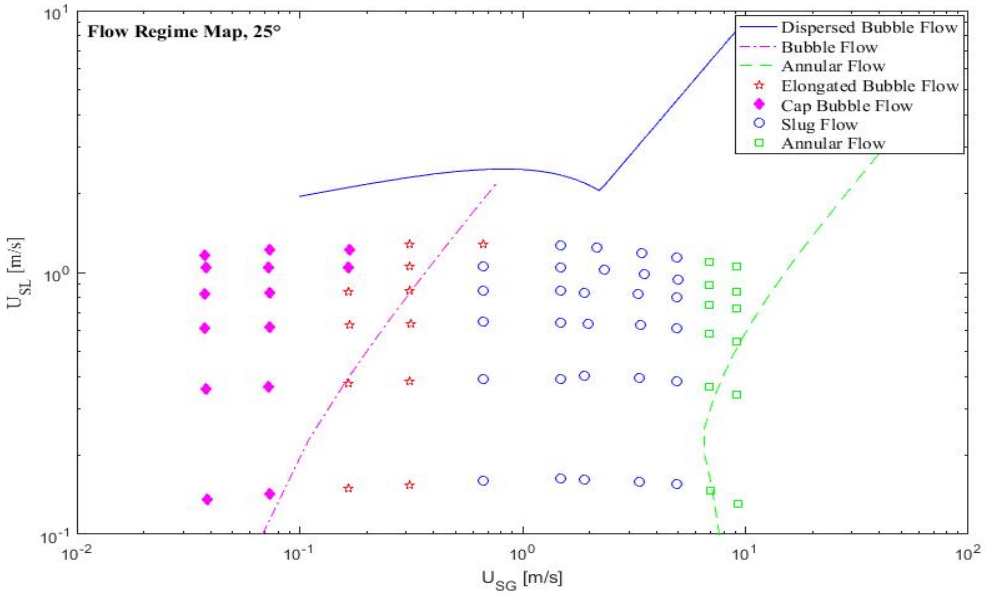

Figure 5.7: Barnea (1987) flow pattern map comparison at 25°.

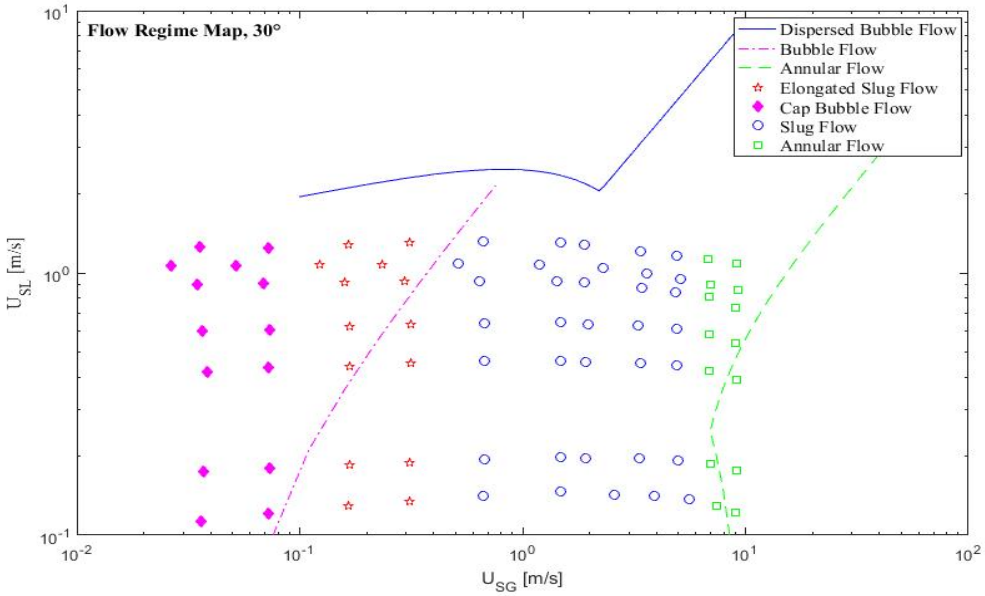

Figure 5.8: Barnea (1987) flow pattern map comparison at 30°.

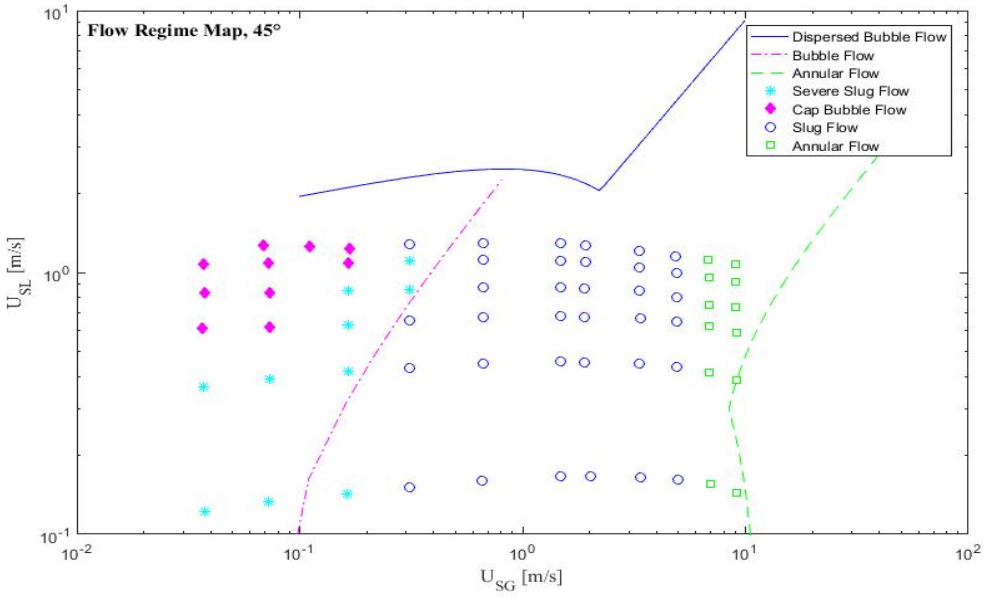

Figure 5.9: Barnea (1987) flow pattern map comparison at 45°.

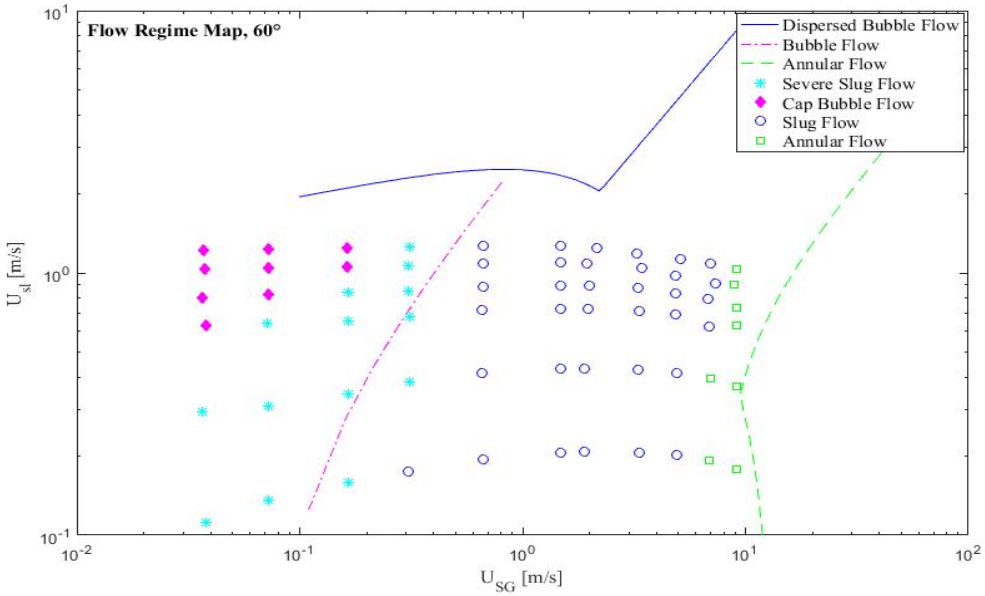

Figure 5.10: Barnea (1987) flow pattern map comparison at 60°.

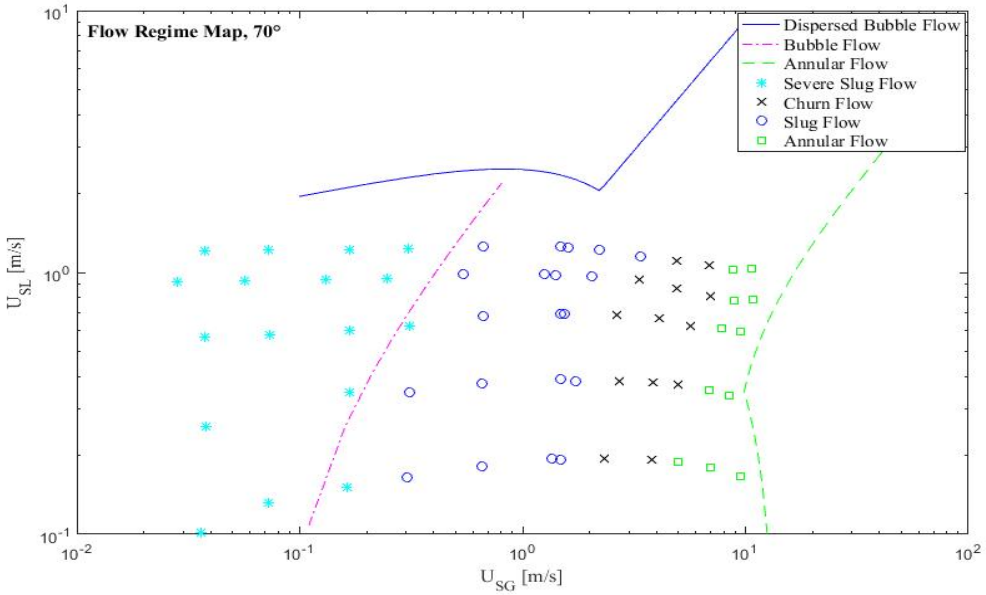

Figure 5.11: Barnea (1987) flow pattern map comparison at 70°.

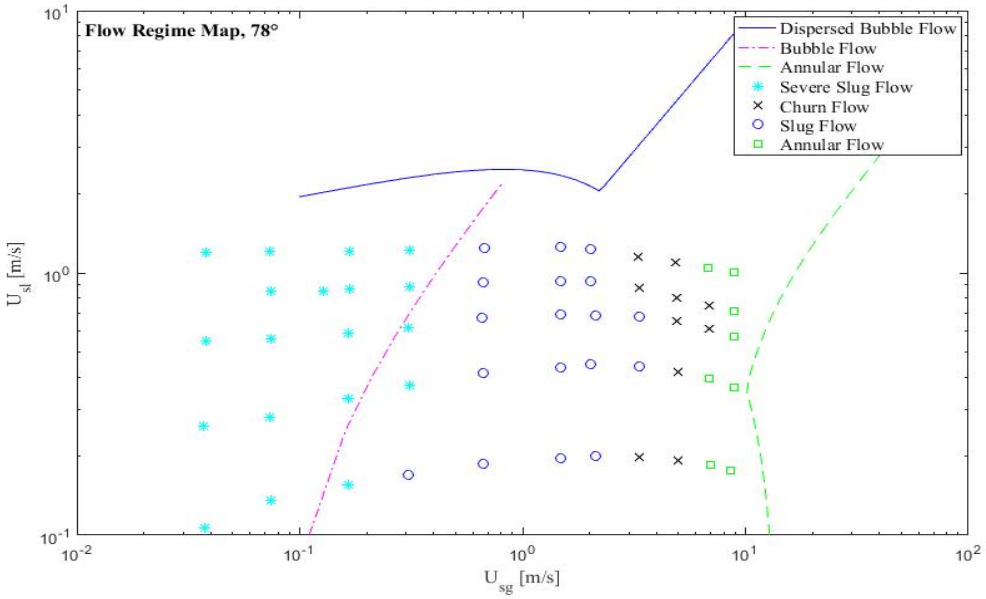

Figure 5.12: Barnea (1987) flow pattern map comparison at 78°.

5.3 OLGA Modeling and Comparison

5.3.1 Flow Regime Comparison with Experimental Results

Overall, the flow regime map predictions in OLGA is not in sufficient agreement with measurements. Similarly to the Barnea (1987) unified model, OLGA predicts the transition to annular flow at higher gas flow rates compared with the experiments. In fact, annular flow exists at superficial gas velocities so high that it is out of range for the presented flow regime maps for inclination angles $10° - 45°$. An explanation for this could be the set conditions for annular flow which is more conservative in OLGA, as discussed in section 2.3.2. For example, it was observed, however not displayed here, that annular flow occurs at superficial gas velocities above 200 m/s at inclination 10°. For the inclination angles, $10° - 45°$, OLGA predicts stratified wavy flow for considerably higher inclinations than in the measurements. The stratified-wavy line in OLGA is closer and similar to the annular transition in the experiments. Barnea et al. (1980b) explains that the annular flow regime could be designated as wavy annular which is characterized by an unstable wavy liquid film around the pipe circumference. This could mean that the transition line is a question about flow regime definition. Figures 5.13-5.18 show that OLGA predicts stratified wavy flow from inclination $10° - 45°$, whereas the same flow regime disappeared at inclination angles above 20° in experiments. From 45°- 60°, the stratified wavy line switches to annular flow.

The agreement with the experimental map is quite good for slug flow at inclination 70° and 78°, although OLGA predictions are more adequate at 78° then 70°. The OLGA predictions are generally not in good agreement with the measurements for slug-annular flow at these inclination angles. OLGA requires significantly higher superficial gas velocity, up to 50 m/s, and the lowest onset to annular flow is at 10 m/s. The experimental measurements had onset at 5 m/s for these inclination angles. However, for low oil flow rates, the OLGA predictions are quite accurate for 60° inclination, but still the predictions requires slightly more gas flow to obtain annular flow.

Overall, the predictions for slug-annular transition is not in good agreement with inclination angles from $10° - 60°$. In the region at which slug flow exist in the measurements, the onset to slug flow is at superficial oil velocity between $1.0m/s - 1.3m/s$, while OLGA predicts no slug flow below 1.5 m/s for superficial gas velocities at approximately $0.7m/s - 3.0m/s$. The same yields for slug-stratified wavy transition which occur at greater air rates in the OLGA prediction throughout angle inclinations $10° - 45°$. This can be explained with the difference of stratified wavy and annular flow definition.

Comparison with the experiment could be improved if OLGA provided extended flow regime description. The experiments separated between elongated and cap bubble flow in addition to slug, severe slug and churn flow.

Although the flow regimes and the transitions disagree with OLGA predictions in many cases, the experimental results are considered as reasonable. OLGA is based on different criteria and also experiments from other facilities which could explain the difference in the results.

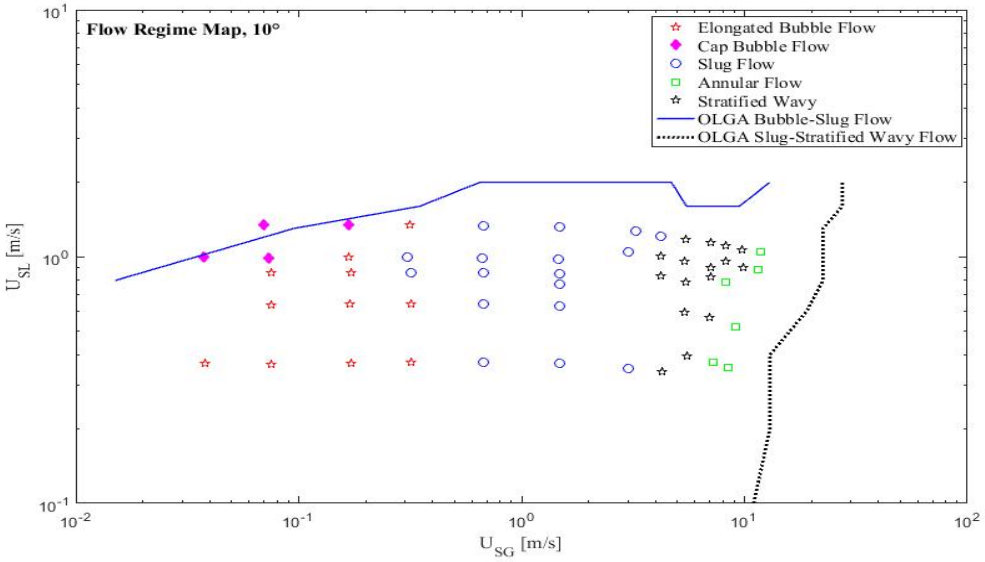

Figure 5.13: Flow regime map compared with OLGA at 10°

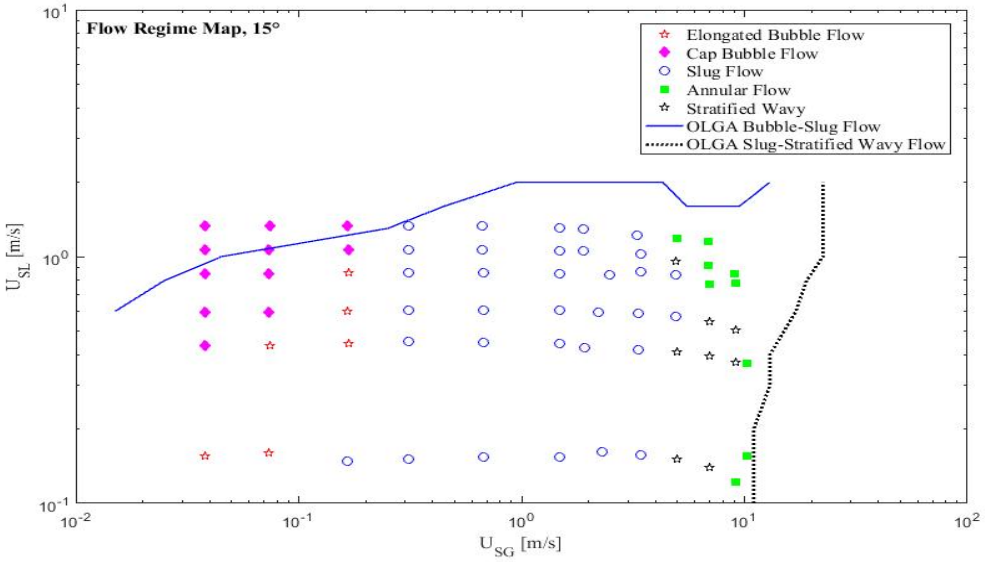

Figure 5.14: Flow regime map compared with OLGA at 15°

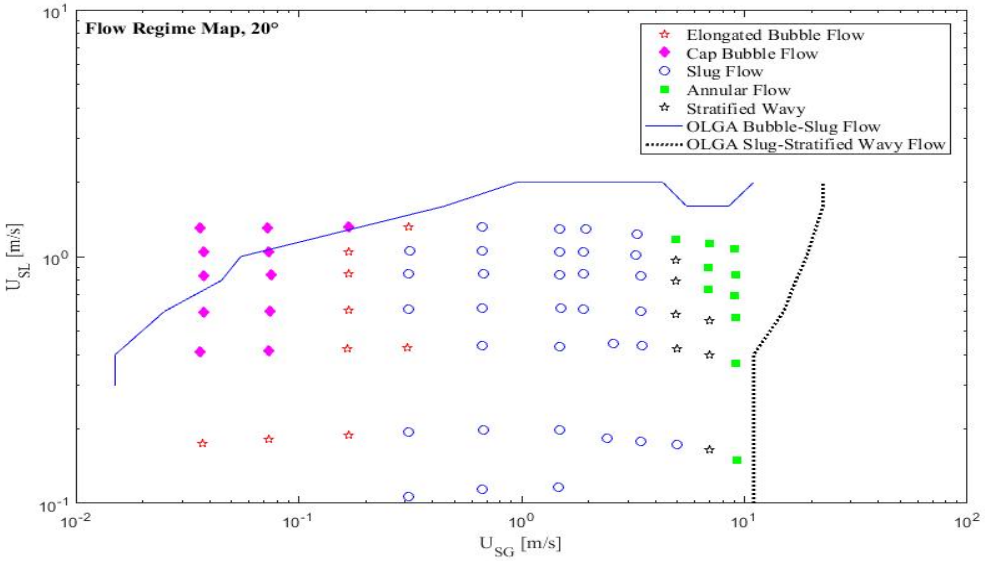

Figure 5.15: Flow regime map compared with OLGA at 20°

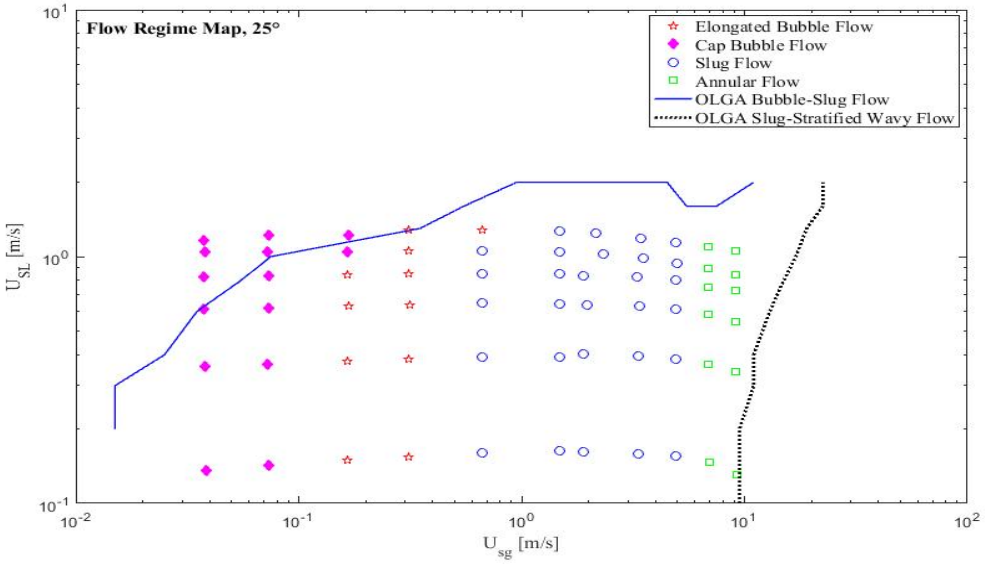

Figure 5.16: Flow regime map compared with OLGA at 25°

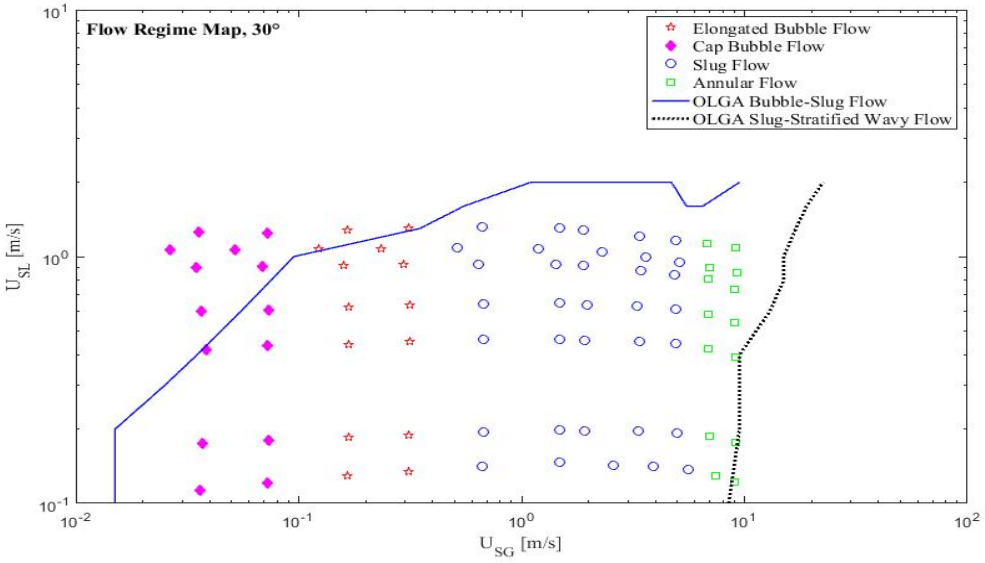

Figure 5.17: Flow regime map compared with OLGA at 30°

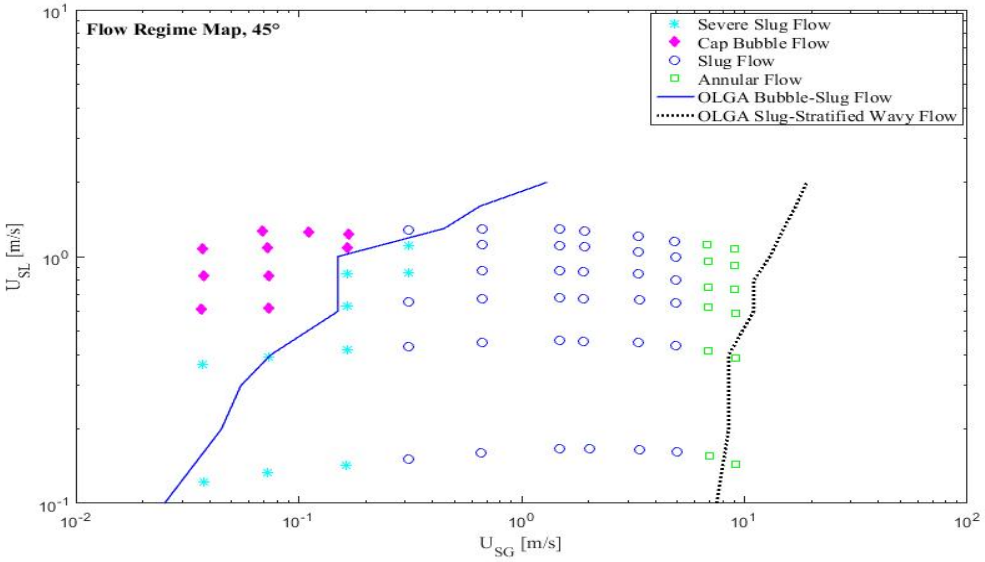

Figure 5.18: Flow regime map compared with OLGA at 45°

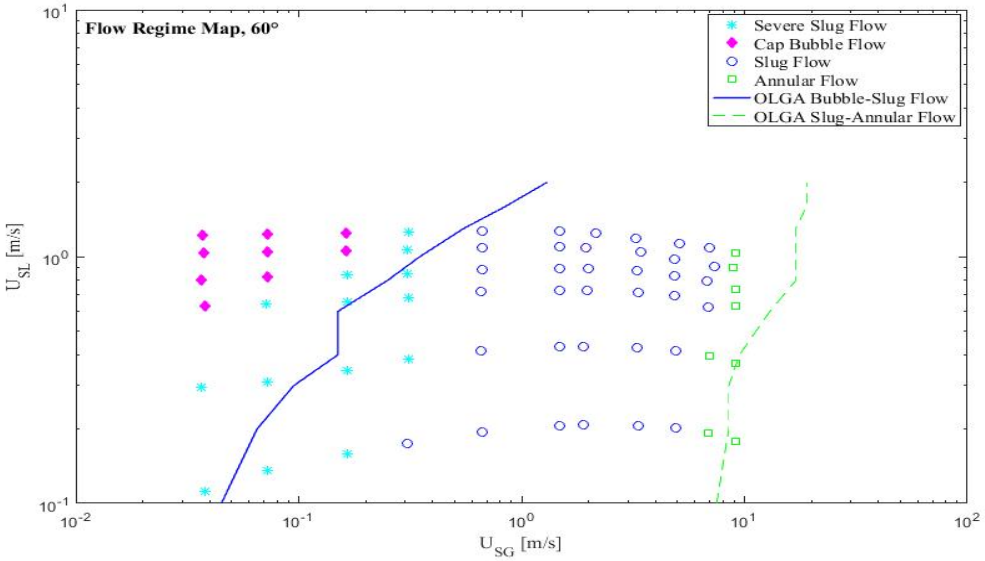

Figure 5.19: Flow regime map compared with OLGA at 60°

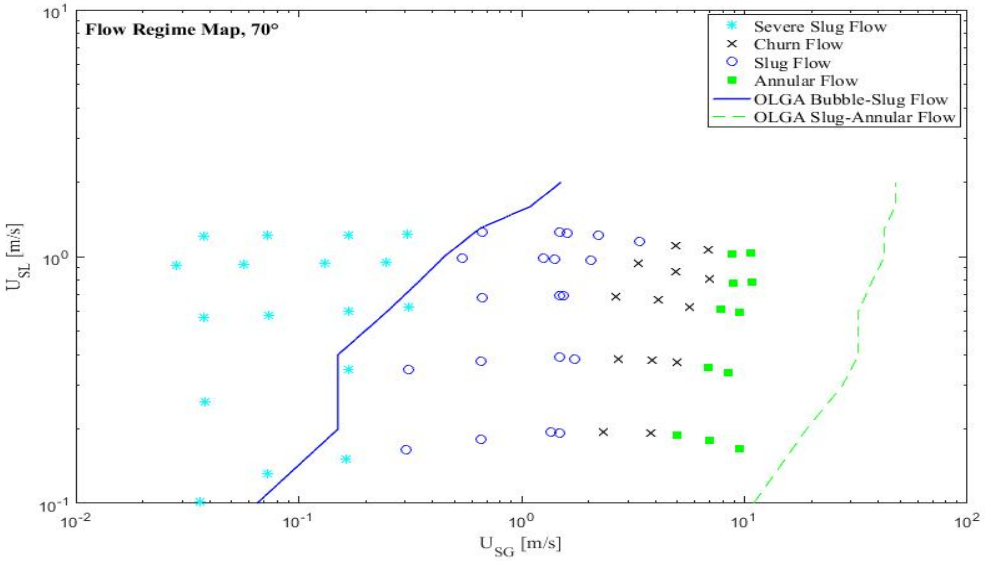

Figure 5.20: Flow regime map compared with OLGA at 70°

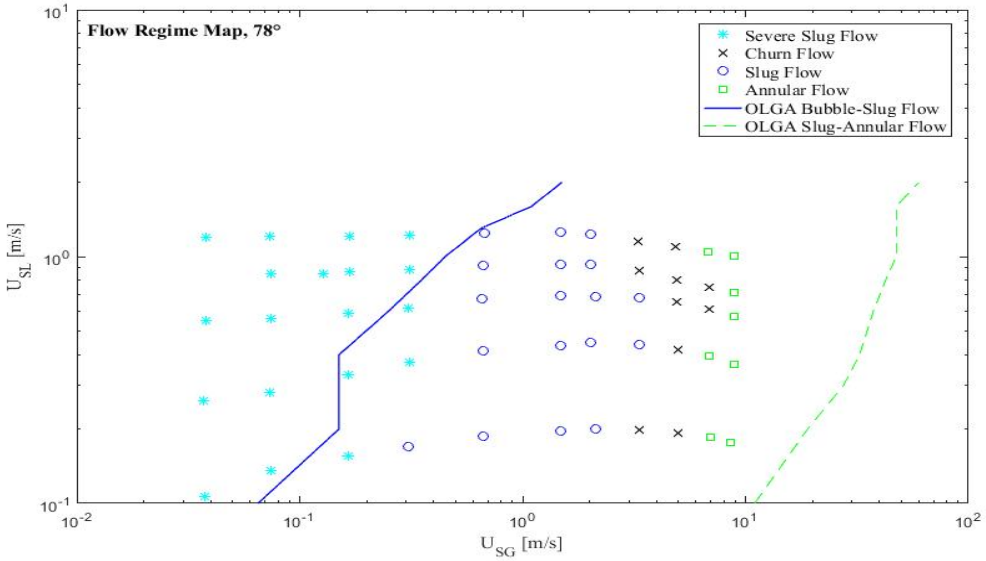

Figure 5.21: Flow regime map compared with OLGA at 78°

5.3.2 Liquid Holdup Comparison with Experimental Results

The liquid holdup in OLGA possesses higher values compared to experimental experimental data. In Figure 5.22 the no slip liquid holdup at selected flow rates studied is plotted to study the effect of inclination angle. The dotted curves are OLGA predictions while the filled lines are the measured values. Parameter c in Figure 5.22 represents the liquid content $Q_L/(Q_L + Q_G)$. Overall, it can be seen that the exprimental no slip liquid hold up is approximately equal at 0° and 78°. OLGA, on the other hand, predicts lower liquid holdup at angle 78° compared to 0° for liquid content $c = 0.65$ and $c = 0.08$. For liquid content $c = 0.11$, the greatest value of liquid holdup is at inclination angle 20°.

The overall trend in the comparison is that the no slip liquid holdup is higher in OLGA simulations compared to measurements. However, the experimental data is obtained from flow measurements, and not capacitance signals, such that the results can be presumed differently for capacitance measurements.

The liquid holdup from capacitance measurements were compared to OLGA as well. However, the liquid holdup deviated, especially for high gas velocities. This can be explained by the fact that the s-curve was developed for stratified flows. Therefore, the correlated s-curve was desired to be applicable for other flow regimes. From Figure 5.23 we can see that both curves have a exponential shape. The correlation was made by taking the difference between the respective exponential fitted curves, and calculate the new liquid holdup by adding the difference to the liquid holdup from the capacitance sensor. Equation 5.1 shows the correlation. The correlation was developed for angle 25°, but it was applied to the other inclination angles as well.

$$a_{Lnew} = a_{LCAP} + 0.7472 * e^{-0.9654 * U_{SG}} + 0.2186 * e^{-0.05905 * U_{SG}} - 0.6829 * e^{-4.583 * U_{SG}} - 0.3372 * e^{-0.604 * U_{SG}} \tag{5.1}$$

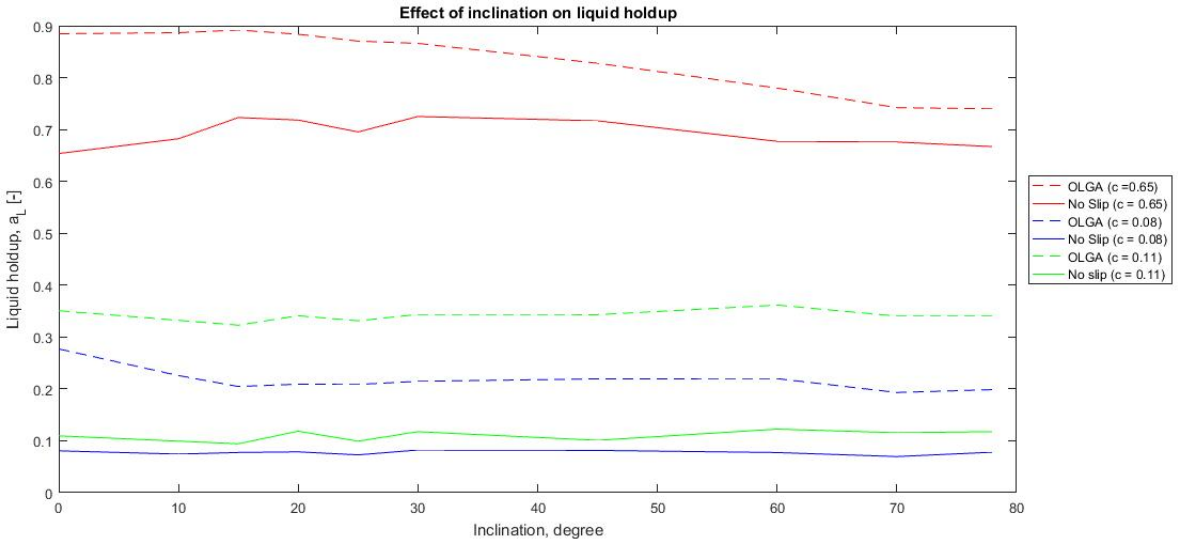

Figure 5.22: Liquid holdup fpr inclination angle $0° - 78°$.

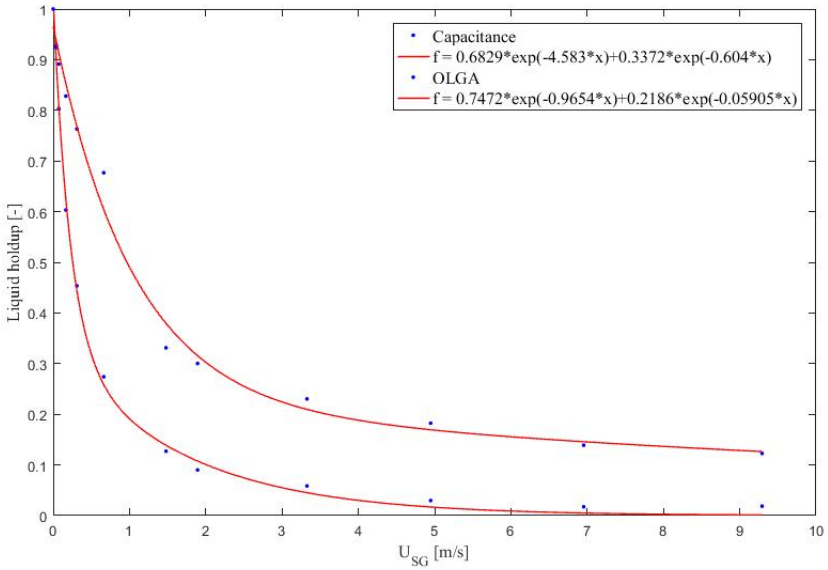

Figure 5.23: Liquid holdup from capacitance sensor and OLGA at 25°.

5.3.3 Pressure Drop Comparison with Experimental Results

In order to measure two-phase air-oil pressure drop it is important to understand where the liquid heights for the low and high pressure side of the PDT are. For a single oil flow,

the low and high pressure side will have the same liquid level, denoted in Figure 5.24b as h. As illustrated, the liquid level will be in the separator right after the test section. The reason is that the fluids in the pipe and the impulse pipes connected to the PDT is both oil. Therefore, the measured pressure drop will be equal to the frictional pressure drop. In the opposite case, where the fluid in the pipe is air, and the impulse pipes are filled with oil, will the measured pressure drop be close to the total pressure drop. The PDT-sensors will experience the height difference between the liquid level of the low pressure and high pressure side, denoted h_1 and h_2 in Figure 5.24a, in addition to the frictional loss. For two-phase flows, the flow in the pipe is simplified to be a mixed phase and the measured pressure drop can be expressed as following

$$(\frac{dP}{dL})_{mea} = (\frac{dP}{dL})_{fric} + (\rho_L - \rho_m)gsin(\beta), \tag{5.2}$$

where the mixed density is defined as

$$\rho_m = \alpha_L \rho_L + (1 - \alpha_L)\rho_G. \tag{5.3}$$

The pressure loss due to gravitation becomes

$$(\frac{dP}{dL})_{grav} = \rho_m gsin(\beta), \tag{5.4}$$

and the total pressure loss

$$(\frac{dP}{dL})_{tot} = (\frac{dP}{dL})_{mea} - \rho_L gsin(\beta). \tag{5.5}$$

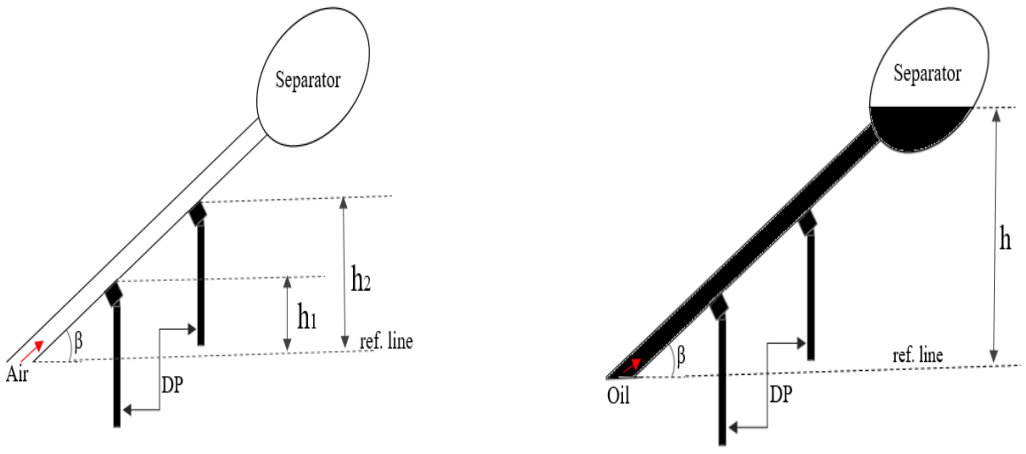

(a) Empty test section pipe.

(b) Filled test section pipe.

Figure 5.24: Illustration of measured pressure drop for empty and filled pipe.

For separated phases, as annular and stratified flow, the described approach can be inaccurate since the fluids will have different liquid level. However, in the thesis, the explained consideration, and the described equations for all flow regimes, were applied. The measured pressure drop was corrected for non-zero value at zero flow, which was found during the calibration.

In all of the pressure gradient plots, means a negative pressure gradient a pressure loss while a positive pressure gradient will mean gained pressure. Figure 5.25 show the measured pressure drop from PDT 4.02 and PDT 4.03 at 0° inclination at a superficial oil velocity of 0.31 m/s. The measured pressure drop is the same as the frictional pressure drop, which also equals the total pressure drop, because the inclination angle is zero. In this particular case, PDT 4.02 reached its maximum pressure gradient at $-1249.6 Pa/m$, at a superficial air velocity around $9 m/s$. The predicted pressure gradient from OLGA is also included in the figure, and for low superficial air velocities, the measured and predicted pressure gradient are within a reasonable range. For high air flow rates, on the other hand, the difference between OLGA and experiments is significant.

Figure 5.26 - 5.29 show the measured frictional, gravitational and total pressure drop for a fixed oil flow rate at 15°, 30°, 45° and 60° angles. The figures also contains the predicted pressure gradient from OLGA. For angles 15°, 30° and 45°, the superficial oil velocity is fixed within a range of 0.8 - 0.9 m/s. For 60°, the pressure drop exceeded the limit of the PDT 4.02 sensor at 0.8 m/s. A superficial oil velocity of 1.07 m/s is therefore used for this angle.

The first observation is the single oil flow pressure drop, $U_{sg} = 0$, where OLGA simulations and the experiments agrees. The pressure drop also increases with increasing angle for single oil flow. The gravitational pressure gradient is relatively easy to predict since it only differs upon liquid holdup calculation. Liquid holdup is achieved by using the s-curve obtained from the capacitance sensor with a correlation for the flow regime. Overall, the predicted and the measured gravitational pressure gradients agrees with each other. However, the experimental liquid holdup is not very good approximated for low gas velocities, which gives an U-shape in the curve. The deviation in the correlated liquid holdup also affects the frictional pressure gradient, giving an opposite U-shape for the experimental curve. Despite the U-curve and difference in pressure drop values, the frictional pressure gradients provide the same trends. An increase in gas flow rate results in a larger frictional pressure drop. There is also an agreement upon the frictional pressure gradients at which become larger than the gravitational for high values of superficial gas velocities. However, the difference between the predicted and measured pressure gradient becomes large in this region. This also affects the total pressure gradients, making the difference similar to the frictional. A reason for these discrepancies could be the flow regime predicted in this region, where OLGA predicts the flow regime to be slug or stratified wavy flow, despite observed stratified wavy or annular flow regime. Another argument could be the liquid

level defined in the experiments, where the assumption of having a mixture is inaccurate.

Figure 5.30 - 5.34, show the total and frictional pressure gradient for three different superficial oil velocities at angles 15°, 25°, 45°, 60° and 78°. The pressure gradient increases for higher superficial liquid velocities for all inclination angles. For 60° and 78°, the pressure sensor reached its limit giving a straight horizontal line in the total pressure gradient plots. This also affects the frictional pressure gradients, so the pressure gradient is invalid in this region. The effect of injecting gas into the oil flow is smaller for high superficial oil velocity. At angle 15°, the difference between pressure gradient at $U_{sg} = 0$ and the minimum pressure gradient is 1435.6 Pa/m for $U_{sl} = 0.15m/s$ and 236.8 $Pa/$ for $U_{sl} = 1.07m/s$. The experiments show that for all the inclinations and superficial liquid velocities there is a minimum total pressure drop. The point for minimum pressure drop appears at higher superficial gas velocities at higher inclination angles. For low inclination angles, where the gravitational effect is less, the total pressure drop is measured at higher values than the initial pressure drop (at $U_{sg} = 0$). This can be explained by the increased turbulence in both gas and liquid phases, which creates a dominant frictional pressure loss. Thus, the dominant frictional pressure loss overcomes the advantage of having less gravitational pressure loss.

OLGA indeed show the same trend as described for the experimental results. Both measurements and OLGA show that the pressure gradient is less for higher air flow rates, for example in annular flow. Although pressure drop provides the same trends, the values from OLGA is not in agreement with the results in the lab. One reason could be different flow regime predictions in OLGA or the simplification with a mixed phase in measurement calculation.

For superficial gas velocities above 1 m/s OLGA underestimates the total pressure drop compared to measured total pressure drop. The difference becomes larger at higher gas flow rates. An interesting observation of the frictional pressure gradient is that it becomes positive, for low gas velocities. This is observed for all inclinations except 0° for the lowest superficial liquid velocity. There is a abrupt increase in the pressure gradient in the frictional pressure drop from approximately $U_{SG} = 0m/s - 2m/s$ compared with OLGA. This can be due to liquid holdup calculations or the instrumental measurements itself.

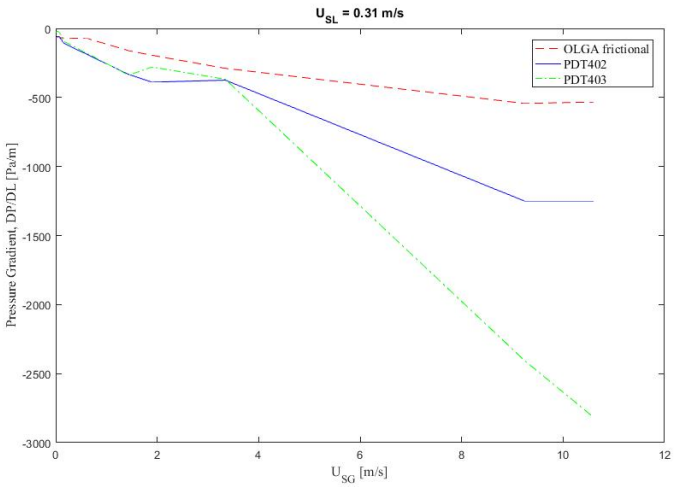

Figure 5.25: Pressure drop at 0° inclination.

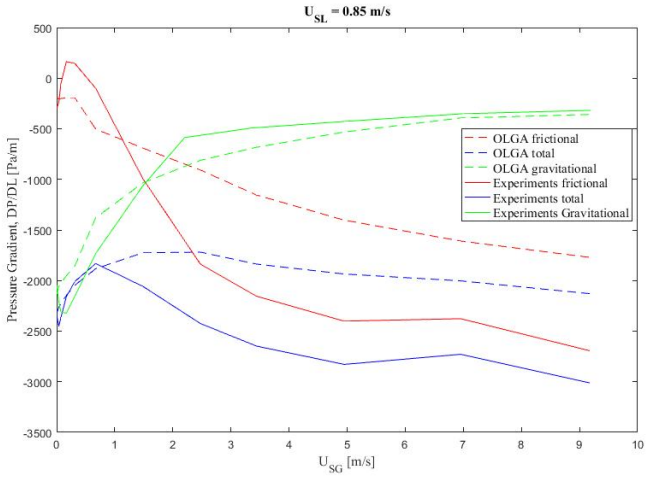

Figure 5.26: Gravitational, frictional and total pressure gradient at 15° angle.

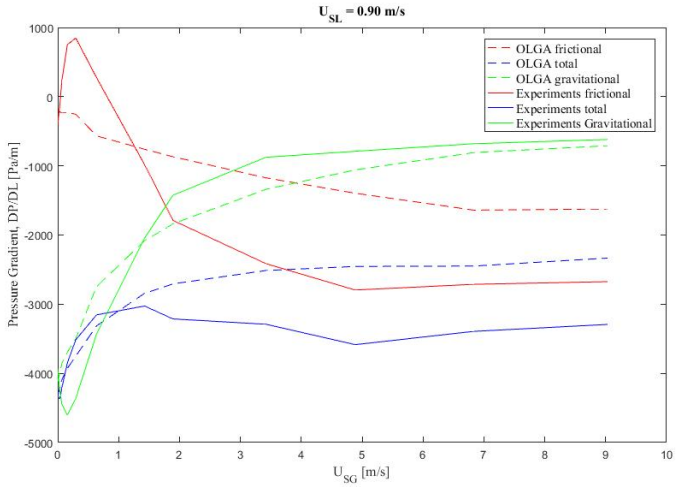

Figure 5.27: Gravitational, frictional and total pressure gradient at 30° angle.

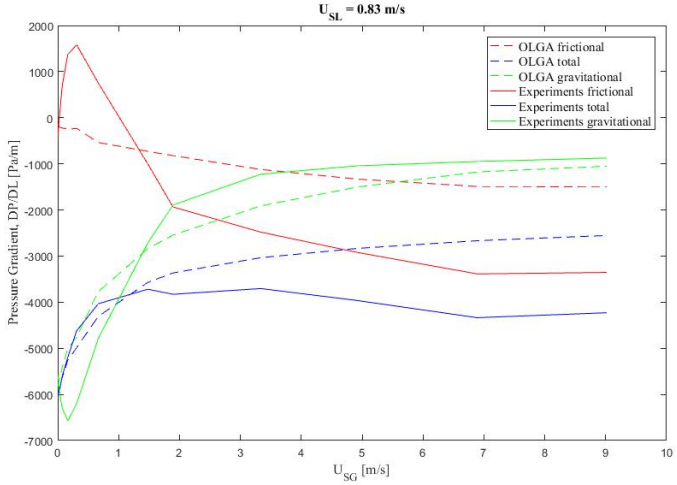

Figure 5.28: Gravitational, frictional and total pressure gradient at 45° angle.

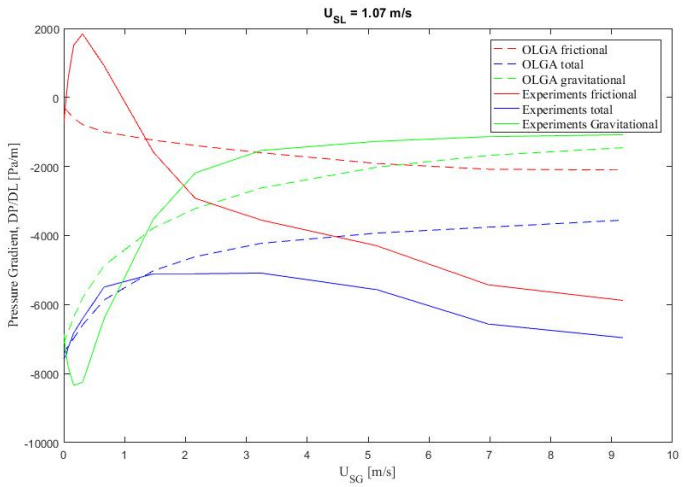

Figure 5.29: Gravitational, frictional and total pressure gradient at 60° angle.

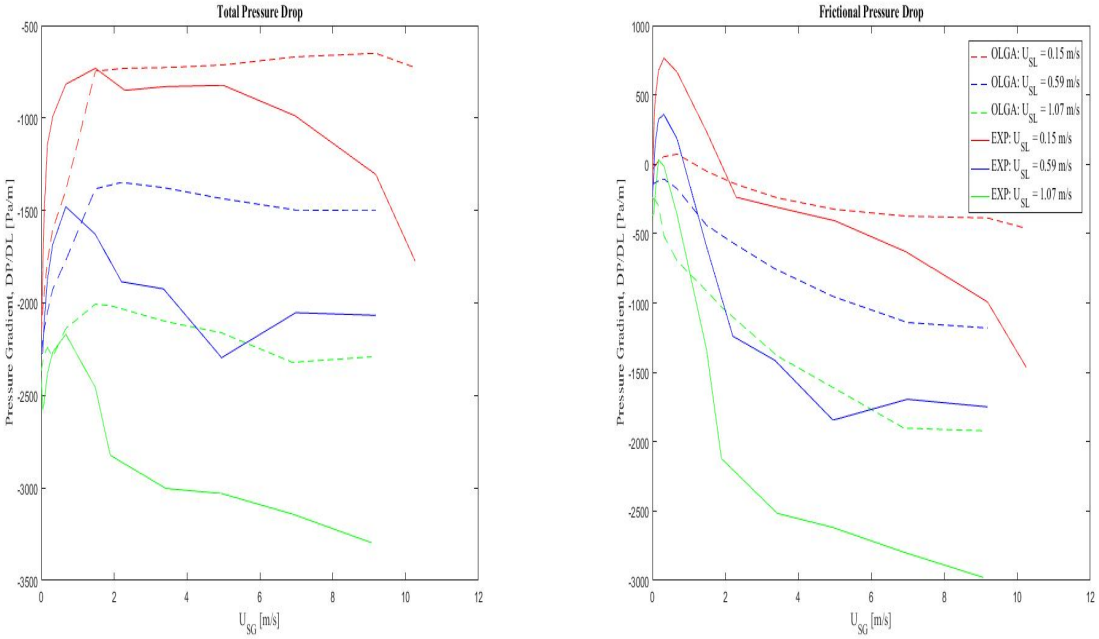

(a) Total pressure drop.

(b) Frictional pressure drop.

Figure 5.30: Pressure drop measurements compared to OLGA at 15° angle.

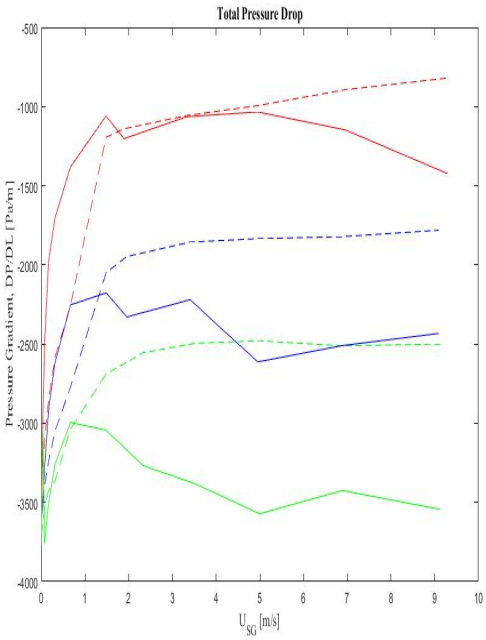

(a) Total pressure drop.

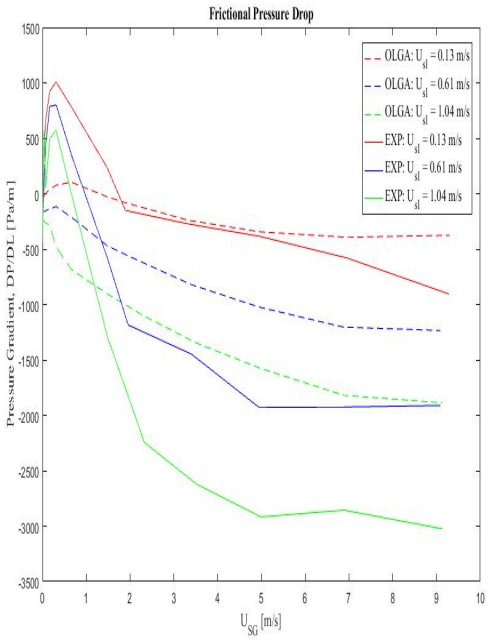

(b) Frictional pressure drop.

Figure 5.31: Pressure drop measurements compared to OLGA at 25° angle .

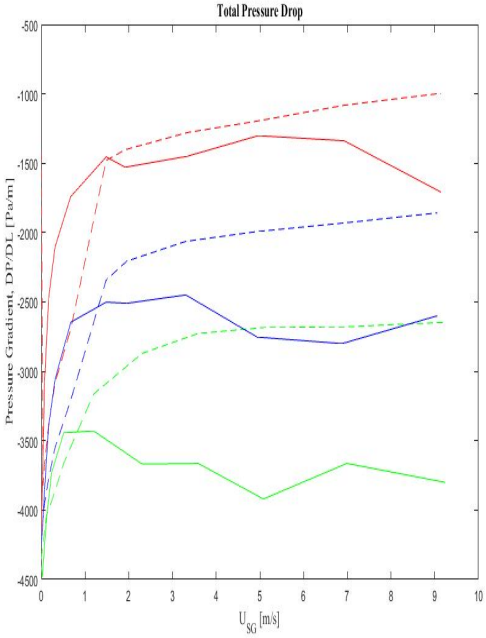

(a) Total pressure drop.

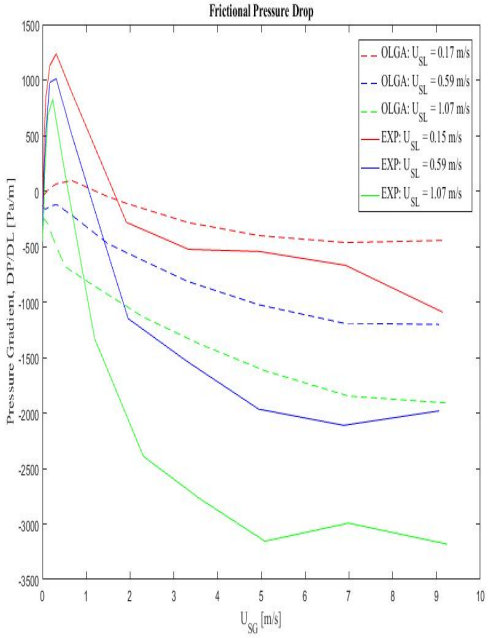

(b) Frictional pressure drop.

Figure 5.32: Pressure drop measurements compared to OLGA at 45° angle.

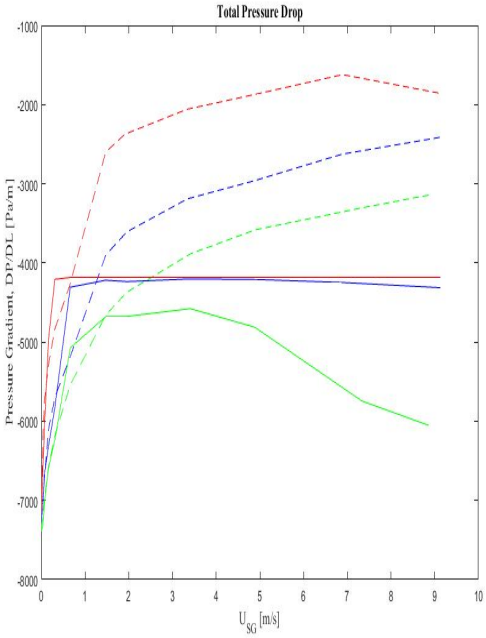

(a) Total pressure drop.

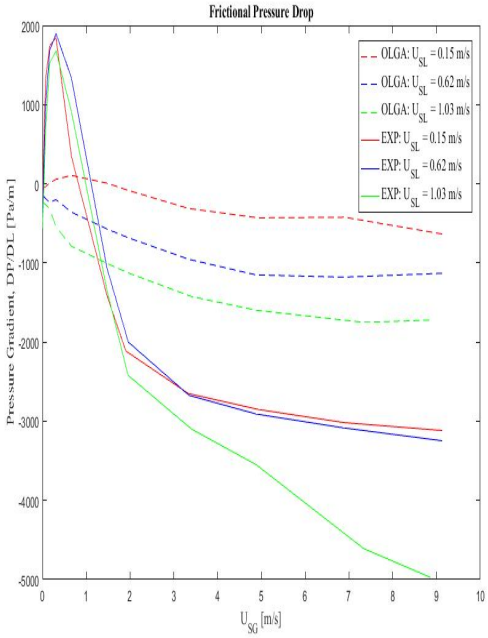

(b) Frictional pressure drop.

Figure 5.33: Pressure drop measurements compared to OLGA at 60° angle.

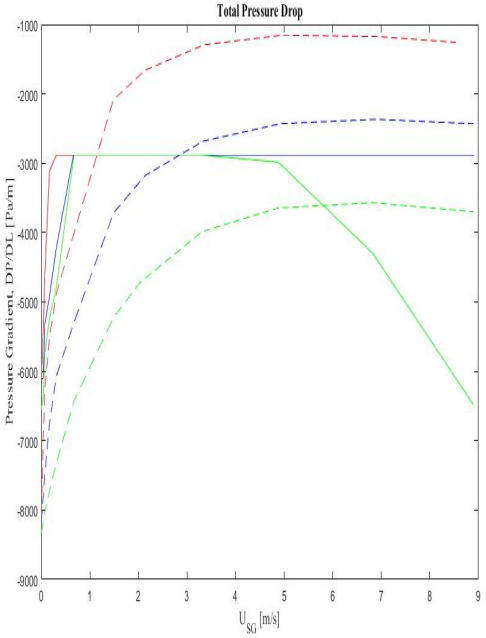

(a) Total pressure drop.

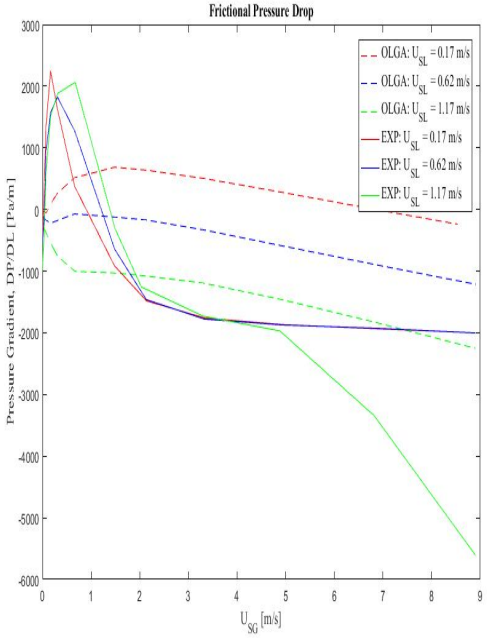

(b) Frictional pressure drop.

Figure 5.34: Pressure drop measurements compared to OLGA at 78° angle.

Chapter 6

Conclusions and Recommendations for Further Work

6.1 Conclusions

This work has focused on examining viscous two-phase flow in an inclined pipe. Relevant literature on two-phase flow at all inclination angles and numerical modeling is presented. It was found that the agreement between experiment and theory was good. The unified model by Barnea (1987) provides sufficient agreement for bubble-slug flow transition, particularly for inclination angles $45° - 78°$. In addition, stratified flow was observed and predicted at maximum 20°. With different degree of severity, annular flow was modelled at higher air flow rates, slug flow was modelled at lower gas flow rates and stratified flow at lower oil flow rates in a unified model compared to experiments.

A comprehensive conclusion of the experimental study is that the effect of inclination angle had a major effect on the flow regime maps. First, the transition between stratified and intermittent flow was highly affected as there was no occurrence of stratified flow above 20°, and upward inclinations causes the intermittent flow regime to take place over a wider range of flow conditions. Secondly, elongated bubble flow was not observed at higher angles than 30°. Finally, churn flow exists only for angles 70° and 78°. These results agree with relevant literature.

Overall, there were no occurrence of dispersed bubble for any inclination angles and according to previous investigations and OLGA it should not exist at the relevant flow rates.

Flow regime predictions in OLGA were not in good agreement with measurements, as it predicts stratified wavy flow for 44% higher inclination angle than the measurements, and the transition to annular flow at significantly higher gas flow rates than what the experiments suggests. It was however found that the flow regime agreement was more

satisfying for higher inclination angles, starting at 60°. The most satisfying bubble-slug flow transition was predicted for angle 70° while slug-annular flow transition was in most agreement with measurements at inclination 60°.

Capacitance measurements were used to classify the flow regimes, and the measurements were compared with OLGA simulations. Capacitance measurements were also used for liquid holdup calculations. The comparison showed higher liquid holdup predictions in OLGA for all inclination angles compared to measurements. It is however concluded that the accuracy of liquid holdup correlations can be improved by considering each flow pattern.

No slip liquid holdup, based on the superficial velocities, was compared with the actual liquid holdup measured with the capacitance sensor. The s-curve calibration was applied in these considerations as well. For slug flow it was found that the no slip holdup was less than the measured holdup at inclinations $10° - 60°$, and in annular flow this yields for inclinations $15° - 60°$, although the deviations are less for annular flow.

Differential pressure was measured and compared with OLGA simulations. The comparison showed that the total pressure gradient agreed quite well with predictions from OLGA for low gas flow rates. Further, the gravitational pressure gradients only differed with the liquid holdup. Both the experiments and the simulations showed that injecting air could lower the total pressure drop for any case, except for horizontal flow. In horizontal flow friction contributed to pressure loss, exclusively. The conditions obtained at increased gas flow rate was specially significant for high inclination angles and when the superficial velocities of air and gas were low.

The total pressure loss reached a minimum point for lower gas flow rates and an increase in gas flow rates resulted in larger pressure drop for all inclinations. In some cases, the pressure gradient exceeded the single phase oil flow value. OLGA and the measured values provides the same trends for frictional pressure gradient, but there were significant discrepancies in the actual values. OLGA predicts a much lower frictional pressure gradient, especially for high gas flow rates. An explanation could be that OLGA calculate the pressure drop on basis that the flow regime is slug flow in the areas where experiments observed stratified wavy and annular flow. Another explanation could be the simplification of using average pressure drop and assuming a mixed phase when calculating the frictional pressure gradients from the measured pressure drop.

6.2 Recommendations for Further Work

- High gravitational pressure drop at high inclinations exceeded the range of the excising pressure transmitters such that the range of the pressure transmitters and transducers limited the accuracy in the measurements. For further work, differential

pressure transmitters with a wider range will enable measuring pressure drop for all cases at high inclination angles.

- An oil pump with higher capacity, providing higher range of flow rates should be installed as the current pumps ruled out the possibility to obtain dispersed bubble flow.
- Liquid holdup measurements could be improved, and could be measured with gamma ray or quick closing valves. Quick closing valves was used by Beggs et al. (1973)
- In further work, an experimental study with gas-liquid three phase flow should be done in such pipe geometry.
- CFD-simulation could be applied as a tool to examine the validity of the experimental investigation.
- Over all, it would be beneficial to conduct experiments with smaller intervals, in particular inclination angles between 20° and 25° to find the exact angle at which transition from stratified (wavy) to annular occurs, inclination angles between 60° and 70° to obtain knowledge at where bubble flow vanishes, and inclination angles above 78° where churn flow could possibly disappear.
- Further work should calculate the pressure drop using the signal and apply the flow regime relation equations to calculate the measured frictional pressure gradient. A better prediction and correlation for the liquid holdup could also increase the accuracy of the pressure drop experimental analysis.
- The experimental measurements should also be compared to the more recent unified model by Zhang et al. (2003).

Bibliography

Ahmed, H. (2006). Capacitance sensors for void-fraction measurements and flow-pattern identification in air–oil two-phase flow. *IEEE sensors Journal*, 6(5):1153–1163.

Barnea, D. (1986). Transition from annular flow and from dispersed bubble flow—unified models for the whole range of pipe inclinations. *International journal of multiphase flow*, 12(5):733–744.

Barnea, D. (1987). A unified model for predicting flow-pattern transitions for the whole range of pipe inclinations. *International journal of Multiphase Flow*, 13(1):1–12.

Barnea, D., Shoham, O., and Taitel, Y. (1980a). Flow pattern characterization in two phase flow by electrical conductance probe. *International Journal of Multiphase Flow*, 6(5):387–397.

Barnea, D., Shoham, O., Taitel, Y., and Dukler, A. (1980b). Flow pattern transition for gas-liquid flow in horizontal and inclined pipes. comparison of experimental data with theory. *International Journal of Multiphase Flow*, 6(3):217–225.

Barnea, D., Shoham, O., Taitel, Y., and Dukler, A. (1985). Gas-liquid flow in inclined tubes: flow pattern transitions for upward flow. *Chemical Engineering Science*, 40(1):131–136.

Beggs, D. H., Brill, J. P., et al. (1973). A study of two-phase flow in inclined pipes. *Journal of Petroleum technology*, 25(05):607–617.

Bendiksen, K. H., Maines, D., Moe, R., Nuland, S., et al. (1991). The dynamic two-fluid model olga: Theory and application. *SPE production engineering*, 6(02):171–180.

Bratland, O. (2009). *Pipe Flow 1, Single-phase Flow Assurance.*

Bratland, O. (2010). *Pipe Flow 2, Multi-phase Flow Assurance.*

Chen, J. and Spedding, P. (1983). An analysis of holdup in horizontal two-phase gas-liquid flow. *International Journal of Multiphase Flow*, 9(2):147–159.

Diaz, M. (2016). *Two-Phase Slug Flow Experiments with Viscous Liquids.* PhD thesis, Norwegian University of science Technology.

Gokcal, B., Wang, Q., Zhang, H.-Q., Sarica, C., et al. (2008). Effects of high oil viscosity on oil/gas flow behavior in horizontal pipes. *SPE Projects, Facilities & Construction*, 3(02):1–11.

Jeyanchandra, B. C. (2011). Effect of pipe inclination on flow characteristics of high viscosity oil-gas two-phase flow.

Johansen, M. (2006). *An experimental study of the bubble propagation velocity in 3-phase slug flow*. PhD thesis, Norwegian University of science Technology.

Kokal, S. and Stanislav, J. (1989). An experimental study of two-phase flow in slightly inclined pipes—i. flow patterns. *Chemical Engineering Science*, 44(3):665–679.

Kosterin, S. (1949). An investigation of the influence of the diameter and inclination of a tube on the hydraulic resistance and flow structure of gas-liquid mixtures. *Izvest. Akad. Nauk. SSSR, Otdel Tekh Nauk*, 12:1824–1830.

Lockhart, R. and Martinelli, R. (1949). Proposed correlation of data for isothermal two-phase, two-component flow in pipes. *Chem. Eng. Prog*, 45(1):39–48.

Mukherjee, H. K. (1979). *An experimental study of inclined two-phase flow*. University of Tulsa.

Piau, J., Bremond, M., Couette, J., and Piau, M. (1994). Maurice couette, one of the founders of rheology. *Rheologica acta*, 33(5):357–368.

Schlumberger (2014). *Used Manual OLGA 3.0*.

Shoham, O. (1982). *Flow Pattern Transition and Characterization in Gas-Liquid Two-Phase Flow in Inclined Pipes*. PhD thesis, Tel - Aviv University, Israel.

Shoham, O. (2005). *Mechanistic modeling of gas-liquid two-phase flow in pipes*.

Spedding, P., Chen, J., and Nguyen, V. T. (1982). Pressure drop in two phase gas-liquid flow in inclined pipes. *International Journal of Multiphase Flow*, 8(4):407–431.

Taitel, Y., Bornea, D., and Dukler, A. (1980). Modelling flow pattern transitions for steady upward gas-liquid flow in vertical tubes. *AIChE Journal*, 26(3):345–354.

Taitel, Y. and Dukler, A. (1976). A model for predicting flow regime transitions in horizontal and near horizontal gas-liquid flow. *AIChE Journal*, 22(1):47–55.

Zhang, H.-Q., Wang, Q., Sarice, C., and Brill, J. P. B. (2003). Unified model for gas-liquid pipe flow via slug dynamics - part 1: Model development. *Journal of Energy Resources Technology*, 125(4):266 – 273.

Appendix A

Flow chart lines

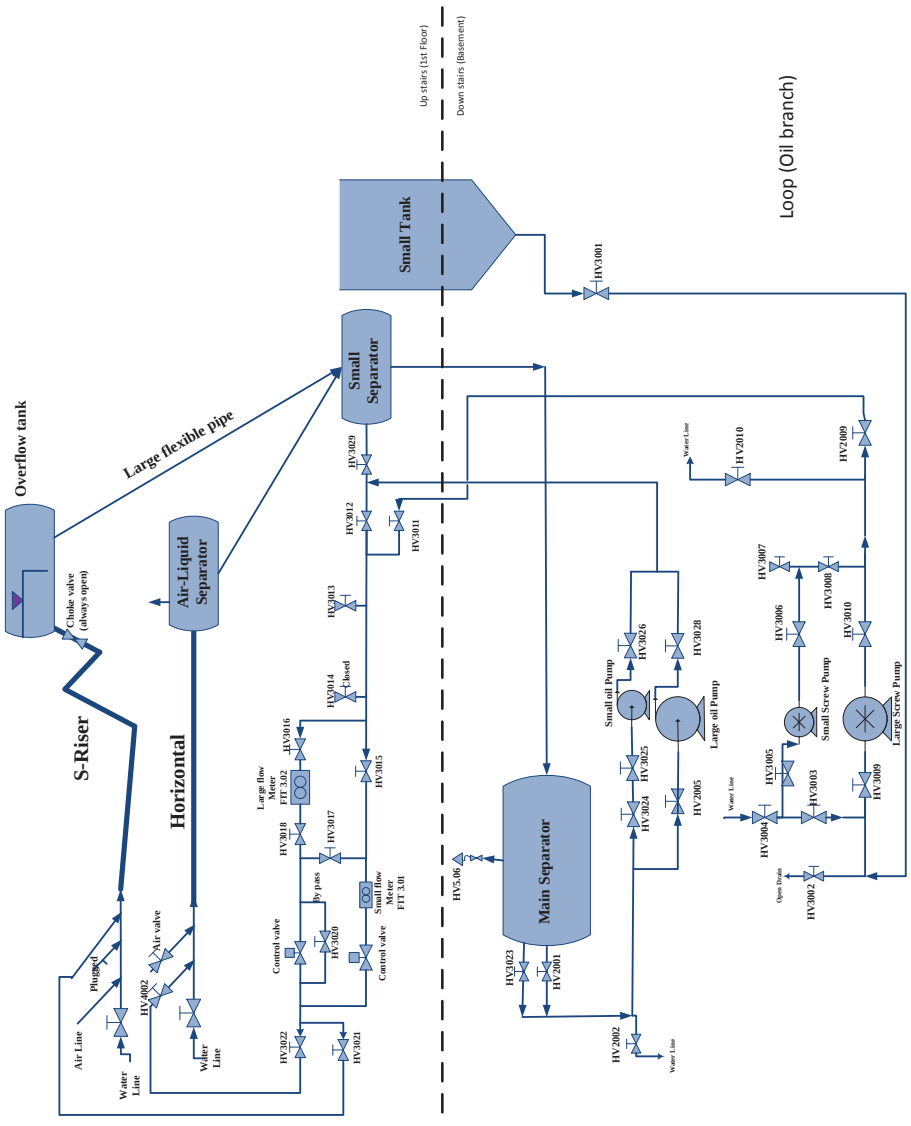

Figure A.1: Oil line.

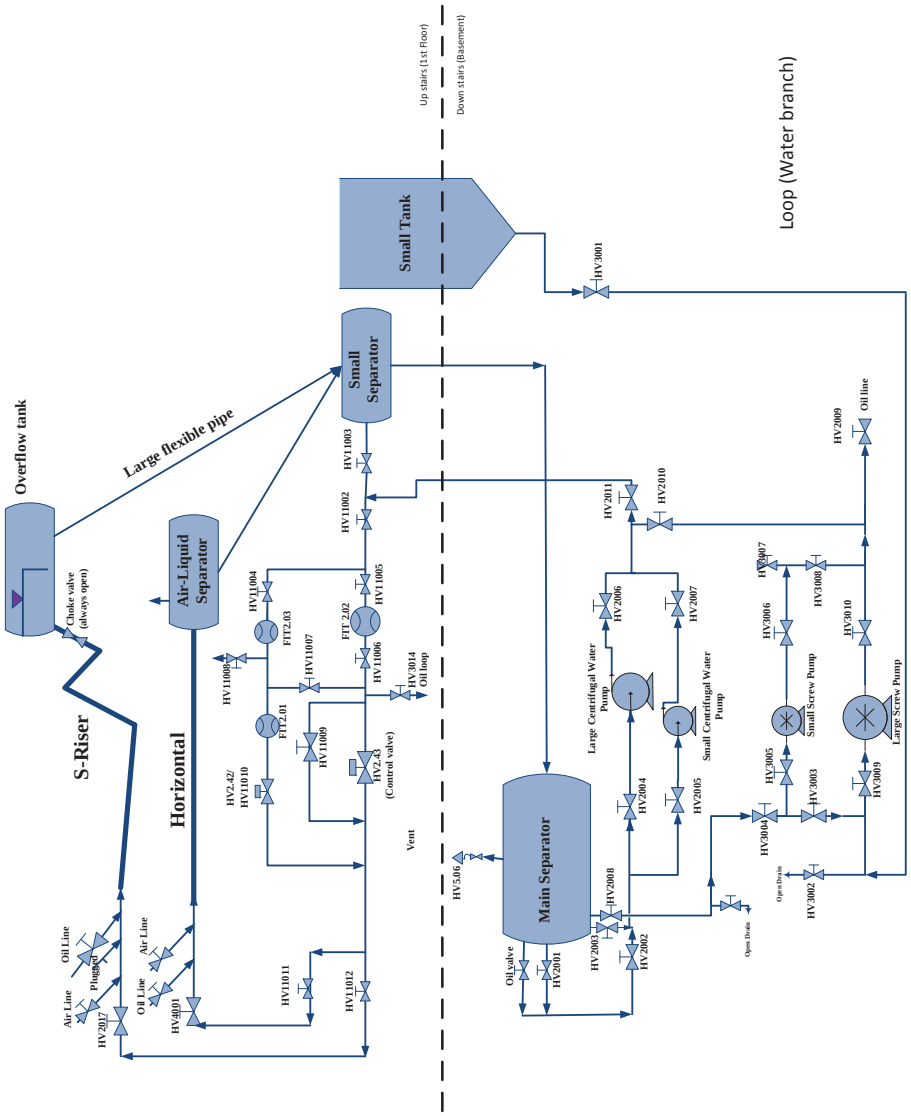

Figure A.2: Water line.

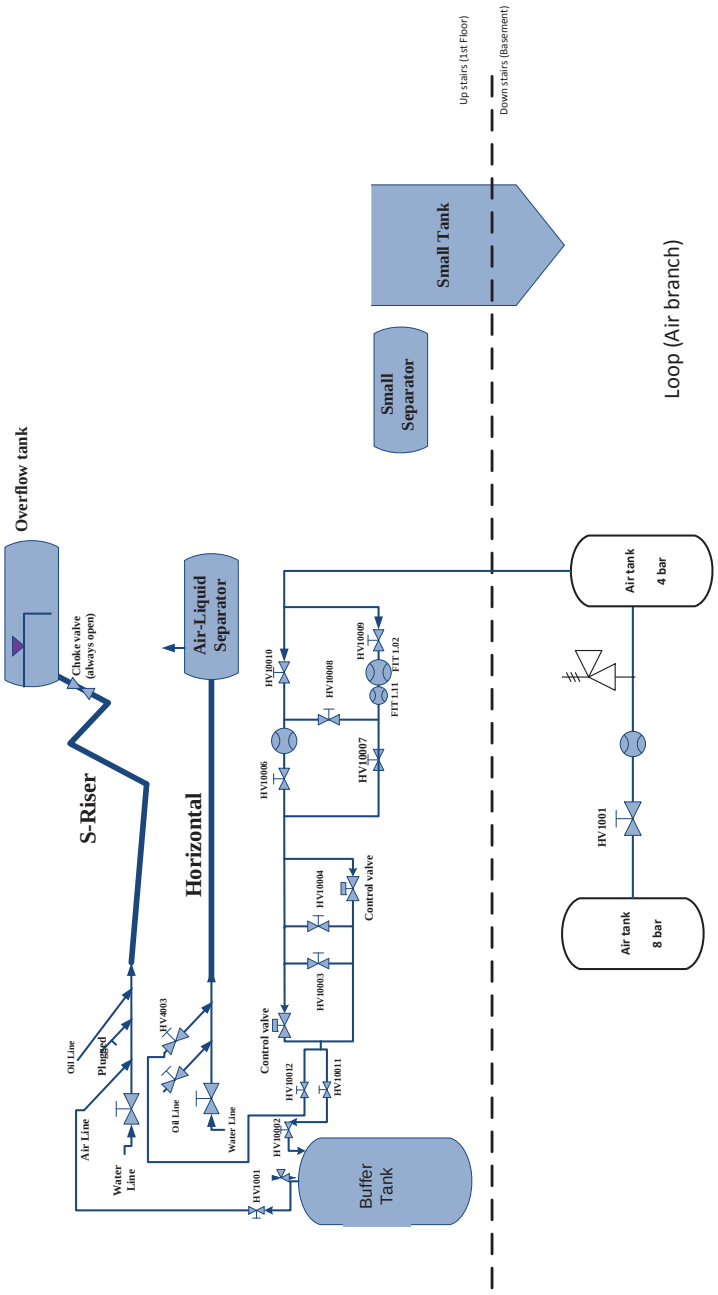

Figure A.3: Air line.

Appendix B

Check List Procedure

DOWN STAIRS

WATER

Large Screw Pump ☐	HV2008 ☐Open	HV2002 ☐Close	HV2001 ☐Close	HV3004 ☐Open	HV3003 ☐Open
	HV3005 ☐Close	HV3009 ☐Open	HV3010 ☐Open	HV3008 ☐Close	HV2009 ☐Close
	HV2010 ☐Open	HV2011☐Open	HV2006 ☐Close	HV2007 ☐Close	
Small Screw Pump ☐	HV2008 ☐Open	HV2002 ☐Close	HV2001 ☐Close	HV3004 ☐Open	HV3003 ☐Close
	HV3005 ☐Open	HV3006 ☐Open	HV3008 ☐Open	HV3010 ☐Close	HV2009 ☐Close
	HV2010 ☐Open	HV2011 ☐Open	HV2006 ☐Close	HV2007 ☐Close	HV3007 ☐Close
Large Centrifugal Water Pump ☐	HV2002 ☐Close	HV2008 ☐Close	HV2001 ☐Close	HV2003 ☐Open	HV2004 ☐Open
	HV2006 ☐Open	HV2007☐Close	HV2011 ☐Open	HV2010 ☐Close	
Small Centrifugal Water Pump ☐	HV2002 ☐Close	HV2008 ☐Close	HV2001 ☐Close	HV2003 ☐Open	HV2005 ☐Open
	HV2007 ☐Open	HV2006 ☐Close	HV2011 ☐Open	HV2010 ☐Close	

OIL

Large Centrifugal Oil Pump ☐	HV3023 ☐Open	HV2001 ☐Close	HV2002 ☐Close	HV3027 ☐ Open	HV3026 ☐ Close	HV3028 ☐ Open
Small Centrifugal Oil Pump ☐	HV3023 ☐Open	HV2001 ☐ Close	HV2002 ☐Close	HV3024 ☐Open	HV3025 ☐Open	HV3026 ☐Open
	HV3028 ☐Close					
Large Screw Pump to be used with the small tank ☐	HV3001 ☐Open	HV3002 ☐ Close	HV3003 ☐ Close	HV3004 ☐ Close	HV3009 ☐Open	HV3010☐ Open
	HV2009☐ Open	HV2010☐ Close	HV3008 ☐Close			
Small Screw Pump to be used with the small tank ☐	HV3001 ☐Open	HV3002 ☐ Close	HV3003 ☐Open	HV3005 ☐Open	HV3004 ☐ Close	HV3006 ☐Open
	HV3007 ☐ Close	HV3008 ☐Open	HV3010☐ Close	HV2009☐ Open	HV2010☐ Close	

AIR HV1001 ☐Open

Figure B.1: Check list procedure down stairs.

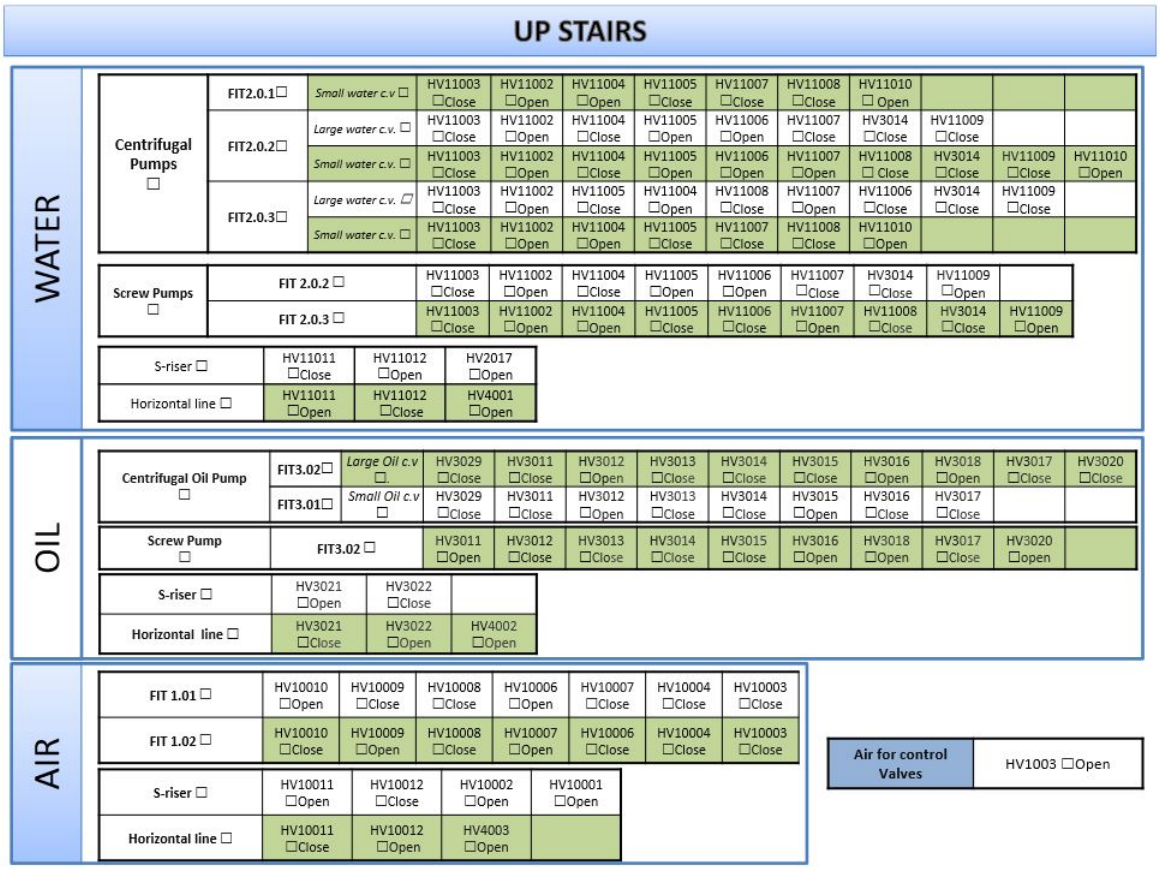

Figure B.2: Check list procedure up stairs.

Appendix C

Experimental Procedure

Firstly, the facility must be started. This includes a check list provided by NTNU. The check list is included in appendix B.

Start up:

1. Visual inspection of the flow loop. Make sure that all flanges are connected correctly, specially the connection to the separator.
2. Basement: Use the check list to verify the position of each valve. Start with the air and then go to either the water or oil. For water/oil, the desired pump must be chosen. The air valve HV1001 should then be opened slowly.
3. Up stairs: Follow the check list and check boxes according to chosen pump and flow meter.
4. Open the valve HV1003 for the control valves.
5. When using acrylic pipes and fluids with viscosities higher than 100 cP special attention have to be paid on the pressure at the acrylic pipe inlet. Pressure higher than 1 barg should be voided.
6. In the case of using centrifugal pumps, the normal operation frequency should be 30 Hz and the maximum should be 45 Hz.

Similarly, the facility has a shut down routine.
Stop:

1. Stop water/oil flow by slowly reduce the frequency of the pump until the pumps are fully switched off.
2. Stop the air flow.
3. Be sure to close the valve HV1001 as well as all valves in the mix unit.

4. Close valve HV1003.
5. Write down activities and changes in the dossier.

Secondly, the experimental procedure for two phase flow experiments was as follows:

1. Centrifugal pumps are controlled from the control valve using the software LabView.
2. Air is controlled by the control valve and a PID controller. The valve is also cntrolled from LabView.
3. Ensure correct inclination angle of test section pipe with angle meter. The angle meter used is presented in Figure C.1
4. Calibration of capacitance sensor and pressure transmitters with single phase flow as explained in section (-).
5. Reach desired air and oil flow rates. Obtain two phase flow stability.
6. Note flow regimes to the corresponding flow rates.
7. Subsequently, pictures and video recording conducted for visual observation and support for decision making.
8. Log experimental results in LabView over a time period of 5 minutes.
9. Insert logged parameters for flow rates, pressure drop, differential pressure and capacitance in a program written in Excel to plot flow regimes.
10. When the flow regimes for all flow rates of oil and gas has been noted, the inclination if the pipe is adjusted and step 1-9 are repeated.

Figure C.1: Angle gauge.

Appendix D

Risk Assessment

Dangerous situation	Why can it occur	Probability	Consequences	Combination	Actions
Slippery scaffold	Oil leakage from test-section	4	B	B3	Check test-section for oil leakage. Routines for removal of oil spillage.
Slippery ground	Oil leakage from set-up	3	B	B3	Check the set-up for any leakages before starting experiments. Oil should be disposed in the available barrels.
Falling object	Loose tools in heights	3	C	C3	Avoid working in heights
Stumbling	Loose cables and components around the rig	5	A	5A	MThe area around the rig should be clean always. System for cables.
Eye damage	Oil spill in contact with eyes	1	A	A1	Use of eye protection

Table D.1: Risk matrix.

CONSEQUEN						
	Svært alvorlig	E1	E2	E3	E4	E5
	Alvorlig	D1	D2	D3	D4	D5
	Moderat	C1	C2	C3	C4	C5
	Liten	B1	B2	B3	B4	B5
N	Svært liten	A1	A2	A3	A4	A5
		Svært liten	Liten	Middels	Stor	Svært Stor
		PROBABILITY				

The principle of the acceptance criterion. Explanation of the colors used in the matrix

Farge		Beskrivelse
Rød		Unacceptable risk Action has to be taken to reduce risk
Gul		Assessment area. Actions has to be concidered
Grønn		Acceptable risk. Action can be taken based on other criteria

Figure D.1: The principle of acceptance criterion.

Appendix E

Experimental Results Pressure Drop, Capacitance and Flow Rates

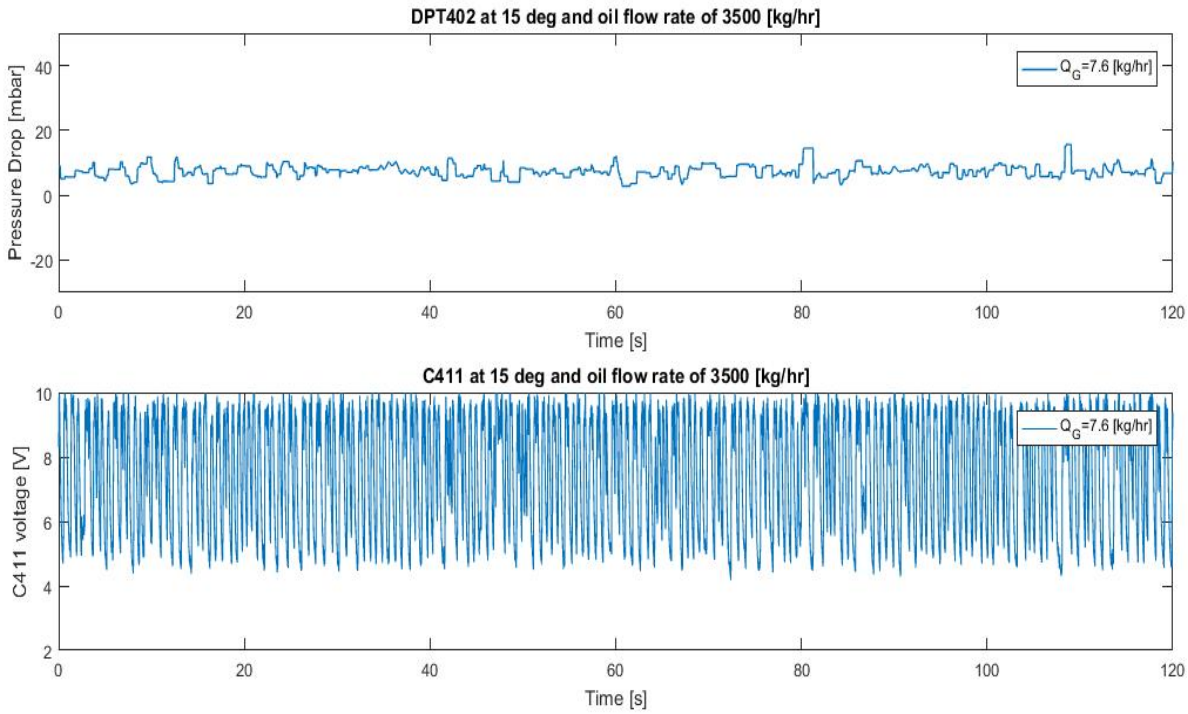

Figure E.1: Differential pressure and capacitance at 15° angle and $Q_L = 3500kg/h$, $Q_G = 7.5kg/h$.

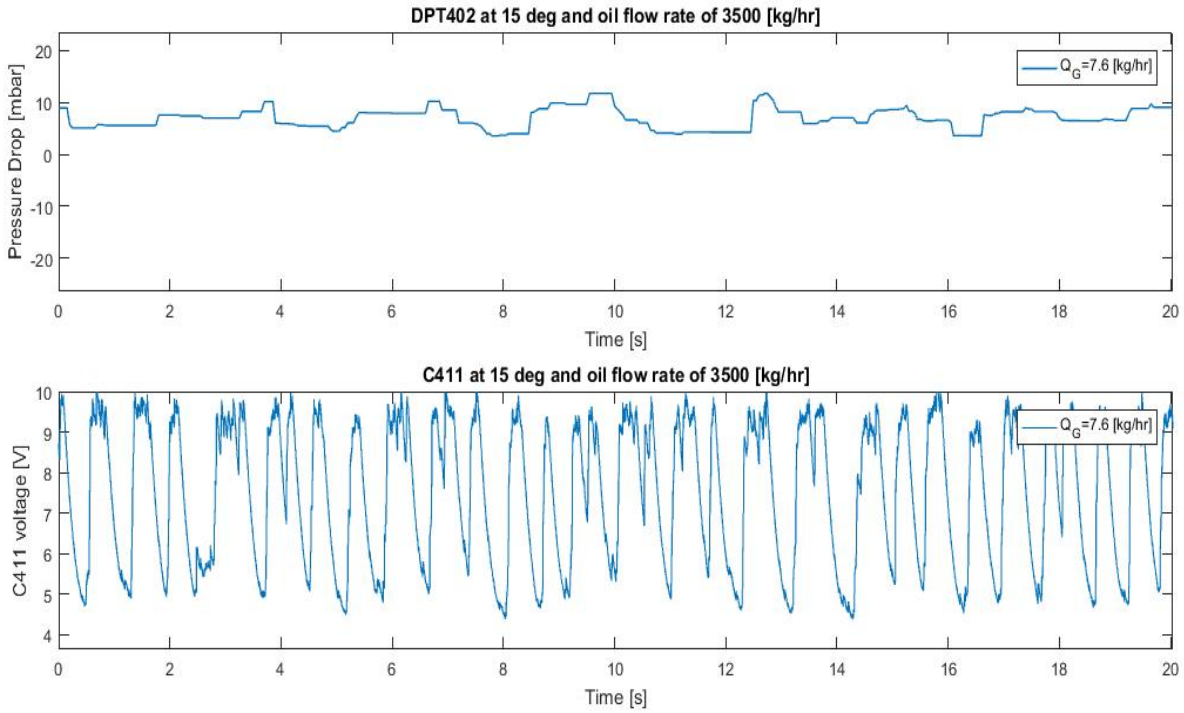

Figure E.2: Differential pressure and capacitance at 15° angle and $Q_L = 3500kg/h$, $Q_G = 7.5kg/h$.

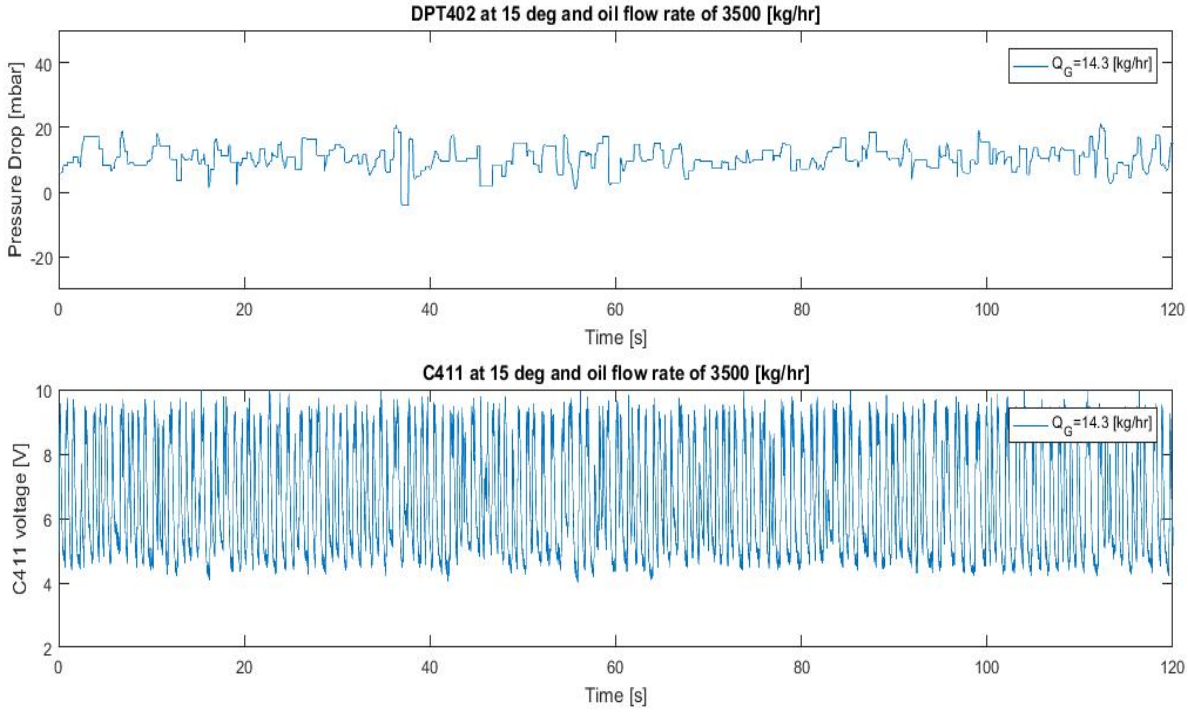

Figure E.3: Differential pressure and capacitance at 15° angle and $Q_L = 3500kg/h$, $Q_G = 14.3kg/h$

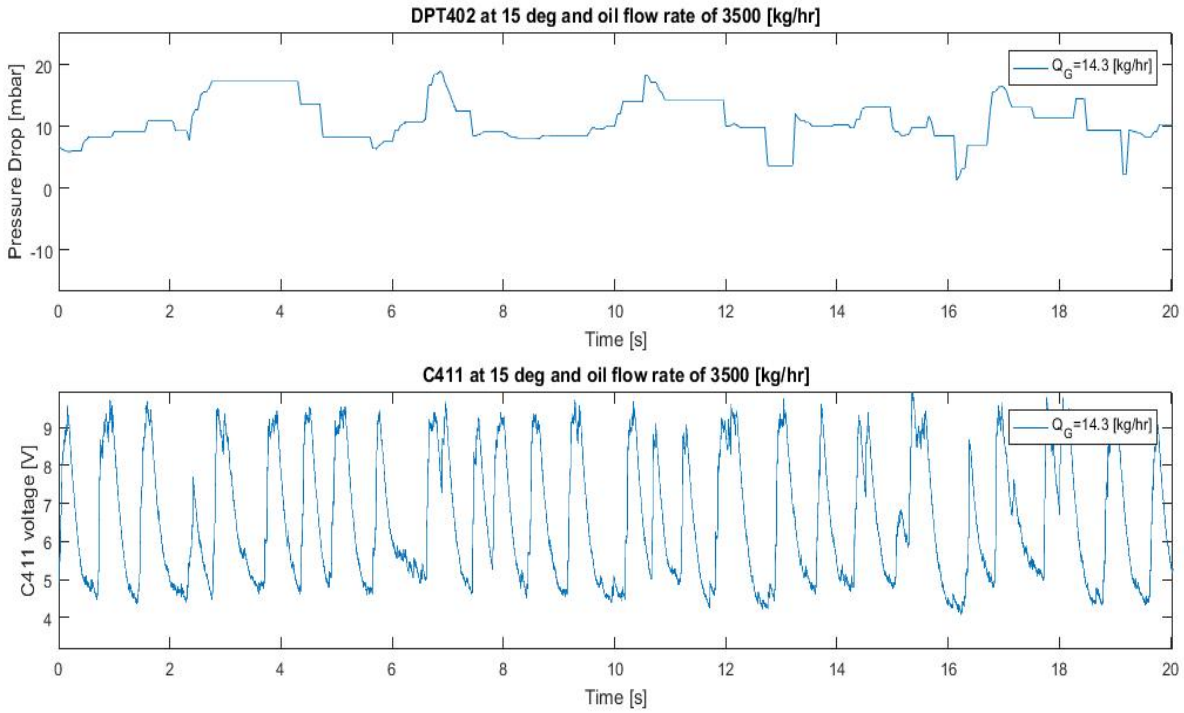

Figure E.4: Differential pressure and capacitance at 15° angle and $Q_L = 3500kg/h$, $Q_G = 14.3kg/h$

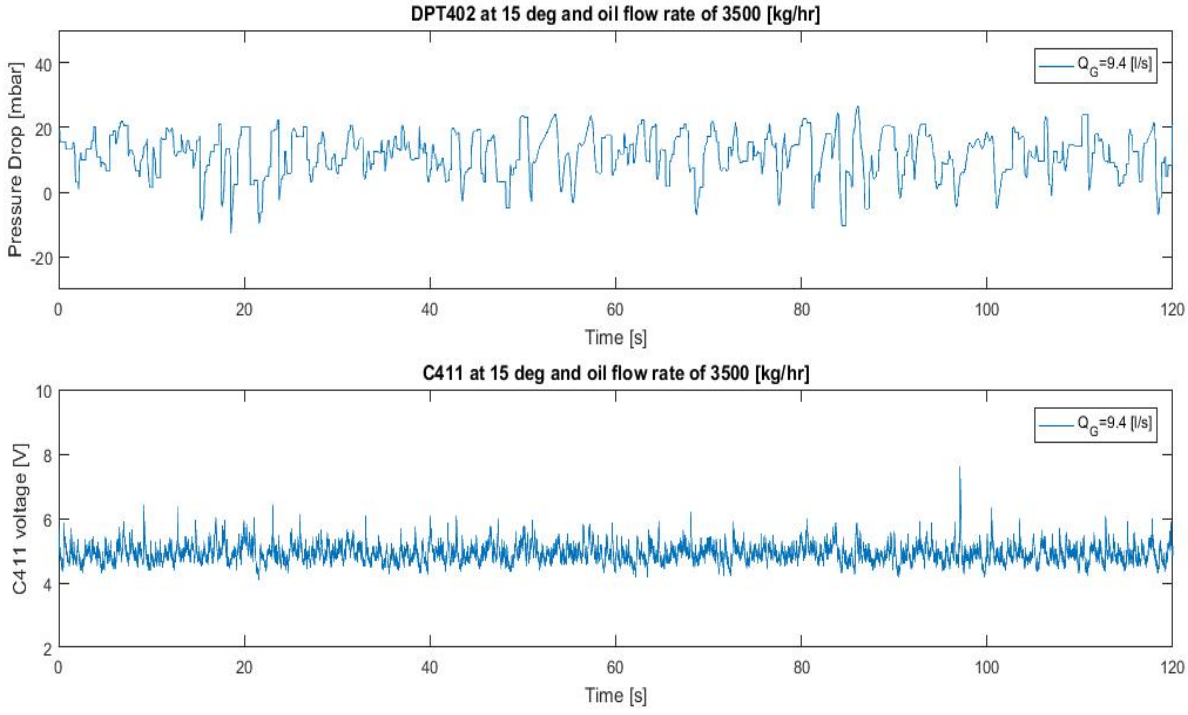

Figure E.5: Differential pressure and capacitance at 15° angle and $Q_L = 3500kg/h$, $Q_G = 9.4l/s$.

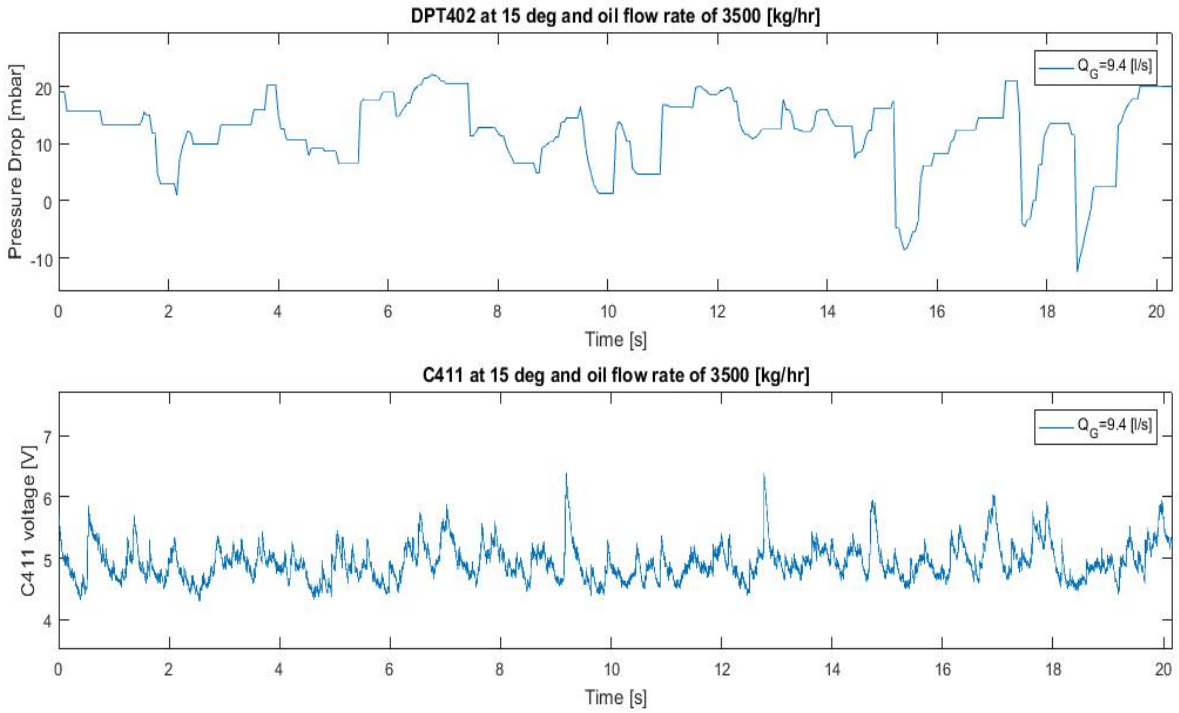

Figure E.6: Differential pressure and capacitance at 15° angle and $Q_L = 3500kg/h$, $Q_G = 9.4l/s$.

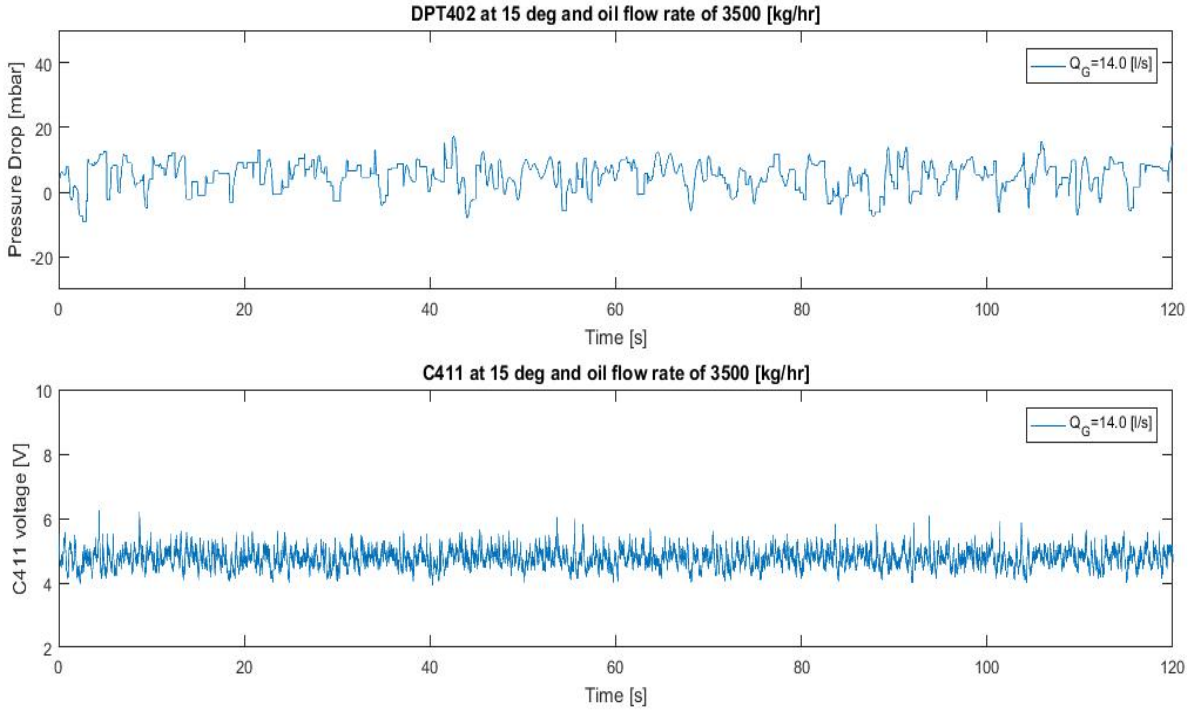

Figure E.7: Differential pressure and capacitance at 15° angle and $Q_L = 3500kg/h$, $Q_G = 14.0l/s$.

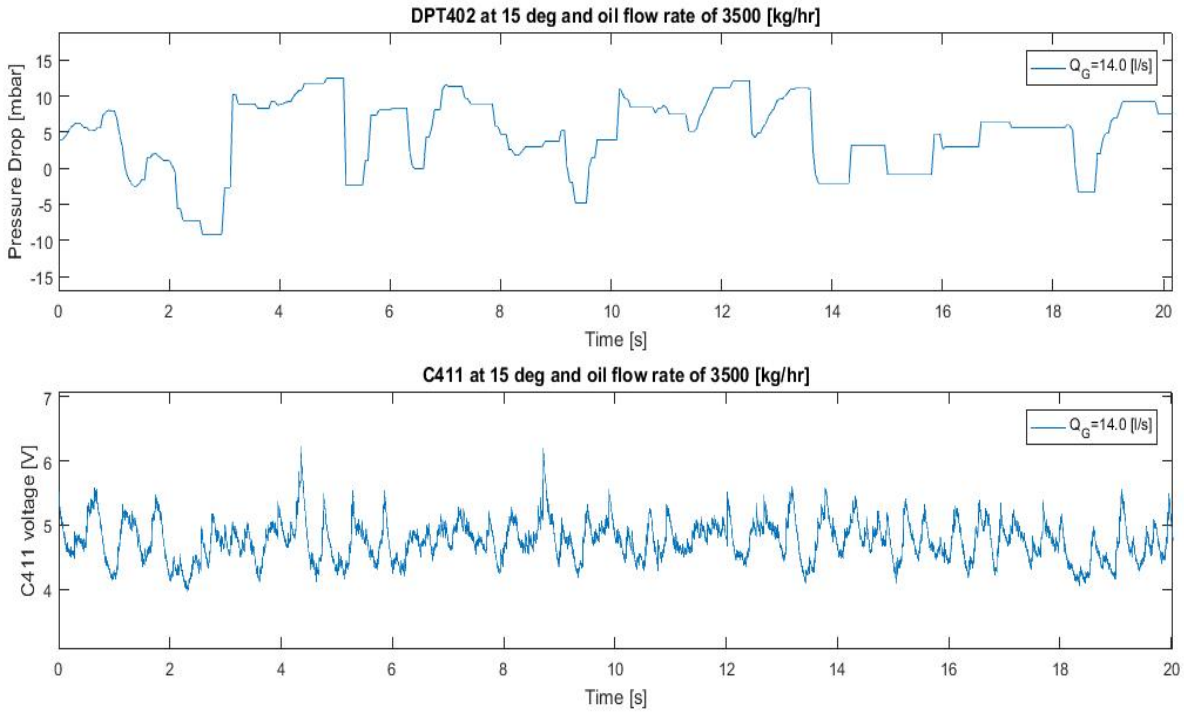

Figure E.8: Differential pressure and capacitance at 15° angle and $Q_L = 3500kg/h$, $Q_G = 14.0l/s$.

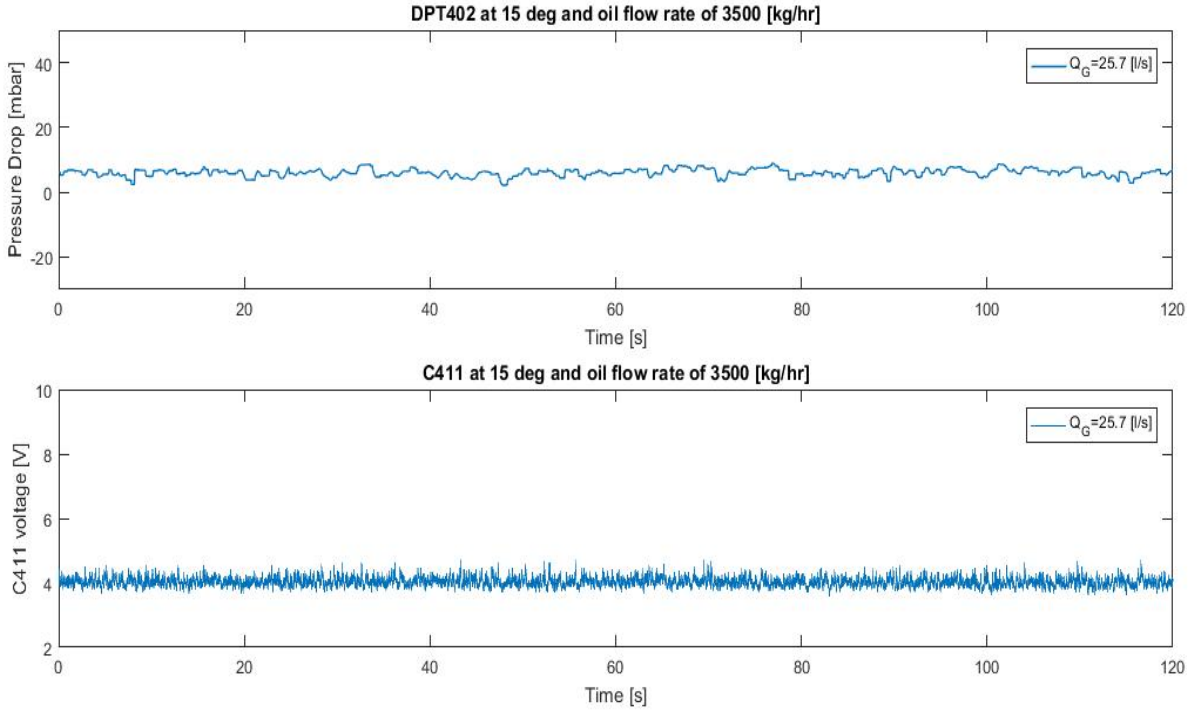

Figure E.9: Differential pressure and capacitance at 15° angle and $Q_L = 3500kg/h$, $Q_G = 25.7l/s$.

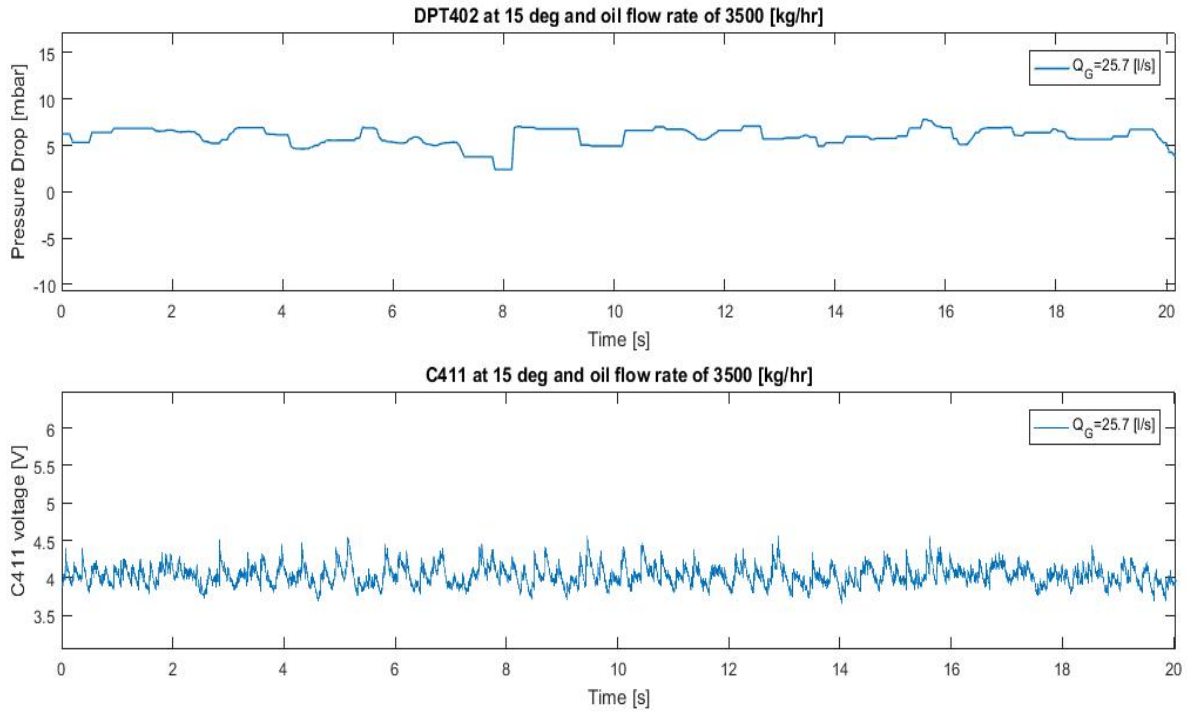

Figure E.10: Differential pressure and capacitance at 15° angle and $Q_L = 3500kg/h$, $Q_G = 25.7l/s$.

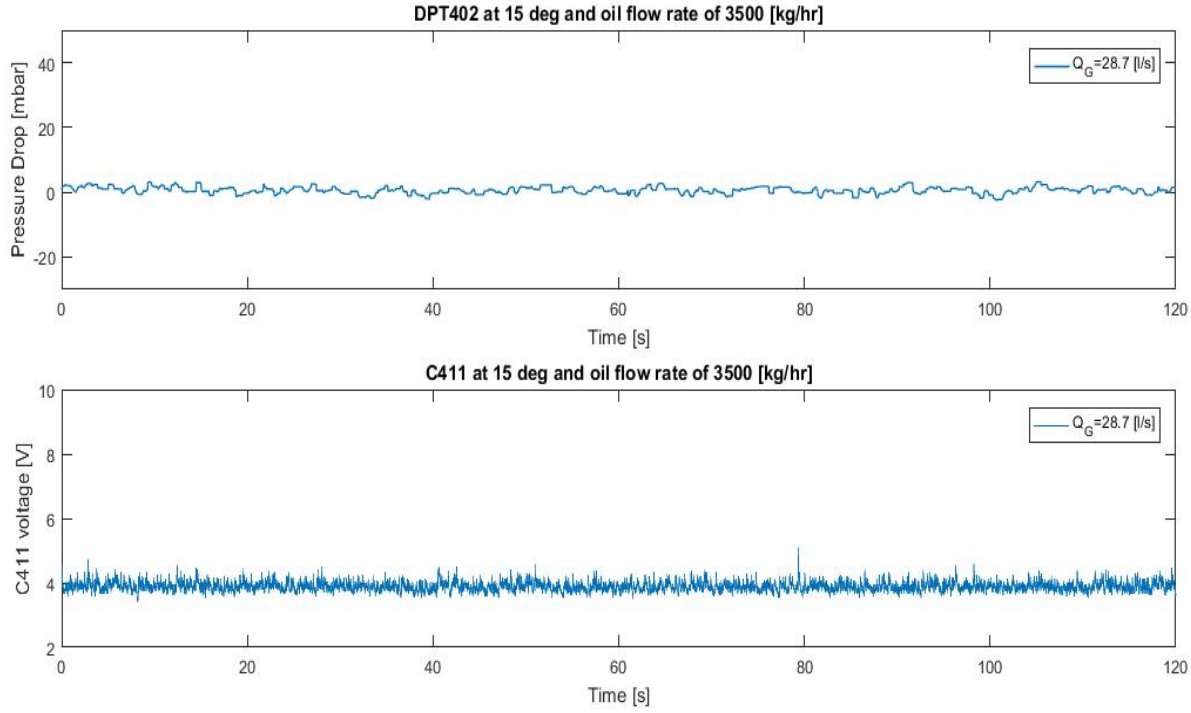

Figure E.11: Differential pressure and capacitance at 15° angle and $Q_L = 3500kg/h$, $Q_G = 28.7l/s$.

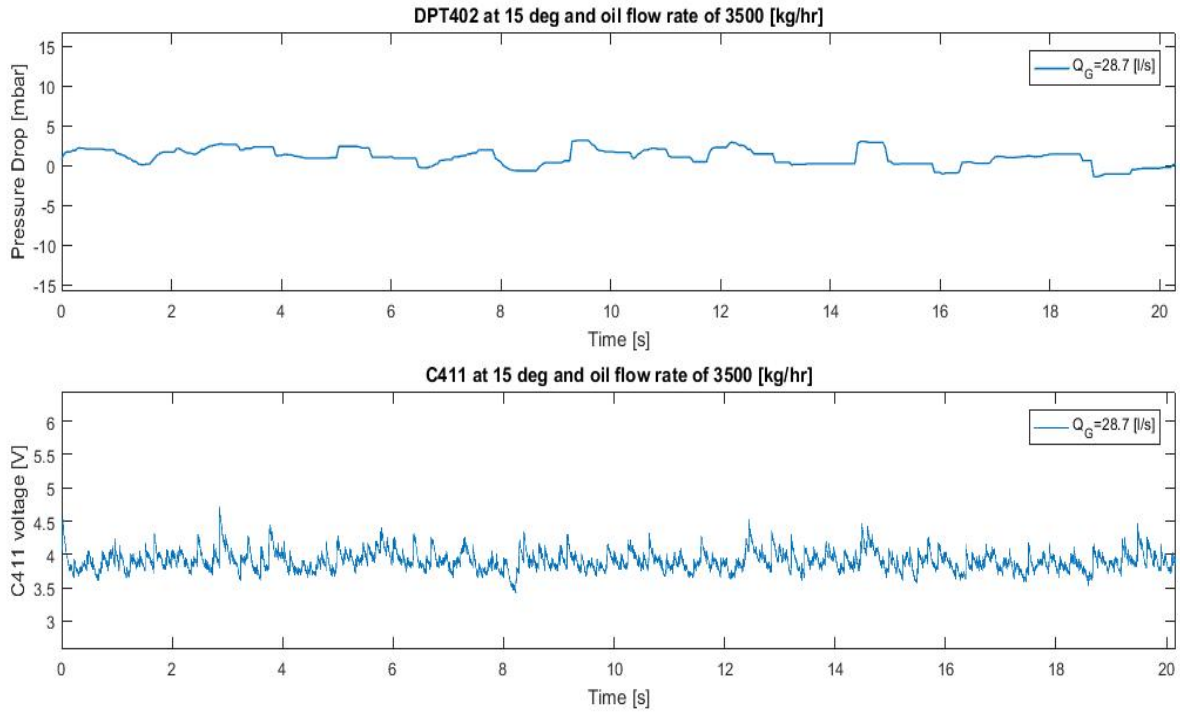

Figure E.12: Differential pressure and capacitance at 15° angle and $Q_L = 3500kg/h$, $Q_G = 28.7l/s$.

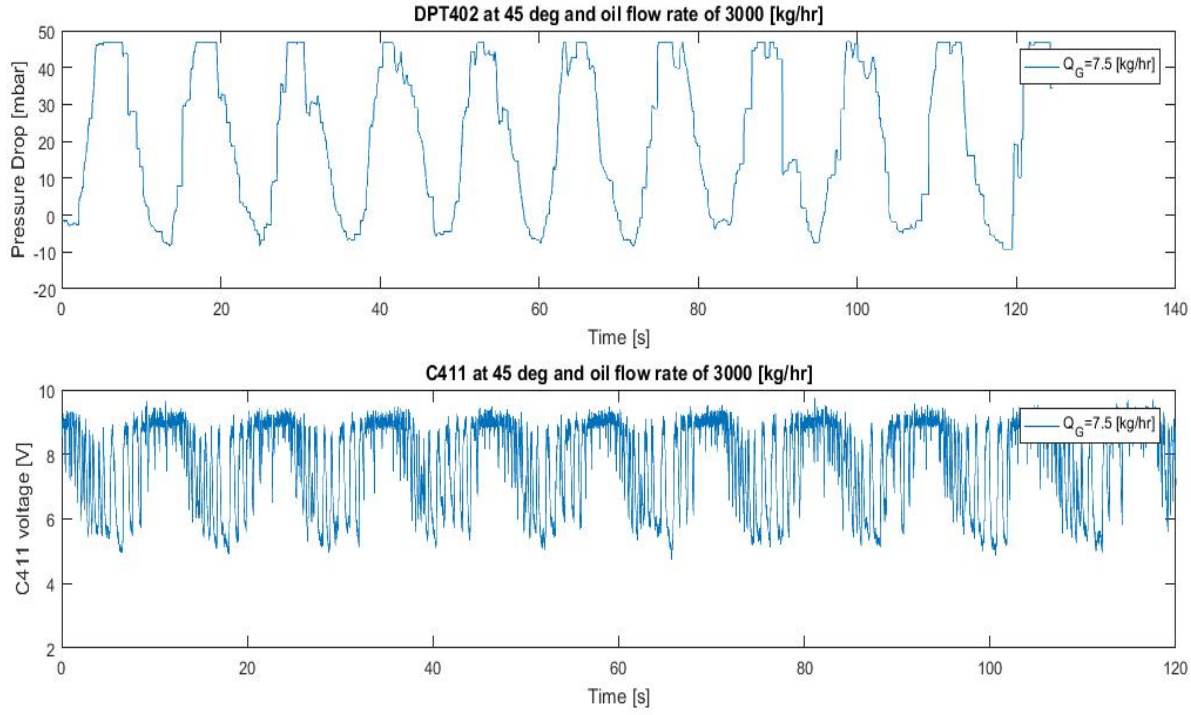

Figure E.13: Differential pressure and capacitance at 45° angle and $Q_L = 3000kg/h$, $Q_G = 7.5kg/h$.

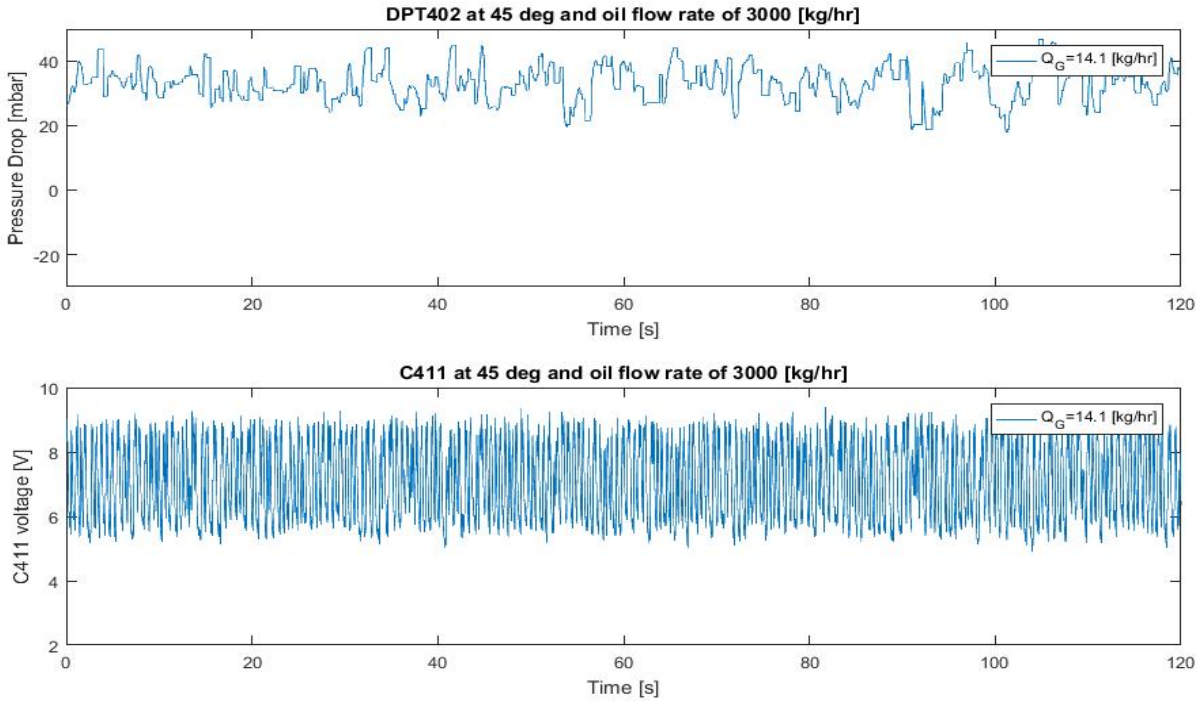

Figure E.14: Differential pressure and capacitance at 45° angle and $Q_L = 3000kg/h$, $Q_G = 14.1kg/h$.

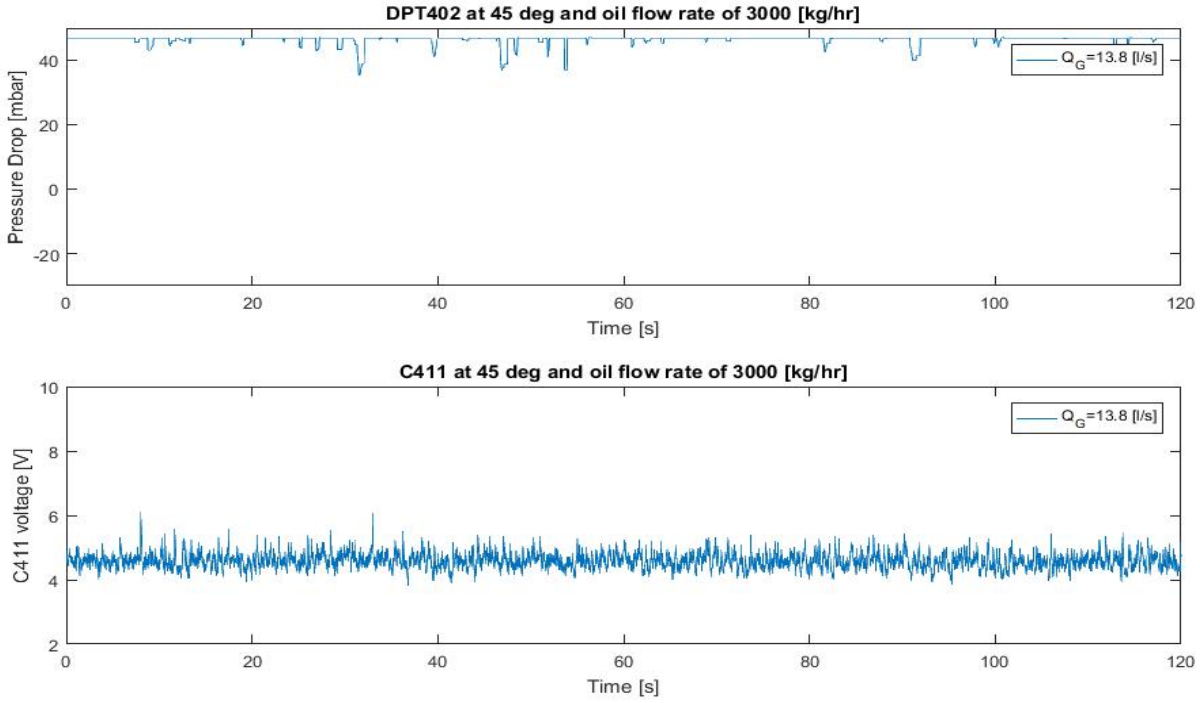

Figure E.15: Differential pressure and capacitance at 45° angle and $Q_L = 3000kg/h$, $Q_G = 13.8l/s$.

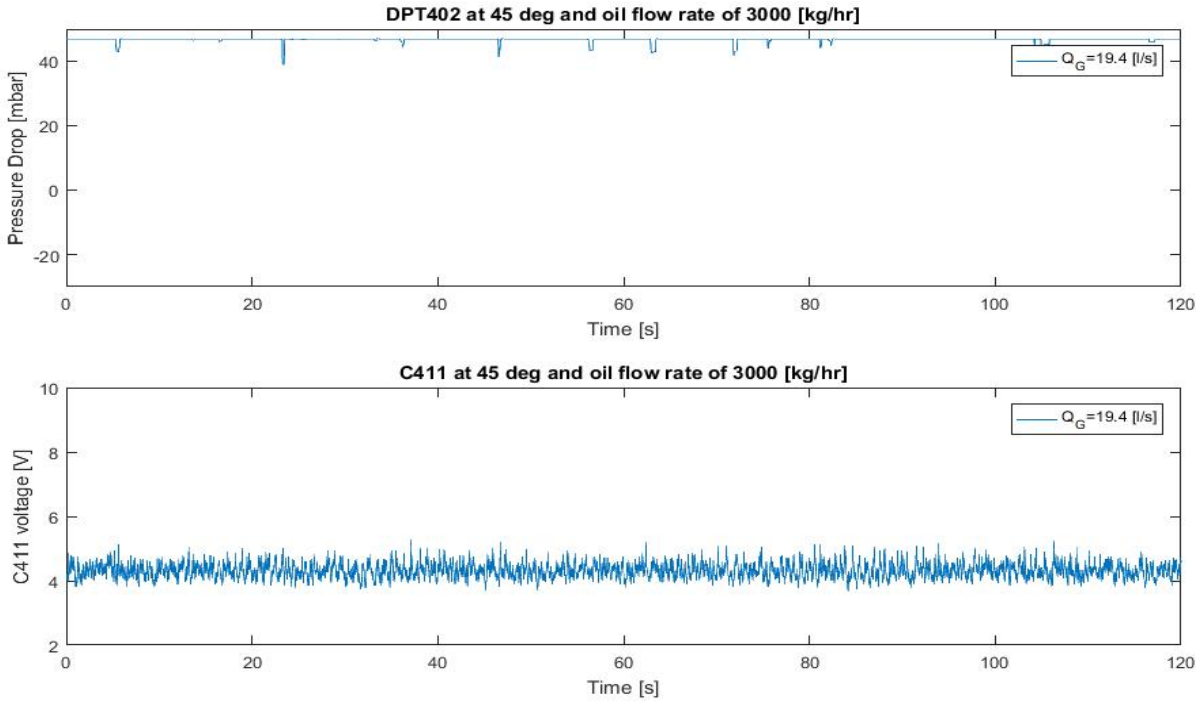

Figure E.16: Differential pressure and capacitance at 45° angle and $Q_L = 3000kg/h$, $Q_G = 19.4l/s$.

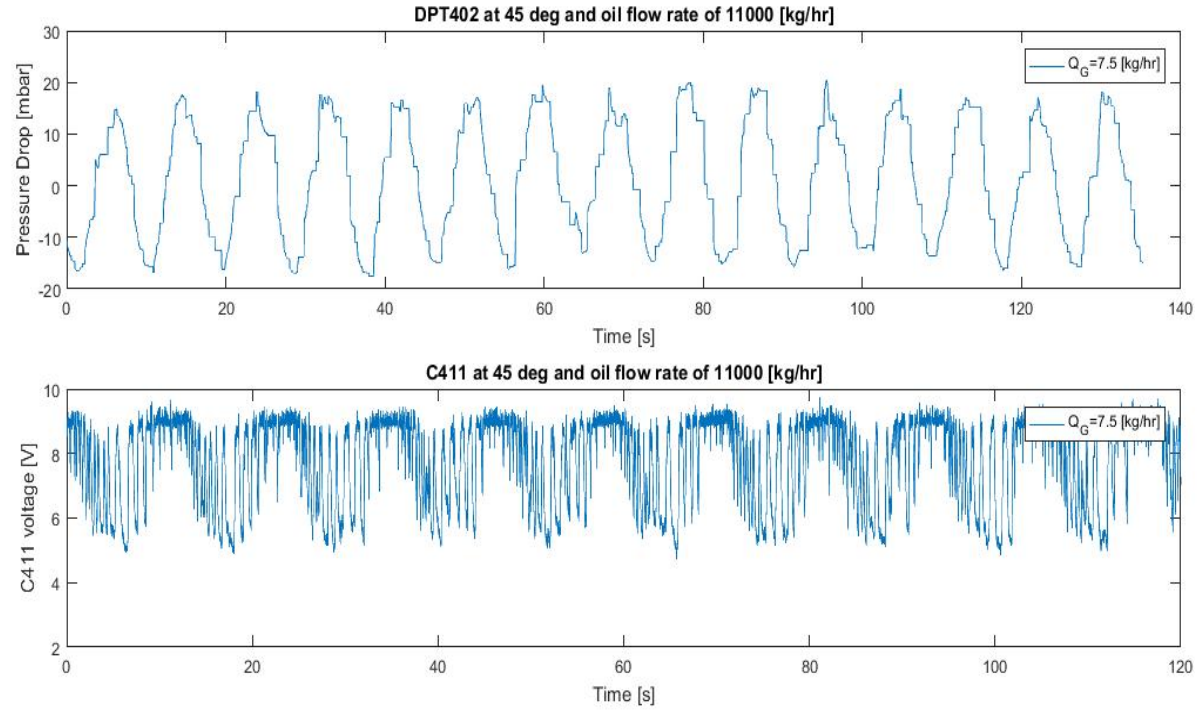

Figure E.17: Differential pressure and capacitance at 45° angle and $Q_L = 11000kg/h$, $Q_G = 7.5kg/h$.

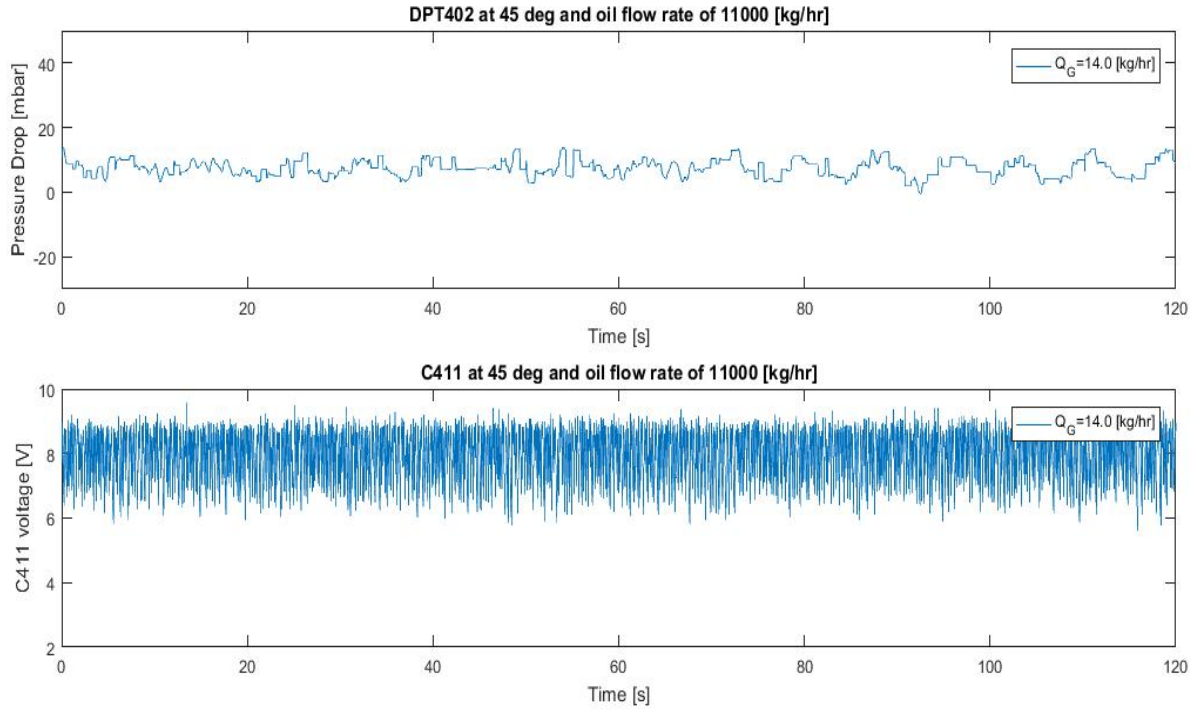

Figure E.18: Differential pressure and capacitance at 45° angle and $Q_L = 11000kg/h$, $Q_G = 14.0kg/h$.

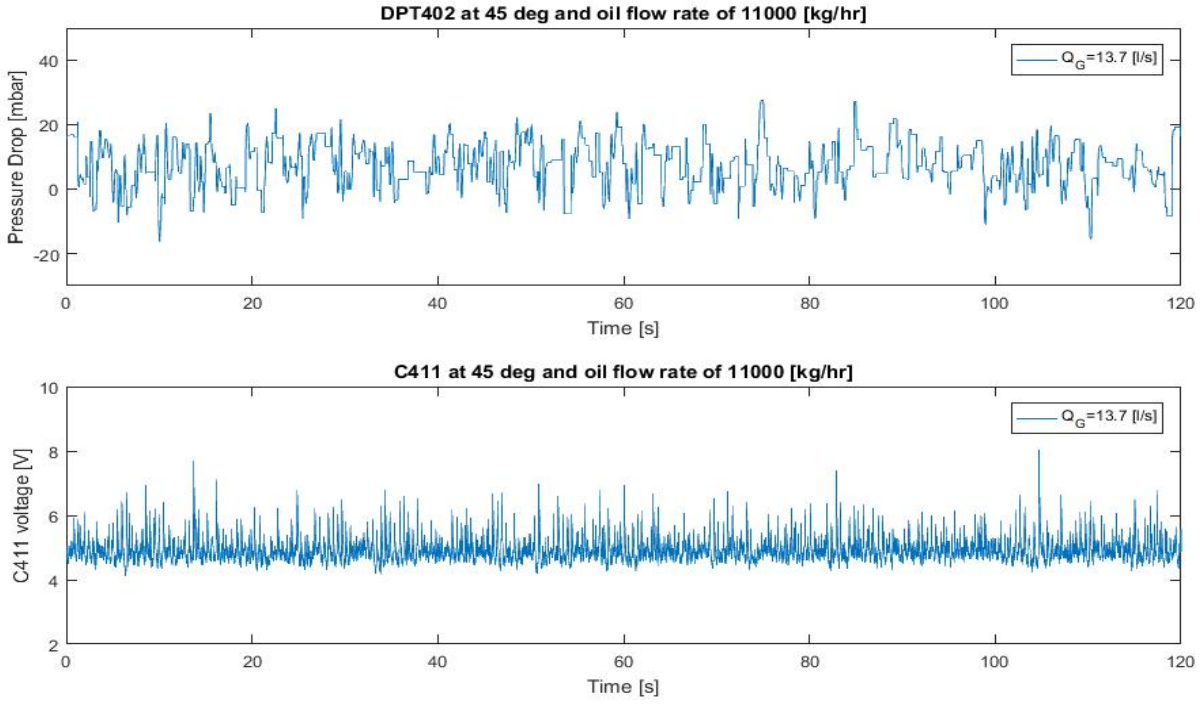

Figure E.19: Differential pressure and capacitance at 45° angle and $Q_L = 11000kg/h$, $Q_G = 13.7l/s$.

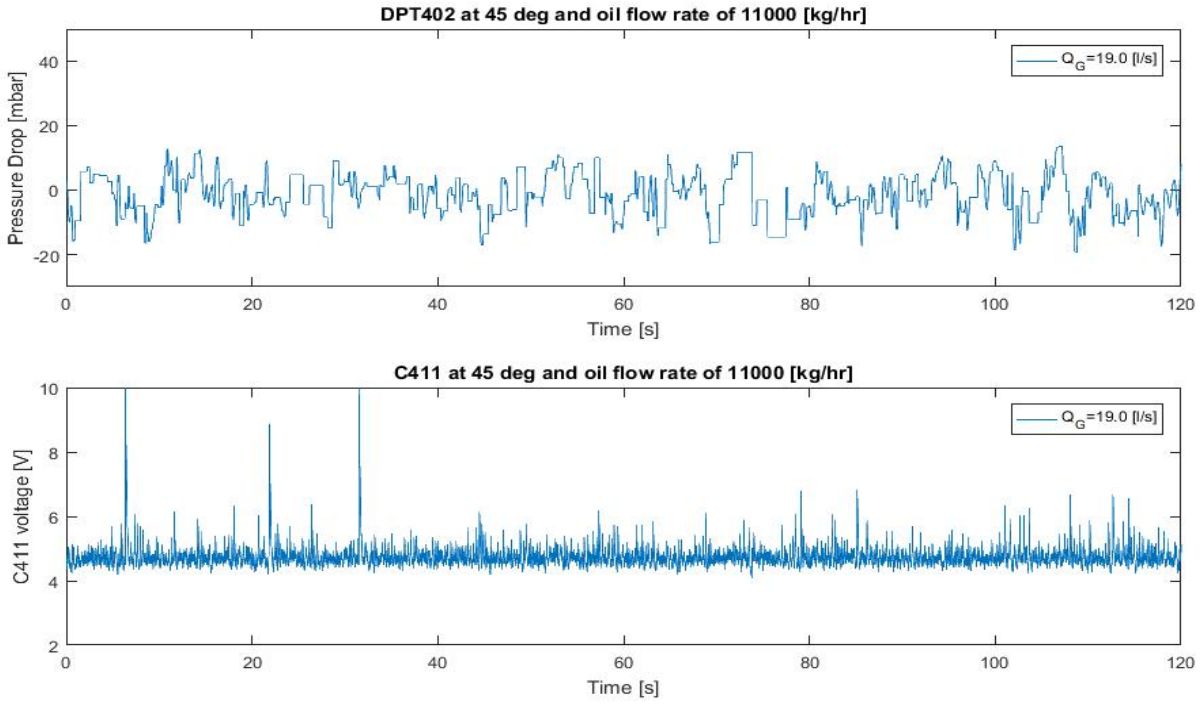

Figure E.20: Differential pressure and capacitance at 45° angle and $Q_L = 11000kg/h$, $Q_G = 19.0l/s$.

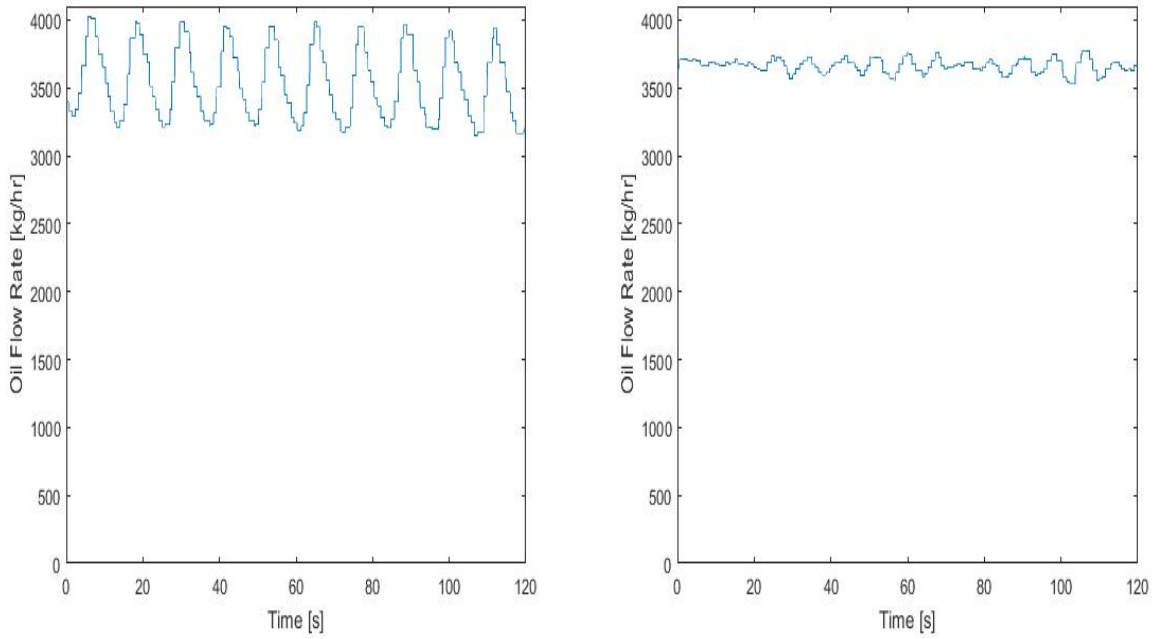

(a) Severe slug flow with $Q_{Gavg} = 7.5kg/h$

(b) Slug flow with $Q_{Gavg} = 14.1kg/h$

Figure E.21: Oil flow rate $3500kg/h$ at 45° angle.

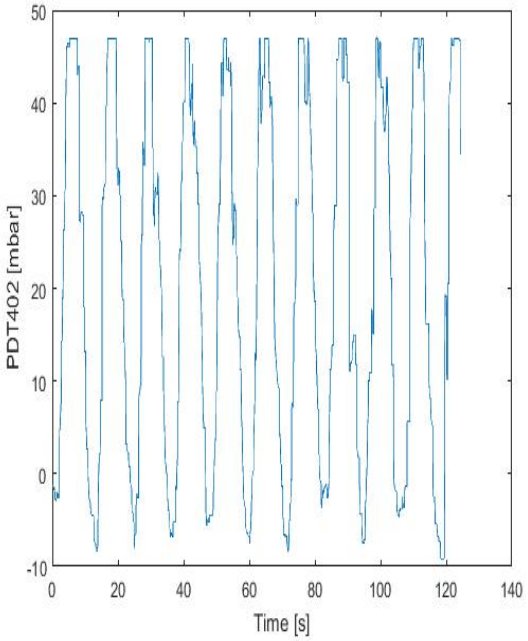

(a) Severe slug flow with $Q_{Gavg} = 7.5kg/hr$

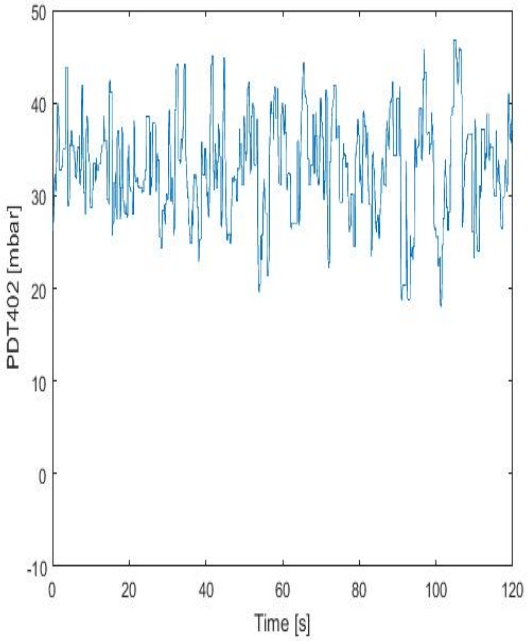

(b) Slug flow with $Q_{Gavg} = 14.1kg/hr$

Figure E.22: Pressure drop with oil flow rate $3500kg/h$ at 45° angle.

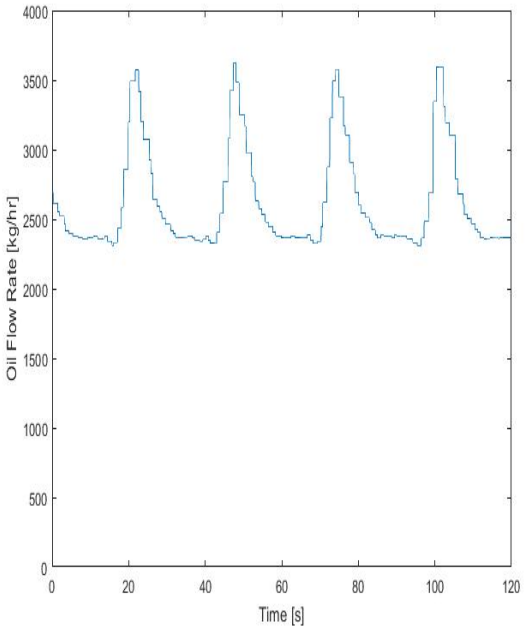

(a) Severe slug flow with $Q_{Gavg} = 3.34kg/hr$

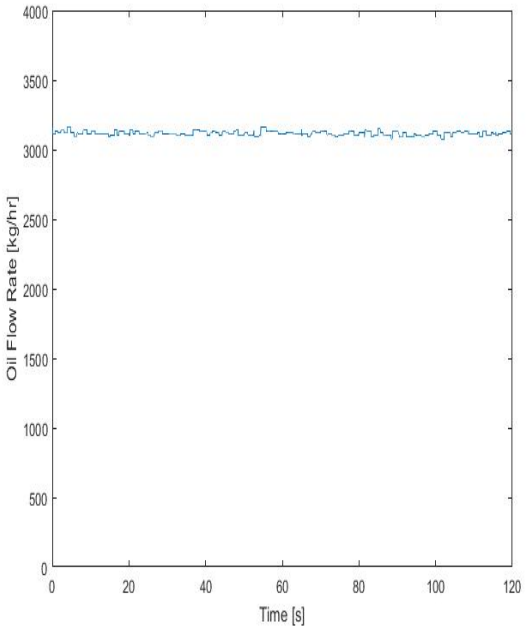

(b) Slug flow with $Q_{Gavg} = 5,7l/s$

Figure E.23: Oil flow rate $3200kg/h$ at 60° angle.

Appendix F

List of Files on Hard Drive

Folder	Name on hard drive	Explanation
Flow regime maps:		
	Flow regime map Xdegree inclination.xls	Processed flow regime maps $10° - 78°$
10 incl:		
	oil230kgh-oil11309	Logged data for all flow rates
15 incl:		
	oil400kgh-oil11200kgh	Logged data for all flow rates
20 incl:		
	oil400kgh-oil11100	Logged data for all flow rates
25 incl:		
	oil1100kgh-oil10500	Logged data for all flow rates
30 incl:		
	oil870kgh-oil11000	Logged data for all flow rates
45 incl:		
	oil950kgh-oil10800	Logged data for all flow rates
60 incl:		
	oil750kgh-oil10300	Logged data for all flow rates
70 incl:		
	oil650kgh-oil10000	Logged data for all flow rates

Folder	Name on hard drive	Explanation
78 incl:		
	oil680kgh-oil10110	Logged data for all flow rates
Liquid holdup:		
	Curvefitting LiqHold	Curve fitting for liquid holdup comparison with OLGA
Videos:		
	Inclination X	Video and pictures for all inclination angles
Matlab:		
		Matlab-codes from Trygve Wangsteen and new codes developed.
Calibration pressure:		
	X degree calibration	Pressure calibration all inclination angles.

Table F.1: Overview of hard drive files.

All files are found in the folder Master Thesis

Appendix G

Paper to be Submitted

EXPERIMENTAL INVESTIGATION OF TWO PHASE FLOW REGIME IN AN INCLINED PIPE

Cleide Vieira [a,*], Magnus Kallager[b], Marit Vassmyr[b], Zhi L. Yang[b], Milan Stanko[a], Ole J. Nydal[b]

[a] *Dept. of Geoscience & Petroleum, Norwegian University of Science and Technology, Norway*
[b] *Dept. of Energy & Process Eng, Norwegian University of Science and Technology, Norway*

Abstract

Flow regime in two phase flow is an important factor that influence both fluid transport and pipeline design. In this experimental work, flow patterns maps in two phase flow for upward inclination between 10° to 78° with respect to the horizontal plane are investigated. The experiments were performed in a 6 m long, 60 mm ID inclinable Plexiglas pipe system, using air and viscous oil as test fluids. The oil density and viscosity was 836 kg/m^3 and 0.025 $Pa\,s$, respectively. Experimental results were compared with existing models (Barnea, 1987) used for the flow pattern map prediction in inclined pipes and with a commercial dynamic multiphase flow simulator (OLGA® 7.3). For the flow regime visualisation and identification high speed cameras were installed in the test section. Pressure gradient and liquid holdup were also measured using differential pressure transmitters and capacitance probes. Experimentally seven flow patterns were recognised: stratified, cap bubble, elongated bubble, churn, slug, annular and severe slugging. Acceptable agreement was seen between the unified model and measured data. On the other hand, the flow patterns simulated in OLGA were not in satisfactory agreement with the measured data.

Keywords:
Air-Oil flow
Two-phase flow
Inclined pipe
Flow regime
Pressure gradient
Liquid holdup

1. INTRODUCTION

The need of understanding two phase gas-liquid flow has been increasing in the recent years and technical solution for handling and controlling the behaviour of such flow is required. Prediction of flow patterns in two phase gas-liquid flow is the main problem in piping systems found in many chemical and petroleum industries. Design of pipelines for deep-water riser, production tubing in offshore oil and gas field development, and parameters including pressure drop and liquid holdup are strongly dependent on the flow pattern. Hence, a better understanding on the behaviour of gas-liquid systems is required to accomplish a consistent design. Generally, flow pattern in two phase gas-liquid flow can exist in a wide variety of forms, depending on the flow rate, physical properties of the phase, geometry and inclination of the tube (McQuillan and Whalley, 1985).[12]

For several years, extensive research on flow pattern in two phase flow has been conducted. Most of this research were aiming to either horizontal or vertical pipe, since such pipe geometry and topology are quite common. Nowadays, the exploration in offshore drilling, several directional well are usually drilled with inclination angle between 10° to 85° and little information on such flow pipe geometry is available.

Considerable numbers of correlation to predict the flow pattern, pressure drop and liquid holdup in either horizontal and vertical flow are available, but these correlations have not been satisfactory when applied to inclined flow. For horizontal and vertical flow in two phase gas-liquid flow several authors have proposed flow pattern maps from experimental work for differ-

*Corresponding author

ent conditions, (Baker (1954), Mandhane *et al.* (1974), Govier and Aziz (1972), Griffith and Wallis (1962)) city by Shoham (2006)[16].

Little information has been published on the effect of pipe inclination on two phase flow. In the 1970s Singh and Griffith (1970) and Bonnecase *et al.* (1971) investigated slug flow of air and water in a small upward inclined pipe. Beggs and Brill (1973) developed a model for predicting pressure gradient from correlation of liquid holdup and friction factor for two phase flow in pipe at all angles for many flow conditions. Gould *et al.* (1974) presented a model to predict pressure distribution in two-phase flow through vertical, horizontal and 45° inclined pipe. Tailel and Dukler (1976) proposed a physical model that predicts the flow regime transitions in horizontal and near horizontal gas-liquid flow.

Barnea *et al.* (1983) developed a mathematical model to predict flow pattern transitions that cover all the range of pipes inclination. The model resulted from the extension of previous model developed for horizontal and slightly inclined pipe (Taitel and Dukler, 1976)[17] and vertical upward flow (Tailel *et al.*, 1980) [5].Later Barnea (1987) proposed a unified model to predict the flow patterns transition for the whole range of pipe inclination in steady gas-liquid flow.

Recently, Zhang *et al.*(2003) presented a unified model for all pipe inclinations which predicted flow pattern, pressure gradient, liquid hold up and slug characteristic. Unified models include correlations and equations for different flow patterns, transitions, inclination angle, liquid hold up, flow rates and other parameters. The two-phase flow is formulated specifically for different flow patterns such as stratified, slug, annular and bubble flows in conjunction with a flow pattern prediction model.[18]

After a literature survey on two phase flow in inclined pipes, it can be concluded that most of the experiment data available for comparing with existing correlations, uses air and water as test fluid. The propose of this experimental work was to obtain reliable data on flow pattern transitions for two phase air-oil in inclined pipe. The flow of air and oil over wide velocity ranges through 60 mm pipe diameter is studied at flow having inclination angles of 10°, 15°, 20°, 25°, 30°, 45°, 60°, 70° and 78°. The unified model for predicting flow pattern transition for the whole range of pipe inclinations proposed by Barnea (1987) and a commercial flow simulator (OLGA® 7.3) is tested by comparison with the experimental results. OLGA is used to validate pressure and liquid holdup in addition.

2. EXPERIMENTAL SET UP AND PROCEDURE

The experiments were carried out at the Multiphase Flow Laboratory at NTNU. The laboratory consist of several flexible test section used for diverse proposed. For this work, an inclined test section was used and air-oil were select as working fluids. The test section consist of a straight 6 m long Plexiglas pipe with 60 mm inner diameter, a separator at the top and could be inclined from 10° to 78° from horizontal (Fig.1). Despite limitations in the choice of range for inclinations angles, due to the support beam in the test section, the inclination angles can be easily changed during operation by adjusting a lift handle connected to a lift mechanism.

The flow loop can be fed with air, water and oil through separated lines and is currently operated at atmospheric pressure and ambient temperature around 20°C. Air is supplied at 7 bar from the main line of the laboratory, but reduced to approximately 4 bar due to pressure loss in valves. Oil is stored with water, separated by gravity, in the main separator located in the basement. The oil is supplied through a oil line by a centrifugal pump.

The inclined loop has two possible mixture section. Thus, two different T-sections allows the air to be injected at two locations (Fig.4). One is located before the flexible pipe, connected to a steel pipe (Fig.2). The other is placed at the test section entrance, right after the flexible pipe (Fig.3) . The second mixture section were preferred in the investigation to prevent instabilities prior to the test section. The two-phase flow propagates through the test section to a separator at the top of the pipe where the air is vented to the atmosphere and the liquid drained to a storage separator.

The fluids flow rate are measured by mean of Coriolis meter. The properties and characterisation of the fluid are shown Table 1, density and viscosity of oil were measured with a picnometer and rheology meter, respectively. Capacitance probe, pressure taps and differential pressure transducers were used to study the correspondent liquid holdup and pressure drop in the test section. To permit visual observation of flow pattern, three synchronised high speed cameras (GigE 120 fps) were installed, and pictures and videos recorded. The location of the camera varied for different inclination angle depending on the accessibility around the test section. All equipment in the lab are connected to a DAQ system and controlled by a main program written in LabVIEW® where output signals and logging are provided. A separate acquisition system, also in LabVIEW, was used for the cameras.

In addition to the inclination angle at which varies

during the experiments, superficial velocities of both air-oil were tested for different values, presented in Table 2. The fluid velocities chosen for the experiments were selected to allowed better observation of the flow pattern along the test section.

Figure 1: Test section

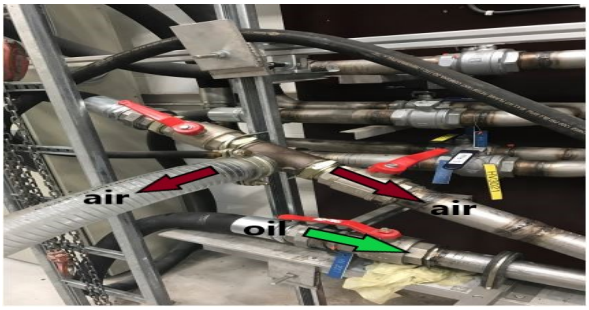

Figure 2: Mixture section before flexible pipe.

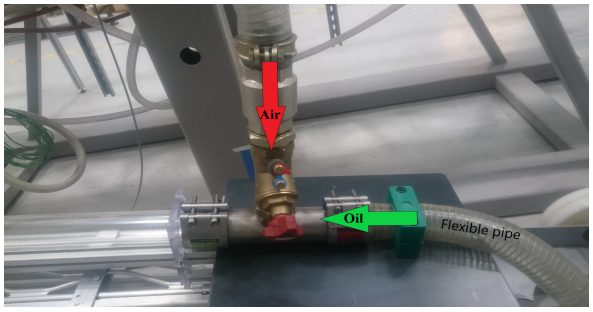

Figure 3: Mixture section after flexible pipe.

3. CHARACTERISTIC FLOW PATTERNS

Flow pattern is normally defined as the result of the mechanical and thermal dynamic equilibrium between the phases that depends on a large number of important parameters such as superficial velocities, flow conditions, fluid properties, geometry and the flow direction (Monni *et al.,* 2014).

The effect of inclination angle on the flow pattern transition boundary was studied in the present paper, by varying the inclination angle in a steps of 5°, 8° and 15°. Diverse classification of the flow pattern in the conduit exit, most of them based on individual interpretation to the visual observation of the fluid distribution within the pipe flow, [4]. This has been a disadvantage, due to different visual interpretations reported under identical flow conditions. Therefore, many researches have proposed to classify the flow pattern quantitatively. Jones and Zuber (1974) proposed gamma ray densitometer to identify the flow patterns by analysing the measured void fraction fluctuation. Hubbard and Dukler (1966), Weisman *et al.*(1979) and Elperin *et al.*(2002) have used pressure drop oscillations. Conductance probe tech-

Figure 4: Air T-section supply

Table 1: Working fluid properties

Physical Property	**Air**[a]	**Oil**[b]
Density, kg/m^3	1.22	$840 \pm 0.4\%$
Viscosity, $Pa.s$	1.8×10^{-5}	$1.79 \times 10^{-3} \pm 1.2\%$
Surface tension, N/m	-	0.025 ± 0.0005

[a]Properties calculated at 1 atm and 20°C

[b]Properties measured at 1 atm and 20°C

Table 2: Experimental test matrix

Incli.	N° Exp.points	U_{sl} (ms^{-1})	U_{sg} (ms^{-1})
10	65	0.017 – 1.34	0.038 – 11.79
15	71	0.048 – 1.33	0.035 – 10.25
20	79	0.047 – 1.31	0.036 – 9.20
25	72	0.13 – 1.28	0.037 – 9.29
30	82	0.10 – 1.32	0.036 – 9.24
45	71	0.11 – 1.29	0.039 – 9.18
60	72	0.088 – 1.27	0.036 – 9.19
70	66	0.077 – 1.25	0.028 – 10.78
78	61	0.082 – 1.25	0.037 – 8.93

nique was also the target of many investigations cited in the paper of Barnea *et al.*(1980a).

In the present work, flow regimes were identified by visual inspection, where video recordings were carefully conducted for stable flow. Based on the observation seven present flow regimes were identified: cap bubble, elongated bubble, slug, stratified wavy, churn, severe slugging and annular. Dispersed bubble flow could not be observed due to limitations of oil flow rate in the experiments. In Figs.5-10 some of the observed flow regimes are presented. The regime identification and their transition were not easily recognised during the experiments. For example in Figures 8 and 9, a long time period on the observations was taken into account and the most dominant flow regime over the time classified the final flow regime. The difference between elongated bubble, slug and cap bubble flow (Fig.6-7) was based on the "bubble shape" and film thickness below the bubble as mentioned in Barnea *et al.*(1980b). Severe slugs were also observed for low superficial velocities of liquid at higher inclination angles, above 45°. This phenomena occurs due to accumulation of liquid at the test section inlet, that creates a blockage for the gas to flow. Overall, as a consequence of the difficulties regarding the visualisation, flow regimes could be misinterpreted during classification of the flow patterns.

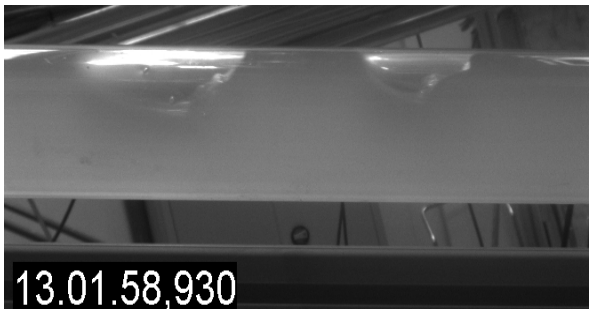

Figure 5: Cap bubble flow

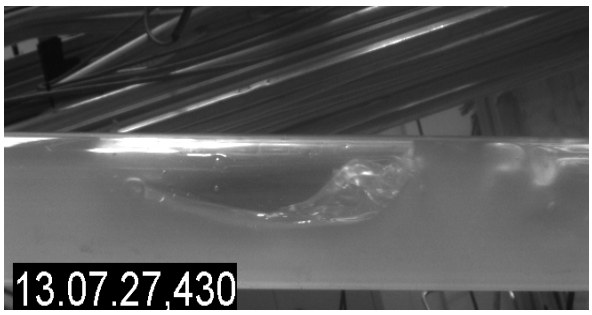

Figure 6: Elongated flow

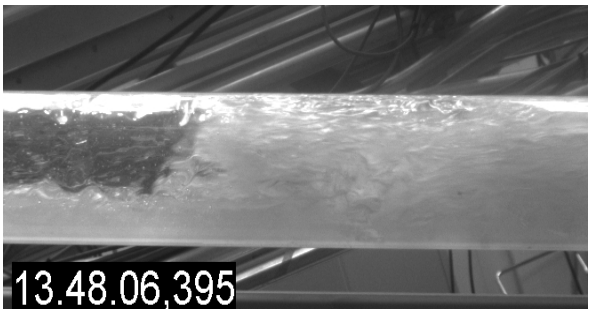

Figure 7: Slug flow

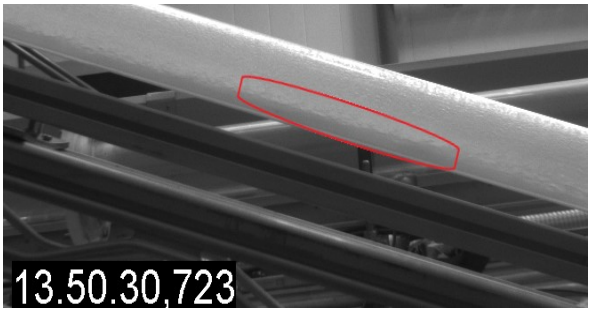

Figure 8: Stratified wavy flow

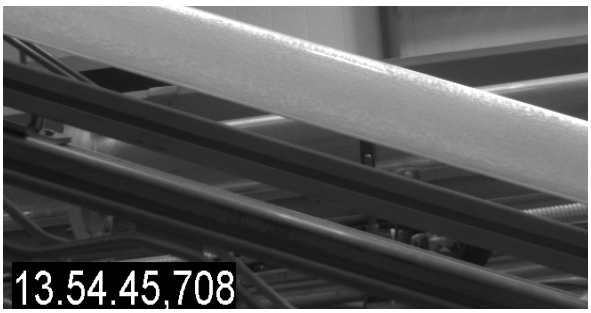

Figure 9: Annular flow

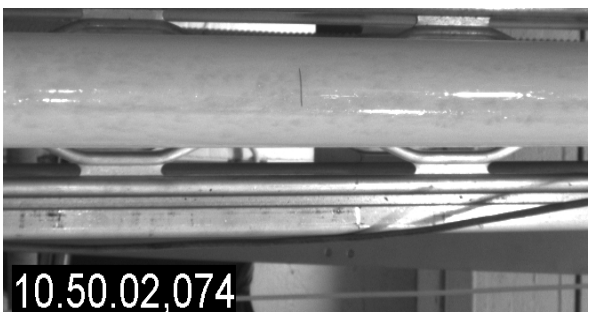

Figure 10: Churn flow

4. COMPARISON OF EXPERIMENTAL DATA WITH BARNEA (1987) UNIFIED MODEL

The unified model developed by Barnea (1987) is compared with the experimental data and presented in Fig.11-19. The model was developed based on previous publication in Barnea (1986) where a unified model for the transition from annular to intermittent flow and from dispersed bubble flow was proposed. Barnea's model was designed with purpose of predicting flow pattern transition for the whole range of pipe inclination. The transition mechanism used to predict the flow patterns transition boundaries and its applicability is given through operative equations or dimensionless maps. The equations and maps incorporate the effect of flow rates, fluid properties, pipe size and the angle of inclination.[3]

The model criteria and equations were implemented in Matlab®. Since the model is based on experimental data for air-water system flowing, the verification of whether this model is also applied for more viscous fluids was set as the aim for the investigation.

In Barnea *et al.* (1980b, 1982a, 1985 and 1987) flow regimes for horizontal, vertical and inclined flow were main classified into four major regions: Stratified, intermittent, annular and dispersed bubble or bubble flow. The stratified region is subdivided into *stratified smooth* and *stratified wavy*. Intermittent is subdivided into *slug* and *elongated flow* for the case of horizontal flow and adding *churn flow* for upward almost vertical flow. For annular region, *annular* and *annular wavy* are defined. At last, dispersed bubble or bubble flow is define as the flow were the gas phase is distributed as discrete bubbles within the liquid phase having no subdivision. In total nine different flow patter are identified. In comparison with the flow pattern identified experimentally, annular wavy, stratified wavy and cap bubbly flow seems to be the difference between them.

Barnea *et al.*(1985) state that annular wavy is a type of flow with a film at the bottom of the pipe, while aerated unstable waves are swept around the pipe which can make the flow appear both stratified wavy and slugging. This are the same characterisations as stratified wavy defined experimentally. Distinction between cap bubble and elongated bubble flow in the region of lower gas rates is done experimentally, while the model only holds as bubble flow.

General agreement between the experimental data and the unified model was found for stratified smooth pattern, that is not observed for any inclination angles. Barnea *et al.* (1985) mentioned that this pattern is only observed for angles less than 0.25°.

Stratified wavy flow defined as annular wavy in the model is not observed for inclination angles above 20° (Figs.14-19), which also agrees with the model prediction and observation in Shoham (1982). However Fig. 11 shows that the stratified flow transition curve does not completely represent the experimental data, due to high liquid flow rates used in the experiments compared with the rates used in Barnea (1987). This is not verified in Fig. 12 where the the liquid flow are much lower. As a consequence of different naming between annular wavy and stratified wavy, the stratified-annular transition curve shows in some cases unclear, which mean that the experimental data could contain marginal deviations from the actual flow regime.

Dispersed flow was not achieved in either experiments due to limitation on the liquid flow rate, which is confirmed with the theoretical transition line located above the maximum superficial velocity of the liquid (U_{SL}) used in the experiments. In Barnea *et al.*(1980b, 1985) dispersed bubble flow exists for superficial velocity of liquid (U_{SL}) approximate to $5m/s$ and higher superficial velocity of gas (U_{SG}) about $10m/s$ to $100m/s$, those rates were not possible to be achieved in the experiments.

Elongated bubble flow region reduces with increasing inclination angle, not existing at inclination angles above 30° in the experiments. Similar condition occurs in Barnea *et al.*(1985, 1987) where the elongated bubble disappears at angles above 50° and 30° respectively for upward inclined pipe with 5.2 cm ID.

Churn flow in the experimental data has a similar behaviour as the one verified in Barnea *et al.* (1985) where the first appearance of this pattern occurs at 70° (Fig.18). In Barnea *et al.*(1985) the range of U_{SL} at which the churn flow appears increase with the pipe diameter, thus it was possible to observe this pattern for the velocities used in the experiment.

The Bubble-slug transition curve better represent the experimental data for inclinations angles above 60°. The criteria used set by the unified model used in this transition were not met for inclination angles 10° and 15°.

In summary, the comparison shown in Figures 11-19 lead to the conclusion that the model presented by Barnea (1987) is applicable to inclined pipes 20°-78° inclination with good accuracy. The agreement is well demonstrated for inclinations were the stratified and intermittent region is quite accurately predict. The only exception to this agreement is the bubble flow region where Barnea (1980b,1985) do not distinguish elongated bubble from cap bubble flow and annular flow that may have some misinterpretation due to the distinction

between stratified wavy and annular flow done experimentally. The superficial velocities used for flow pattern prediction and comparison should be approximated the same range to avoid inaccuracy.

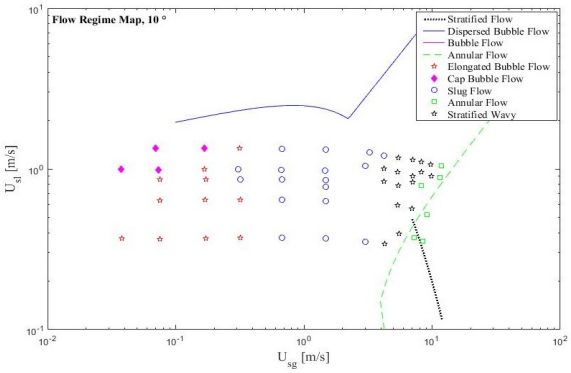

Figure 11: Experimental vs theory 10° inclination

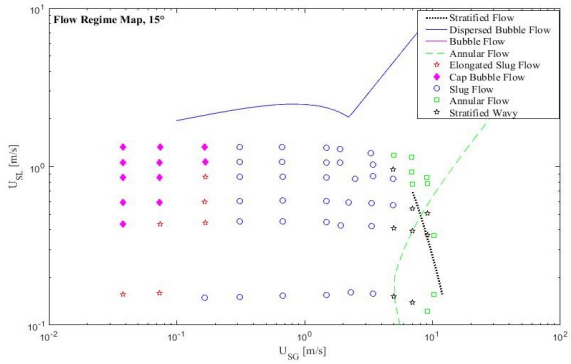

Figure 12: Experimental vs theory 15° inclination

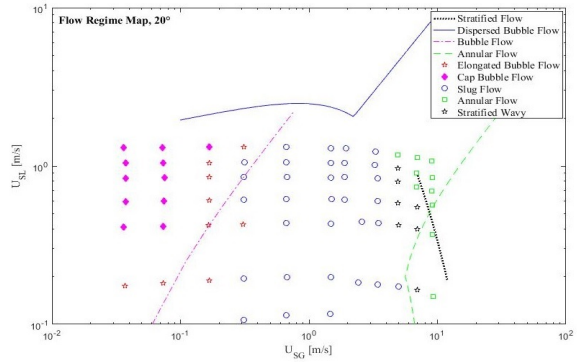

Figure 13: Experimental vs theory 20° inclination

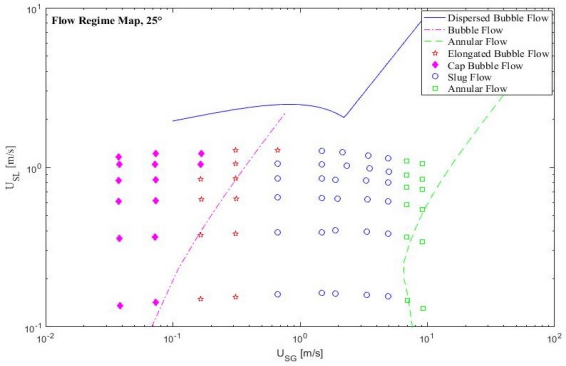

Figure 14: Experimental vs theory 25° inclination

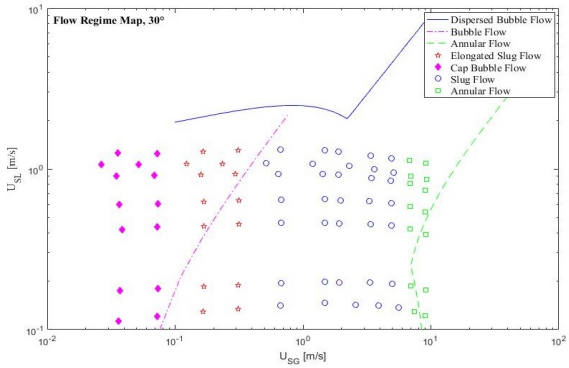

Figure 15: Experimental vs theory 30° inclination

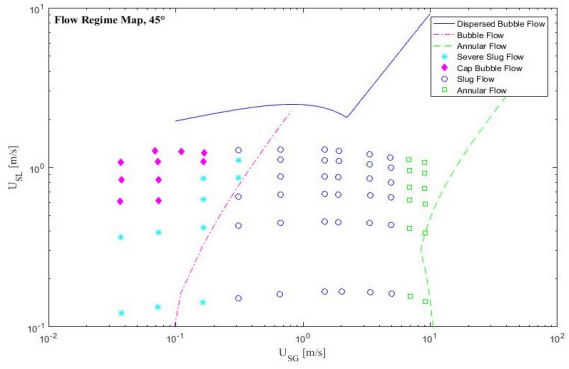

Figure 16: Experimental vs theory 45° inclination

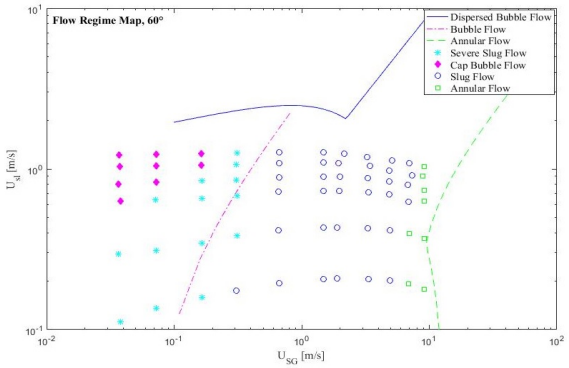

Figure 17: Experimental vs theory 60° inclination

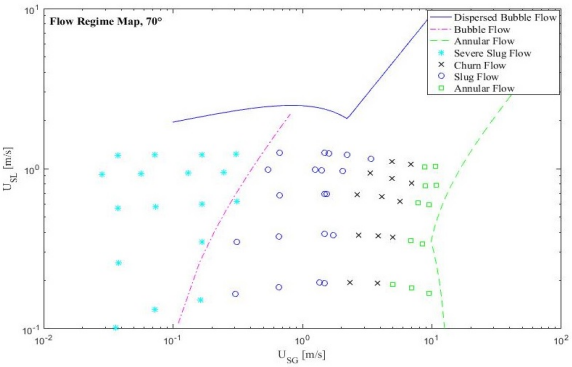

Figure 18: Experimental vs theory 70° inclination

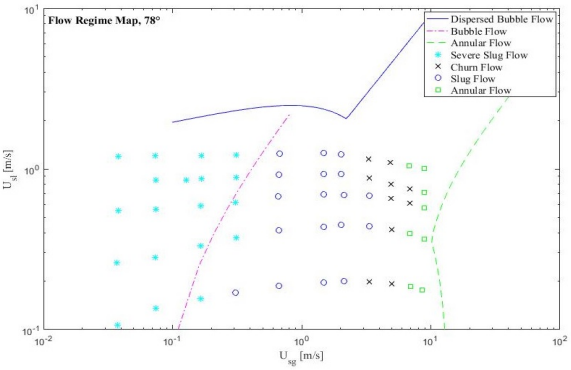

Figure 19: Experimental vs theory 78° inclination

5. COMPARISON OF EXPERIMENTAL DATA WITH COMMERCIAL SIMULATOR

Besides the prediction of the flow pattern transition using the unified model of Barnea (1987), a dynamic multiphase flow simulator (OLGA® 7.3.) have been used with the desire to validate the performance of flow regime determination, pressure drop and liquid holdup for upwards inclined systems. Comparison between the measured data and the simulated are presented in Figs. 20-28. The flow regimes were plotted by fixing necessary parameters and provide superficial velocities from experiments in addition to inclination angles (Table 2).

The fluid properties were specified through a pvt-table, where the properties for air-oil are presented in Table 1. Heat and mass transfer were not considered during the simulations. The geometry of the simulation were set to be the same as the test section.

According to Bendiksen *et al.* (1991) flow regime transition identification in OLGA, is basic two flow regime classes *distributed* and *separated*. The distributed is where the contribution of bubble and slug flow are present, while separated including stratified and annular flow. In total, OLGA distinguish between four flow regimes: stratified, bubble, slug and annular. It should be mentioned that the stratified flow is classified either as smooth of wavy. The transition between distributed and separated flow regime is based on the assumption of continuous average void fraction which means that the flow pattern yielding when the minimum gas velocity is chosen.

Similar to Barnea (1987), slug-annular flow transition in the simulator occurs at higher gas flow rates compared to the experiments. Simulation out of the range presented in the paper were performed in order to reach the annular flow. It was observed that to predict annular flow using the simulator, higher gas velocity is necessary around 200 m/s for 10° inclination. The required gas flow rate for annular flow to be seen, decreases as the angle increases around 50 m/s for 70° inclination. Since in the experiment maximum U_{SG} was approximate 12 m/s, slug-annular transition were not achieved for inclination angles below 60°. In Figs. 26-28 slug-annular transition line is presented, but are not consistent with the experimental observed flow pattern. This may be due to the fact that experimentally some data can be named as annular flow, while stratified wavy flow are treated. The bubble-slug curve moves to the right down when the inclination angle increase, hence the experimental slug flow region in better represented for inclination above 30°. Also in the case bubble flow region that is the left side of the bubble-slug transition curve

better match with the measured flow pattern is verified (Figs. 25-28). This conclusion is based on the fact that cap bubble and elongated bubble exists in the bubble flow region.

Overall, OLGA prediction are not in successful agreement with the experimental data, Although the obtained the experimental results could be considered reasonable. OLGA is based on models and also experiments on other facilities which does not agree completely with the experimental conditions in this investigation.

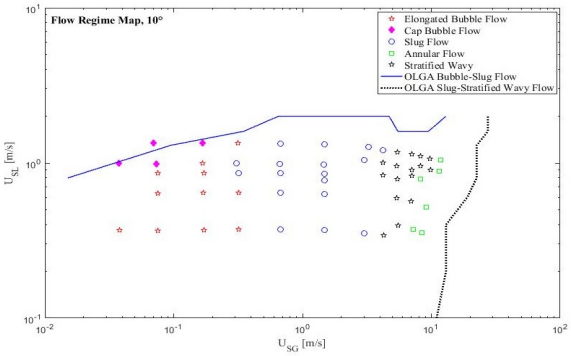

Figure 20: Experimental vs simulator 10° inclination

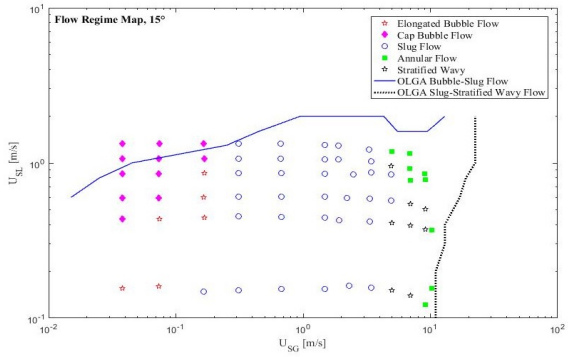

Figure 21: Experimental vs simulator 15° inclination

5.1. LIQUID HOLDUP

Beggs (1973) mentioned that the prediction of liquid loading is essential for the designing field processing equipment's, such as gas separator. In this investigation capacitance probes were used for liquid holdup measurements. They were designed to detect liquid fraction in air-oil two phase flow through a electrical signals. The electrical circuit had a power supply that provided

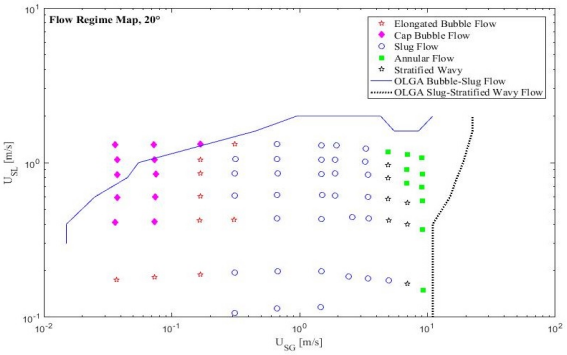

Figure 22: Experimental vs simulator 20° inclination

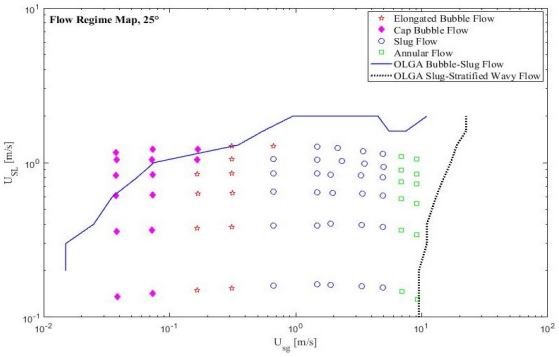

Figure 23: Experimental vs simulator 25° inclination

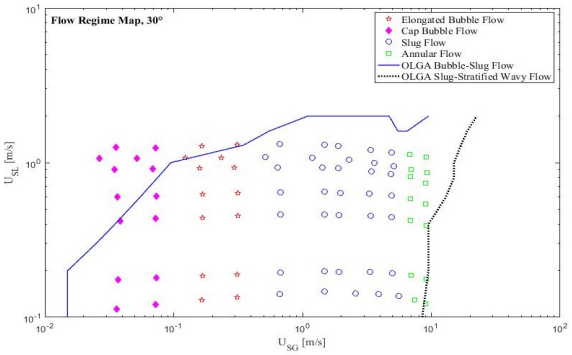

Figure 24: Experimental vs simulator 30° inclination

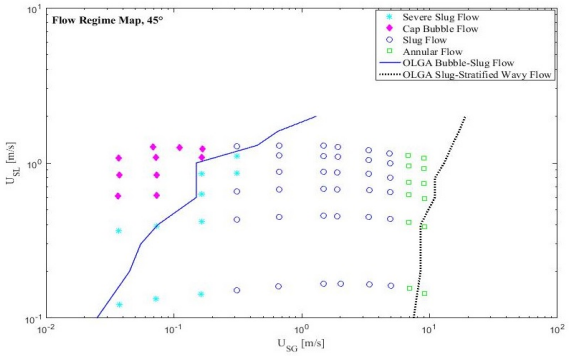

Figure 25: Experimental vs simulator 45° inclination

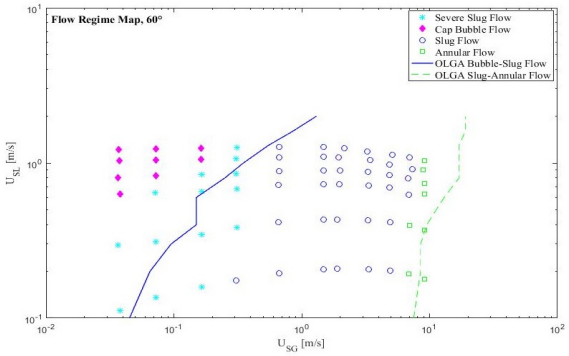

Figure 26: Experimental vs simulator 60° inclination

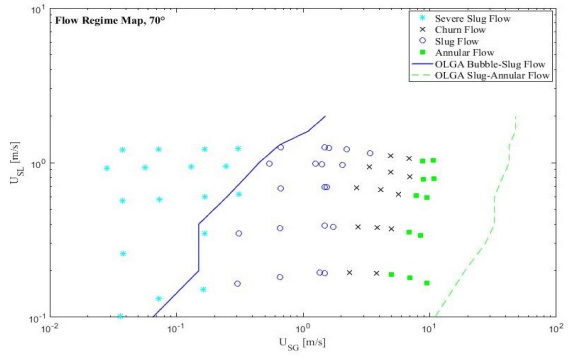

Figure 27: Experimental vs simulator 70° inclination

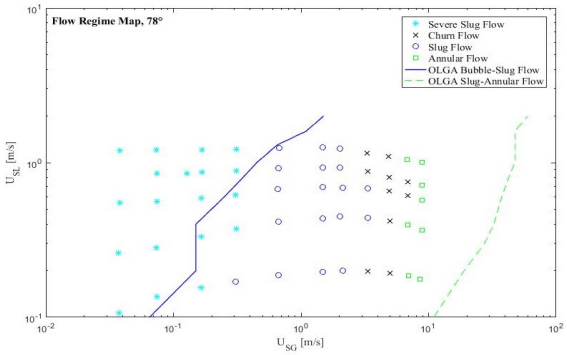

Figure 28: Experimental vs simulator 78° inclination

voltage range from 2 V to 10 V. Before any measurement calibration were performed in order to register the reference limit for a empty pipe (3.2 V) and pipe fully filled with liquid (9.2 V), respectively.

Reading the liquid holdup for a inclined section is challenging, and for that reason horizontal stratified flow was used as a reference calibration. The reference calibration was performed in horizontal stratified flow. The calibration utilised the wet perimeter and voltage output to provide a s-curve for liquid holdup, which can be seen in Fig.29. Adding a trend line to the s-curve, a third order polynomial equation is found. Therefore, the equation can be used to correlate the output voltage signal on the estimation of liquid holdup in the test section.[9]

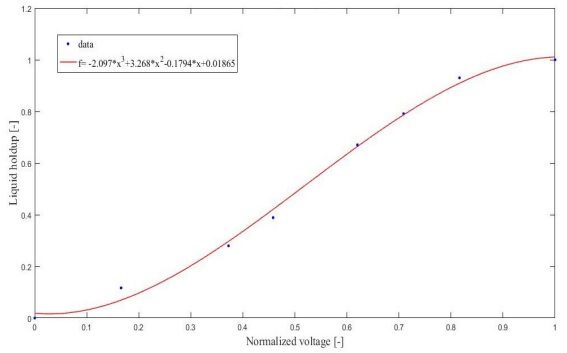

Figure 29: Capacitance probe calibration curve

Experimental liquid holdup results were only compared with the liquid volume fraction estimated in OLGA. The unified model uses a critical void fraction as boundary condition for flow pattern transition. Therefor, no comparison were preformed with experimental results. In Fig.30 variation of liquid holdup with

the superficial gas velocity is present for both experimental and OLGA results for 25° inclination angle. It can be seen that the liquid holdup deviates, specially for high gas velocities and both curves have a exponential shape. This can be explained by the fact that the s-curve was developed for horizontal stratified flows.

The correlation was made by taking the difference between the respective exponential fitted curves, and calculate the new liquid holdup by adding the difference to the liquid holdup from the capacitance sensor. The correlation was developed for angle 25, but it was applied to the other inclination angles as well.

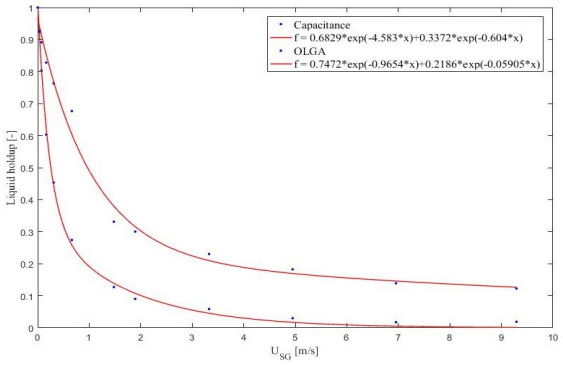

Figure 30: Liquid holdup from capacitance sensor and OLGA at 25°.

A no-slip liquid holdup was also estimated based on some of the experimental flow rates and liquid content (c) was set as constant, to study the effect of this parameter with the inclination angle. A comparison between the no-slip liquid holdup and OLGA is displayed in Fig.31. It was observed that for all ranges of flow condition tested the liquid holdup estimated in OLGA gives higher values that the experimental results. However, the experimental data is obtained from flow measurements, and not capacitance signals, such that the results can be presumed differently for capacitance measurements.

5.2. PRESSURE DROP

Normally, pressure drop is dependent on fluid properties such as density and viscosity, and flow parameters (velocity and friction factor). Beggs and Brill (1973) developed an equation for the pressure gradient when gas or liquid, or both, flow in a pipe. Pressure gradients in directional wells are usually calculated using a vertical flow correlation such that of Hagedorn and Brown (1965) or of Orkiszewski (1967) cited by Begg and Brill (1973). Pressure drop in two phase flow is more complex and difficult to predict compared with single phase flow.

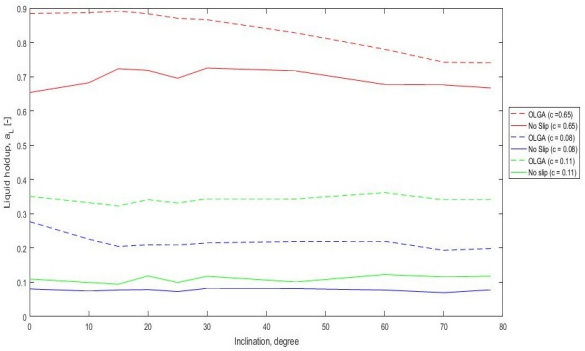

Figure 31: Liquid holdup for $0° - 78°$ inclination angle

Differential pressure transducer were used to measure the pressure drop in the test section. The output pressure signal (from LabVIEW) was then processed and compared only with the pressure drop estimated by the simulator, since the unified model is basically a set of equation and criteria solved for superficial velocities of the fluid, void fraction and pipe geometry having no relation with the pressure drop. Overall, it was observed that the pressure drop response changed with the flow pattern present in the test section and the inclination angles. Experimentally the measured pressure drop was corrected for non-zero value at zero flow, during calibration. The following equations were used to transfer the measured pressure gradient to gravitational, frictional and total pressure drop.

$$(\frac{dP}{dL})_{mea} = (\frac{dP}{dL})_{fric} + (\rho_L - \rho_m)g\,sin(\beta), \qquad (1)$$

where the mixed density is defined as

$$\rho_m = \alpha_L\rho_L + (1 - \alpha_L)\rho_G. \qquad (2)$$

The pressure loss due to gravitation becomes

$$(\frac{dP}{dL})_{grav} = \rho_m g\,sin(\beta), \qquad (3)$$

and the total pressure loss

$$(\frac{dP}{dL})_{tot} = (\frac{dP}{dL})_{mea} - \rho_L g\,sin(\beta). \qquad (4)$$

The measured pressure gradient used in the plots are time-averaged values from the experiments.

Figure 32-35 show that the total pressure loss reach a minimum point for lower gas flow rates and a further increase in gas flow rates resulted in larger pressure drop for all inclinations. In the area of high gas flow rates, the frictional losses are more dominant. The curves for

frictional pressure gradients indicates that the pressure gradient becomes positive for low gas and liquid flow rates. Although OLGA and experiments show the same trends, the lines for frictional and total pressure gradients deviates a lot, especially for high gas flow rates.

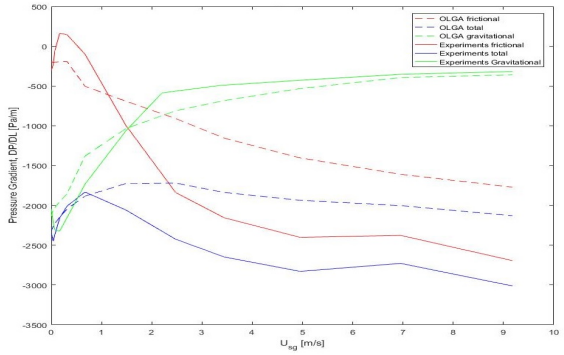

Figure 32: Gravitational, friction and total pressure gradient at 15° inclination and $U_{SL} = 0.85m/s$

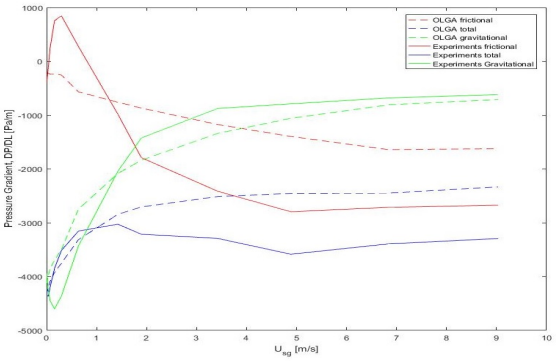

Figure 33: Gravitational, friction and total pressure gradient at 30° inclination and $U_{SL} = 0.90m/s$

6. SUMMARY AND CONCLUSION

Experimental results were collected for a air-oil two phase flow system in 60 mm ID pipe and compared with the theoretical model of Barnea (1987) and a commercial simulator (OLGA®) for a inclined flow with 10° to 78° variation of inclination angle. Experimentally, the flow regime consist of stratified wavy from 10° - 20°, bubble flow from 10° - 60° (elongated bubble and cap bubble flow), severe slugging 45° - 78°, churn flow 70° - 78°, while slug and annular flow were observed for the entire angles range. A comprehensive conclusion of the experimental study is that variation on the inclination

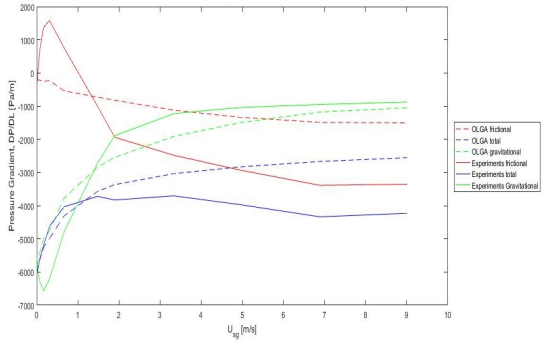

Figure 34: Gravitational, friction and total pressure gradient at 45° inclination and $U_{SL} = 0.83m/s$

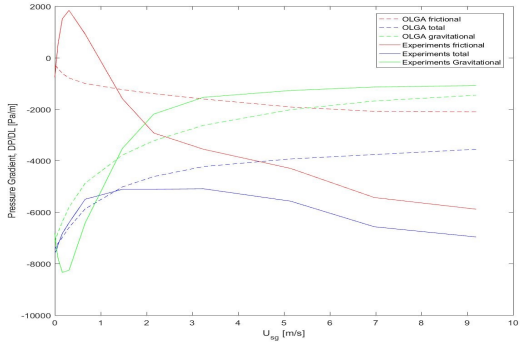

Figure 35: Gravitational, friction and total pressure gradient at 60° inclination and $U_{SL} = 1.07m/s$

angle has a major effect on the flow pattern. Comparison of experimental flow pattern with the theoretical model indicates that the unified model, which is obtain based on two phase air-water to predict flow patterns, shows a good agreement with the experimental measurements. Most of the flow pattern regions defined by Barnea *et al.* (1980a, 1980b, 1985 and 1987) are observed.

In general, flow pattern prediction in the simulator is not in successful agreement with the measured data. The simulated pattern has the exception for the slug flow 70°-78° inclination angles, but fail on the slug-annular flow transition for the same inclination. Experimental results for pressure drop and liquid holdup were also compared with the simulation results. It was shown that the higher liquid holdup is predicted by the simulation comparing with the measured data and the total pressure gradient measured agreed quite well with the predictions in OLGA for the tested inclination angles.

References

[1] Baker, O., et al., 1953. Design of pipelines for the simultaneous flow of oil and gas. In: Fall Meeting of the Petroleum Branch of AIME. pp. 607–617.

[2] Barnea, D., 1986. Transition from annular flow and from dispersed bubble flowunified models for the whole range of pipe inclinations. International journal of multiphase flow 12 (5), 733–744.

[3] Barnea, D., 1987. A unified model for predicting flow-pattern transitions for the whole range of pipe inclinations. International Journal of Multiphase Flow 13 (1), 1–12.

[4] Barnea, D., Shoham, O., Taitel, Y., 1980a. Flow pattern characterization in two phase flow by electrical conductance probe. International Journal of Multiphase Flow 6 (5), 387 – 397.

[5] Barnea, D., Shoham, O., Taitel, Y., Dukler, A., 1980b. Flow pattern transition for gas-liquid flow in horizontal and inclined pipes. comparison of experimental data with theory. International Journal of Multiphase Flow 6 (3), 217–225.

[6] Barnea, D., Shoham, O., Taitel, Y., Dukler, A., 1985. Gas-liquid flow in inclined tubes: flow pattern transitions for upward flow. Chemical Engineering Science 40 (1), 131–136.

[7] Beggs, D. H., Brill, J. P., et al., 1973. A study of two-phase flow in inclined pipes. Journal of Petroleum technology 25 (05), 607–617.

[8] Bendiksen, K. H., Maines, D., Moe, R., Nuland, S., et al., 1991. The dynamic two-fluid model olga: Theory and application. SPE production engineering 6 (02), 171–180.

[9] Diaz, M. J., 2016. Two-phase slug flow experiments with viscous liquids. Ph.D. thesis, NTNU.

[10] Gould, T. L., Tek, M. R., Katz, D. L., et al., 1974. Two-phase flow through vertical, inclined, or curved pipe. Journal of Petroleum Technology 26 (08), 915–926.

[11] Jones, O. C., Zuber, N., 1975. The interrelation between void fraction fluctuations and flow patterns in two-phase flow. International Journal of Multiphase Flow 2 (3), 273–306.

[12] McQuillan, K., Whalley, P., 1985. Flow patterns in vertical two-phase flow. International Journal of Multiphase Flow 11 (2), 161–175.

[13] Monni, G., De Salve, M., Panella, B., 2014. Horizontal two-phase flow pattern recognition. Experimental Thermal and Fluid Science 59, 213–221.

[14] Schlumberger, 2014. Used Manual OLGA 3.0.

[15] Shoham, O., 1982. Flow pattern transition and characterization in gas-liquid two-phase flow in inclined pipes. 1982. PhD Disertation.

[16] Shoham, O., 2006. Mechanistic modeling of gas-liquid two-phase flow in pipes. Richardson, TX: Society of Petroleum Engineers.

[17] Taitel, Y., Dukler, A., 1976. A model for predicting flow regime transitions in horizontal and near horizontal gas-liquid flow. AIChE Journal 22 (1), 47–55.

[18] Zhang, H.-Q., Wang, Q., Sarica, C., Brill, J. P., 2003. Unified model for gas-liquid pipe flow via slug dynamicspart 1: model development. Journal of energy resources technology 125 (4), 266–273.